



UNIFORMED SERVICES UNIVERSITY OF THE HEALTH SCIENCES
F. EDWARD HÉBERT SCHOOL OF MEDICINE
4301 JONES BRIDGE ROAD
BETHESDA, MARYLAND 20814-4799



March 6, 2007

**BIOMEDICAL
GRADUATE PROGRAMS**

Ph.D. Degrees

Interdisciplinary
-Emerging Infectious Diseases
-Molecular & Cell Biology
-Neuroscience

Departmental
-Clinical Psychology
-Environmental Health Sciences
-Medical Psychology
-Medical Zoology
-Pathology

Doctor of Public Health (Dr.P.H.)

Physician Scientist (MD/Ph.D.)

Master of Science Degrees

-Molecular & Cell Biology
-Public Health

Masters Degrees

-Comparative Medicine
-Military Medical History
-Public Health
-Tropical Medicine & Hygiene

Graduate Education Office

Dr. Eleanor S. Metcalf, Associate Dean
Janet Anastasi, Program Coordinator
Tanice Acevedo, Education Technician

Web Site

www.usuhs.mil/geo/gradpgm_index.html

E-mail Address

graduateprogram@usuhs.mil

Phone Numbers

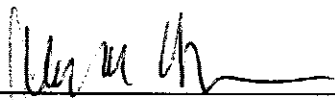
Commercial: 301-295-9474
Toll Free: 800-772-1747
DSN: 295-9474
FAX: 301-295-6772

APPROVAL SHEET

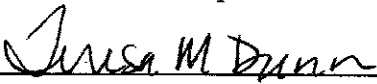
Title of Dissertation: "Characterization of Enzymes Involved in Fatty Acid Elongation"

Name of Candidate: Shilpi Paul
Doctor of Philosophy Degree
11 April 2007

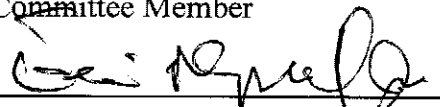
Dissertation and Abstract Approved:


Jeffrey Harmon, Ph.D.
Department of Pharmacology
Committee Chairperson

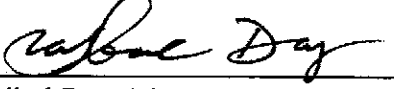
4/14/07
Date


Teresa Dunn, Ph.D.
Department of Biochemistry
Committee Member

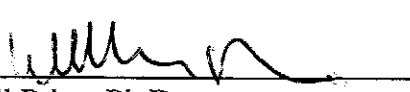
4/17/07
Date


Ernest Maynard, Ph.D.
Department of Biochemistry
Committee Member

4/11/07
Date


Saibal Dey, Ph.D.
Department of Biochemistry
Committee Member

4/16/07
Date


Will Prinz, Ph.D.
NIDDK, National Institutes of Health
Committee Member

4/11/07
Date

The author hereby certifies that the use of any copyrighted material in the thesis manuscript entitled:

"Characterization of Enzymes Involved in Fatty Acid Elongation"

is appropriately acknowledged and, beyond brief excerpts, is with the permission of the copyright owner.

Shilpi Paul 04/12/2007
Shilpi Paul
Molecular and Cell Biology Program
Uniformed Services University

ABSTRACT

Title of Dissertation: Characterization of Enzymes Involved in Fatty Acid Elongation

Name: Shilpi Paul
Molecular and Cell Biology Graduate Program,
Uniformed Services University of the Health Sciences
4301 Jones Bridge Road
Bethesda, MD 20814

Dissertation Directed by: Teresa M. Dunn, Ph.D.
Professor and Interim Chair
Department of Biochemistry and Molecular Biology
Uniformed Services University of the Health Sciences
4301 Jones Bridge Road
Bethesda, MD 20814

The very long chain fatty acids, synthesized by a microsomal chain-elongating enzyme system known as the elongase, are essential components of many cellular lipids. Each cycle of elongation involves four successive enzymatic reactions: condensation, reduction, dehydration, and a second reduction, and lengthens the fatty acid by 2 carbon units. Several enzymes that mediate condensation, including the soluble fatty acid synthases and the FAE1-like 3-ketoacyl-CoA synthases (FAE-KCSs) possess a catalytic triad of Cys, His, and His/Asn. In contrast, the Elop proteins, which are implicated in the condensation reaction lack any homology to the well-characterized condensing enzymes. There are three Elop proteins (Elo1p, Elo2p and Elo3p) in yeast and our *in vitro* assays with microsomes from wild type and the single *elo* mutants (*elo1* Δ , *elo2* Δ and *elo3* Δ) demonstrate that the Elops are essential for condensation. Heterologous expression of

several *Arabidopsis* FAE-KCSs can substitute for the Elops in yeast. Similar to the Elop proteins, genetic and coimmunoprecipitation experiments provide evidence that the FAE-KCSs work in conjunction and are physically associated, with the reductases of the elongase complex. These studies indicate that FAE-KCSs and Elops might have evolved independently, but are still able to utilize similar reductases.

Since the elongase proteins localize to the ER, behave as integral membrane proteins, and are predicted to have several membrane spanning domains, an important step toward elucidating the organization of the elongase complex is to determine the membrane topology of the elongase proteins. Several biochemical approaches including protease protection, glycosylation, factor Xa protease cleavage and the split-ubiquitin yeast two hybrid assays were utilized to resolve the topology of the 3-ketoreductase and enoyl-CoA reductase of the elongase complex. A six membrane-spanning topology model with both termini facing the cytosol for both yeast and *Arabidopsis* Tsc13p, the enoyl-CoA reductases is proposed. By alanine substitution two conserved functionally critical residues of yeast Tsc13p were identified. Based on this model, these residues (K140 and R141) lie towards the cytosolic side of TMD2. These studies also revealed that Ybr159p, the 3-ketoreductase of the elongase system, has an N-terminal membrane-associated domain with the active site lying in the cytosol.

Characterization of Enzymes Involved in Fatty Acid Elongation

By

Shilpi Paul

Thesis submitted to the Faculty of the Molecular
and Cell Biology Program of the Uniformed Services
University of the Health Sciences in partial fulfillment
of the requirements for the degree of Doctor of Philosophy, 2007

Acknowledgements

The work in this thesis could never be done on my own without the support of Teresa Dunn, who not only helped me on my projects but encouraged me to think like an independent scientist. I am grateful to Dunn lab members for being friendly and helping me whenever I am stuck with any experiments. Especially, I would like to thank Ken Gable for his support, his friendship and made everyday work a pleasure; Gongshe Han and Sita Gupta for their helpful comments during lab meetings. I must thank my committee members Dr. Jeffery M. Harmon, Dr. Teresa M. Dunn, Dr. Saibal Dey, Dr. Ernie Maynard and Dr. Will Prinz (NIH) for guidance and intellectual inputs. I would also like to thank the collaborators of the “2010 Arabidopsis project”, Dr. Jan Jaworski (Donald Danforth Plant Science Center, St. Louis), Dr. Edgar Cahoon (USDA-ARS, Donald Danforth Plant Science Center, St. Louis), Dr. Johnathan Napier and Frederic Beaudoin (Rothamsted Research, Harpenden, UK) for their helpful suggestions.

Without monetary help it would have been impossible to do this research, I am grateful to Colonel A. N. Bose travel award by University of Calcutta for higher studies abroad, Henry M. Jackson Graduate Student Award provided by USUHS, graduate student research support fund from USUHS and predoctoral fellowship from American Heart Association for supporting my graduate stipend and “2010 NSF Collaborative research”.for funding the research.

This thesis is a product of all the love and support I have received from so many special people over the years. I dedicate this thesis to my parents and parents-in-law, who sacrificed so much so that I could have every opportunity to succeed. To my brother, Supriyo Roy and brother-in-law, Suman Paul for their encouragement and support. Finally, I would like to express my deepest love and gratitude to my husband and bestfriend Anirban, who is doing research at Cold Spring Harbor Lab. for his intellectual input and emotional support. You have provided me with so much love and support that I will never be able to say thank you enough.

TABLE OF CONTENTS

APPROVAL SHEET	i
COPYRIGHT STATEMENT	ii
ABSTRACT	iii
TITLE PAGE	v
LIST OF FIGURES	x
ABBREVIATIONS	xi
INTRODUCTION	1
What is fatty acid?	1
Difference between de novo FA and VLCFA synthesis	1
Fatty acid synthase required for de novo FA synthesis	2
A. Type I FAS	3
B. Type II FAS	4
Condensing enzymes	8
Microsomal elongase complex for VLCFA biosynthesis	10
A. Enzymes required for the condensation step, the Elops	10
<i>ELO</i> homologs identified in several organisms	13
Elops elongating short chain FAs	14
Fatty acid elongase-3 ketoacyl CoA synthases (FAE-3KCSs)	15
FAE-KCS involved in PUFA elongation	21
Difference between Elops and FAE-KCSs	21
Condensation is the rate-limiting step of VLCFA synthesis	22
B. Enzymes required for the 3-ketoacyl reduction - 3-ketoacyl reductases	22

C. Enzymes required for enoyl-CoA reduction - Trans 2,3-enoyl CoA reductases .	26
Towards understanding the structure of the organization of the Elongase Complex ...	28
1. Hydropathy analyses.....	28
2. Epitope Protease Protection	29
3. Glycosylation Scanning.	29
4. Factor Xa Protease.	31
5. Membrane Based Split-ubiquitin Assay	32
Importance of VLCFAs	34
1. Organ development and morphogenesis.....	34
2. Lipids, wax and seed oil synthesis.....	35
3. Industrial applications.....	35
4. Ceramide and sphingolipid synthesis.....	36
SPECIFIC GOALS OF THIS STUDY.....	39
PAPER 1 (Published in 2006, <i>JBC</i> Vol 281, 14, 9018-9029)	41
MEMBERS OF THE ARABIDOPSIS FAE1-LIKE 3-KETOACYL-coa SYNTHASE GENE FAMILY SUBSTITUTE FOR THE Elop PROTEINS OF <i>SACCHAROMYCES</i> <i>CEREVISIAE</i>	41
PAPER 2 (Accepted in <i>JBC</i>)	
A Six-Membrane-Spanning Topology for Yeast and Arabidopsis Tsc13p, the Enoyl Reductases of the the Microsomal Fatty Acid Elongating System.....	67
PAPER 3	Error! Bookmark not defined.

Topological Analysis of <i>Saccharomyces cerevisiae</i> Ybr159p, the Major 3-ketoreductase of the Microsomal Fatty Acid Elongating System.....	90
DISCUSSION.....	121
The Elops are required in the condensation step	122
Several Arabidopsis FAE-KCSs substitute for the Elops	123
FAE-KCSs and Elops utilize similar elongase components	125
The VLCFAs Synthesized by the FAE-KCS rescued yeast are incorporated into sphingolipids.....	126
Topological mapping of the reductases of the elongase complex	127
A. Six membrane-spanning topology model of yeast and Arabidopsis Tsc13p, the enoyl-CoA reductases	127
B. Topology model of yeast Ybr159p, the 3-ketoreductase	130
Comparing the topology of Tsc13p and Ybr159p	132
FUTURE DIRECTIONS	133
CONCLUSION.....	136
BIBLIOGRAPHY.....	139
Statement of Author's Contribution:	151

LIST OF FIGURES

Figure 1. Pathway of fatty acid synthesis.....	2
Figure 2. Fatty acid biosynthesis pathway in bacteria.....	7
Figure 3. Reduction reactions of fatty acid elongation	8
Figure 4. Condensation reaction in fatty acid biosynthesis	9
Figure 5. Plot showing protein sequence alignment between the yeast Elops.....	12
Figure 6. Phylogenetic tree for known and putative <i>A. thaliana</i> FAE-KCSs	16
Figure 7. Primary sequence alignment for CUT1, KCS1 and FAE1.....	19
Figure 8. Hydropathy analysis of FAE1 KCS.....	20
Figure 9. Schematic representation of the split-ubiquitin assay.....	33
Figure 10. Pathways of fatty acid elongation, LCB, ceramide and sphingolipid synthesis in <i>S. cerevisiae</i>	38
Figure 11. Schematic representation of the Elongase Complex.....	126
Figure 12. Schematic of altering the location of the active site of Ybr159p.....	136
Figure 13. Schematic representation of the topology models of the yeast elongase components.....	138

ABBREVIATIONS

ACC	acetyl coenzyme A carboxylase
ACP	acyl-carrier protein
At	prefix designating an <i>Arabidopsis thaliana</i> gene or gene product
ATP	adenosine triphosphate
CoA	coenzyme A
DHA	docosahexaenoic acid
DHS	dihydrosphingosine
EM	electron microscopy
EndoH	endoglycosidase
ER	endoplasmic reticulum
FA	fatty acid
FAE-KCS	FAE1-like 3-ketoacyl-CoA synthase
FAMES	fatty acid methyl esters
FAS	fatty acid synthase
FASI	fatty acid synthase type I
FASII	fatty acid synthase type II
FOA	5-fluoroorotic acid
fXa	factor Xa
GC	glycosylation cassette
GCMS	gas chromatography-mass spectrometry
GFP	green fluorescent protein
GPI	glycosylphosphatidylinositol
HA	hemagglutinin
His	histidine
HMMTOP	Hidden Markov Model for Topology Prediction
HSD	hydroxysteroid dehydrogenase
IPC	inositolphosphoceramide
kDa	kilodalton
KCS	ketoacyl-CoA synthase
KS	3-ketosphingosine
LCB	long chain base
M	molar

MIPC	mannosylinositolphosphoceramide;
M(IP)2C	mannosyldiinositolphosphoceramide
NaCl	sodium chloride
NV	nucleus-vacuole
NVJ	nucleus–vacuole junction
OH	hydroxyl group
ORF	open reading frame
PHS	phytosphingosine
PMN	piecemeal microautophagy of the nucleus
PUFA	polyunsaturated fatty acid
SC	prefix designating a <i>Saccharomyces cerevisiae</i> gene or gene product
SPL	sphingolipid
TAG	triacylglycerols
TLC	thin layer chromatography
TM	transmembrane
TMHMM	transmembrane prediction using hidden markov model
TMD	transmembrane domain
TSC	temperature-sensitive <i>csg2Δ</i> suppressor
VLCFA	very long-chain fatty acid
Wt	wild type
<i>Wdal</i>	Wax-deficient anther1

INTRODUCTION

What is fatty acid?

A fatty acid (FA) is a carboxylic acid with an aliphatic tail (chain), which is either saturated (double bonds or other functional groups absent along the chain) or unsaturated (one or more alkenyl functional groups exist along the chain, i.e, a carbon double bonded to another carbon). FAs are essential components of all biological membranes and also represent an important form of stored energy in both animals and plants. Because their biosynthesis begins with the two carbon unit acetic acid, the naturally occurring FAs have an even number of carbon atoms. This *de novo* FA synthesis occurs in the cytoplasm, and through repeated cycles generates palmitate, a 16 carbon unit FA. The palmitate is further elongated to very long chain fatty acids (VLCFAs) by a microsomal enzyme system, which is distinct from the cytoplasmic enzyme system.

Difference between *de novo* FA and VLCFA synthesis

Both *de novo* FA biosynthesis and microsomal FA elongation follow a similar pathway involving the following four steps: (i) condensation of a primer with a malonyl group, (ii) reduction of the resulting β -keto compound to a secondary alcohol, (iii) dehydration of the alcohol to form a *trans*- $\alpha\beta$ -unsaturated intermediate, and (iv) reduction of the *trans*- $\alpha\beta$ -unsaturated intermediate to give an acid two carbon units longer than the primer (Fig. 1).

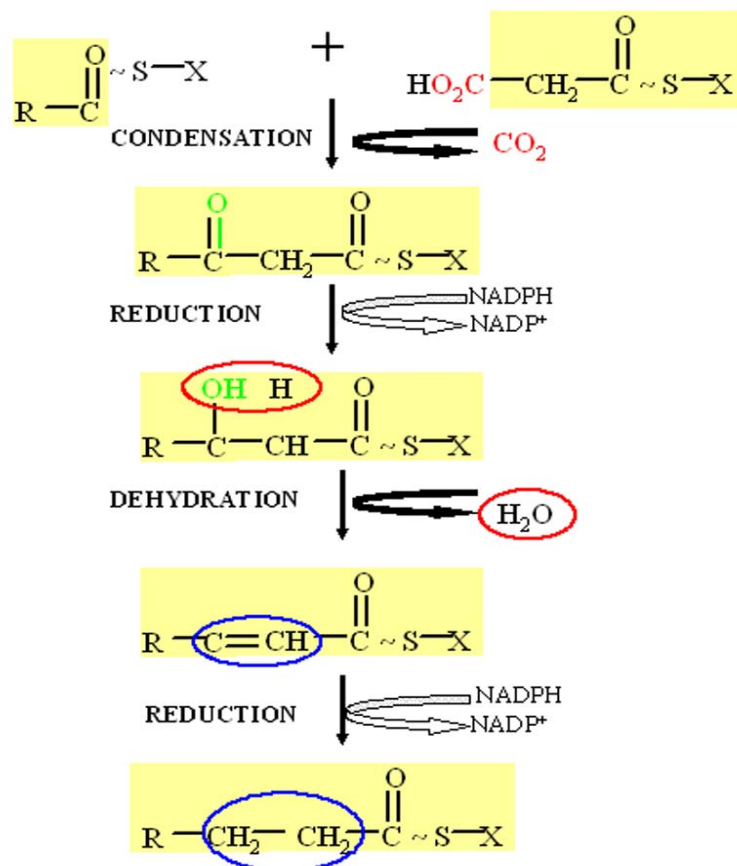


Figure 1. Pathway of fatty acid synthesis. In a cycle of four steps, the FA is elongated by 2 carbon units that are donated from a malonyl group. During condensation, carbon dioxide is liberated, and a β -keto acid intermediate is formed, which is reduced to an alcohol in the second step. The alcohol is dehydrated to form an unsaturated intermediate, which is reduced in the final step to generate the elongated FA. NADPH is used as the cofactor for both reductions. $X=CoA$ or ACP , $R=$ carbon chain.

Fatty acid synthase required for *de novo* FA synthesis

FA can be synthesized, *de novo*, by type I or type II fatty acid synthase [1] complexes [2, 3] that differ in their structural organization but that catalyze a similar reaction sequence. In both systems the growing carbon chain is esterified to an acyl-carrier protein (ACP). The overall reaction sequence is summarized below:





A. Type I FAS

Mammals and fungi have the Type I FAS system that in yeast possesses seven separate catalytic domains [2] residing on two nonidentical polypeptides in yeast [$\alpha_6\beta_6$ subunit organization [4] and in mammals contains two identical polypeptides with subunit molecular masses of ~ 270 kDa [α_2 [5]]. The conventional model posits that the two monomers of Type I FAS are arranged in a fully extended head-to-tail anti-parallel fashion that allows functional interactions across the monomer interface [6, 7]. However, an alternative model based on the results of mutant complementation, chemical crosslinking and monomer interactions, suggests that the FAS monomers adopt a coiled conformation that allows intra- and inter-monomer domain interactions [8-10]. Recently, cryo-EM analysis of a single FAS particle, combined with gold labeling of the N-termini and structural analysis of the FAS monomer, revealed two coiled monomers in an overlapping arrangement requiring limited rearrangements for catalytic interaction between the functional domains [11]. The N-terminal domain, comprised of ~ 400 residues, exhibits significant sequence similarity to the *E. coli* ketoacyl synthase (KS), with both possessing a highly reactive thiol group contributed by an active-site cysteine residue [12]. A second catalytic domain contains the malonyl/acetyl transferase, which with the exception of the conserved active-site serine, exhibits weak sequence similarity with the *E. coli* malonyltransferase [12]. A third domain comprises the dehydrase activity that includes a catalytically important histidine residue [13]. The enoylreductase activity resides in a fourth domain [14] and the ketoreductase in a fifth domain [15]. The reductase domains were identified by the virtue of the presence of glycine-rich motifs:

Gly-Ser-Gly-Gly-Val-Gly and Gly-Leu-Gly-Gly-Phe-Gly, respectively, which exhibit significant sequence similarity to the pyridine nucleotide-binding sites of several enzymes, including alcohol dehydrogenase and dihydrofolate reductase [16]. The first of these two putative nucleotide binding domains also contains the sequence Gly⁶⁹⁴-Ser-Ale-Glu-**Lys**-Arg. The lysine residue within this region was identified by peptide mapping as the residue that, when modified with pyridoxal phosphate, results in specific inactivation of the enoyl reductase activity. Thus, the fourth catalytic domain was identified as the enoylreductase and, by deduction, the fifth as the ketoreductase. The two reductase domains are followed by the acyl carrier protein (ACP) domain, with a Gly-Leu-Asp-Ser-Leu motif, the serine of which is esterified to the 4'-phosphopantetheine prosthetic group. The ACP domain helps in sequestering the reaction intermediates. The C-terminal domain is the thioesterase that releases the palmitoyl moiety from its thioester linkage to the 4'-phosphopantetheine as a free fatty acid [17].

B. Type II FAS

Type II FAS is a dissociated system, with separate proteins responsible for each catalytic step of the elongation pathway. Type II FAS is found in bacteria, plants, parasites and in an eukaryotic cell organelle (mitochondria) [3, 18]. The mitochondrial Type II FAS pathway functions in lipoic acid synthesis [19]. In contrast to Type I FAS, which produces only palmitate, Type II FAS is capable of producing diverse products (with different chain lengths, unsaturated, branched-chain, and hydroxyl FAs). The *E. coli* FAS II pathway (Fig. 2) is outlined below [3]:

The acetyl coenzyme A (CoA) carboxylase (ACC) catalyzes a key step that

synthesizes malonyl-CoA from acetyl-CoA. The *acpP* gene encodes ACP, produced as an apoprotein and converted to its active form by transferring the 4'-phosphopantetheine prosthetic group from CoA by [ACP]synthase. The malonyl group of malonyl-CoA is transferred to ACP by malonyl-CoA:ACP transacylase (FabD). All subsequent intermediates in FAS remain attached to the terminal sulphhydryl of ACP. The β -ketoacyl-ACP synthase III (FabH) catalyzes the first condensation step in the pathway using acetyl-CoA and malonyl-ACP. The acetoacetyl-ACP formed by FabH (with Cys-Asn-His as the catalytic triad) enters the elongation cycle that progressively elongates the acyl chain attached to ACP by two carbons in each cycle. The structures of β -ketoacyl-ACP reductase (FabG) and enoyl-ACP reductase (FabI) were determined for enzymes isolated from three organisms, *E. coli* [20-25], *M. tuberculosis* [26, 27], and *Brassica napus* [28, 29]. FabG is a NADPH-dependent reductase that catalyzes the reduction of the carbonyl group at the C3 position to a hydroxyl group by addition of two hydrogen atoms, one to the carbonyl carbon and the second to the carbonyl oxygen giving rise to β -hydroxyacyl-ACP. This intermediate is dehydrated to *trans*-2-enoyl-ACP by the β -hydroxyacyl-ACP dehydratases (FabA and FabZ). The biochemical characterization of these enzymes suggests that FabA efficiently processes acyl chains of length $\leq C_{10}$, whereas FabZ functions in the synthesis of long-chain acyl-ACPs that are greater than C_{10} [30]. The FabI uses NADH to reduce the C2–C3 carbon-carbon double bond generated by the dehydratase enzyme to complete the synthesis of the acyl chain.

The 3-keto and enoyl reductases involved in fatty acid elongation (or *de novo* synthesis, and by analogy, probably also fatty acid elongation) are both members of the short-chain dehydrogenase/reductase (SDR) superfamily, which contain a signature

YX_nK motif within their active sites. The lysine stabilizes binding of the cofactor by hydrogen bond interactions and a proton is donated by the tyrosine hydroxyl group to the enolate anion formed on the C1 carbonyl oxygen to generate the enol. The members of the SDR family, including the 3-keto and enoyl reductases share structural similarities in that they are tetrameric α/β proteins containing the Rossmann fold that binds the nucleotide cofactor. However, the two reductases of the FAS system differ in the spacing between Y and K in the YX_nK motif, to accommodate the relative positions of the substrate carbonyl oxygen atom that is reduced by the 3-keto reductase and the C=C double bond of the enoyl intermediate that is reduced by enoyl reductase. The position of the lysine side chain relative to the nicotinamide ring is fixed by the ribose interaction. Thus to protonate the oxygen atom on the substrate the position of the tyrosine must shift. In FabI, the motif is longer (YX₆K), reflecting that the C3 carbon and the enolate oxygen are separated by three bonds in the *trans*-2-enoyl-ACP, whereas in FabG the motif is shorter (YX₃K) since the carbon and oxygen in the substrate lie in the same carbonyl group and are separated by only one bond (Fig. 3).

Subsequent rounds of elongation are initiated by the condensing enzymes FabB or FabF (Cys-His-His in the active site), which condense the growing acyl-ACP with malonyl-ACP to extend the fatty acid chain by two carbons.

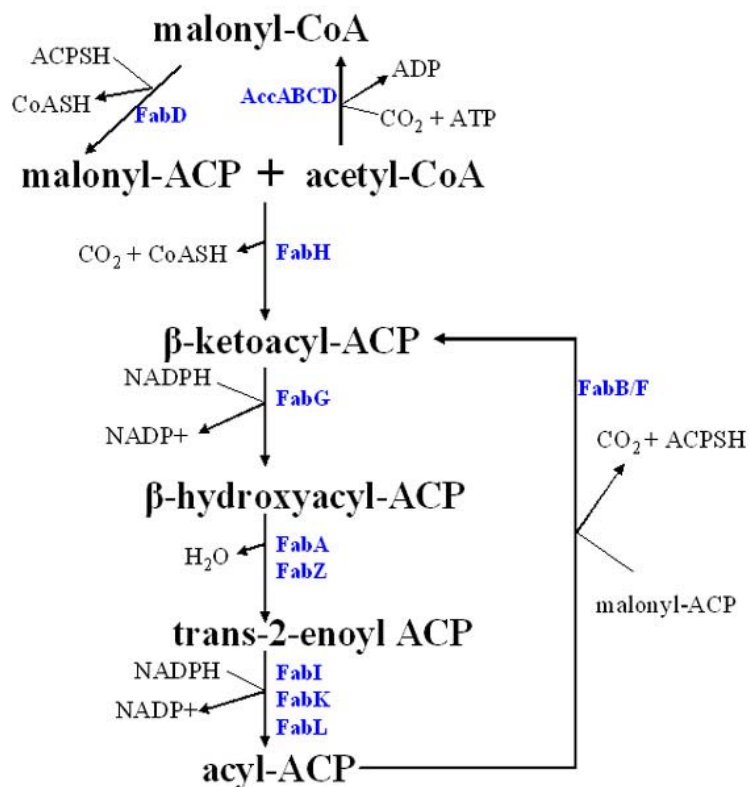


Figure 2. Fatty acid biosynthesis pathway in bacteria (adapted from Heath *et al.* 2002). Malonyl-ACP is made by the ATP-dependent carboxylation of acetyl-CoA, followed by a transacylation step, catalyzed by FabD. FA synthesis is initiated by the condensation of acetyl-CoA and malonyl-ACP by the enzyme FabH, generating acetoacetyl-ACP. A cyclical series of reduction, dehydration, and reduction reactions produces an acyl-ACP. This compound is a substrate for elongation by the FabB or FabF condensing enzymes to produce a β-ketoacyl-ACP two carbons longer than in the previous round.

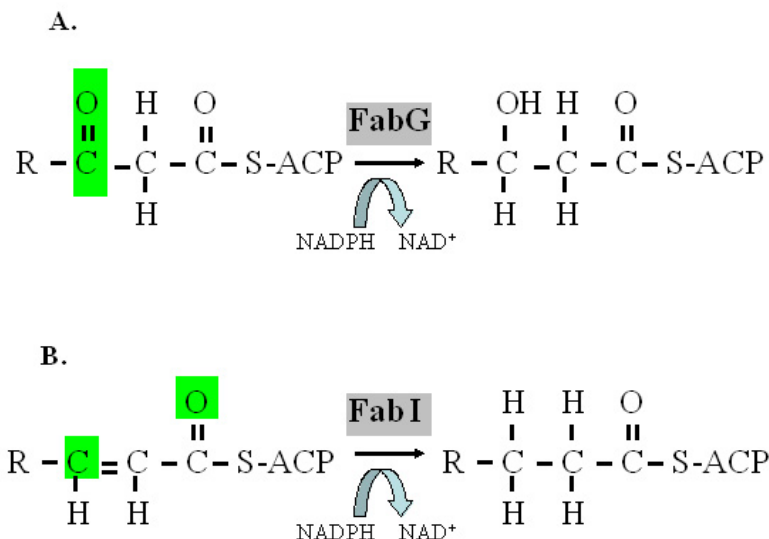


Figure 3. Reduction reactions of fatty acid elongation. A. 3-keto acyl CoA reduction catalyzed by FabG in *E.coli*, B. enoylCoA reduction catalyzed by FabI in *E.coli*. The *green boxes* mark the position of the carbon and the oxygen atoms in the substrates of each reaction that in the β -ketoacyl ACP are separated by only one bond, but in the trans 2-enoyl ACP are separated by three bonds.

Condensing enzymes

The mechanism of carbon-carbon bond formation in FAs and in polyketide synthesis proceeds by a decarboxylative Claisen condensation (Fig. 4), with the enzymes required for catalysis collectively referred to as condensing enzymes. Several members of this family have been crystallized, and the structures reveal a common 3-dimensional fold and a conserved active site. Based on primary sequence alignments, the condensing enzymes can be divided into two classes. The initiation condensing enzymes that include the β -ketoacyl-ACP synthase (KAS) III (FabH) utilize acyl-CoAs as substrates whereas the elongating condensing enzymes, which include the condensing domains of FASI, the β -ketoacyl-ACP synthase I and II from bacteria (FabB and FabF) and plants, use ACP thioesters. The fundamental difference between them lies in their active site residues,

which in the case of the initiation condensing enzymes consist of Cys, His, Asn whereas the elongating condensing enzymes possess Cys, His, His in the catalytic triad. However, both enzymes catalyze identical chemical reaction in FA biosynthesis [31].

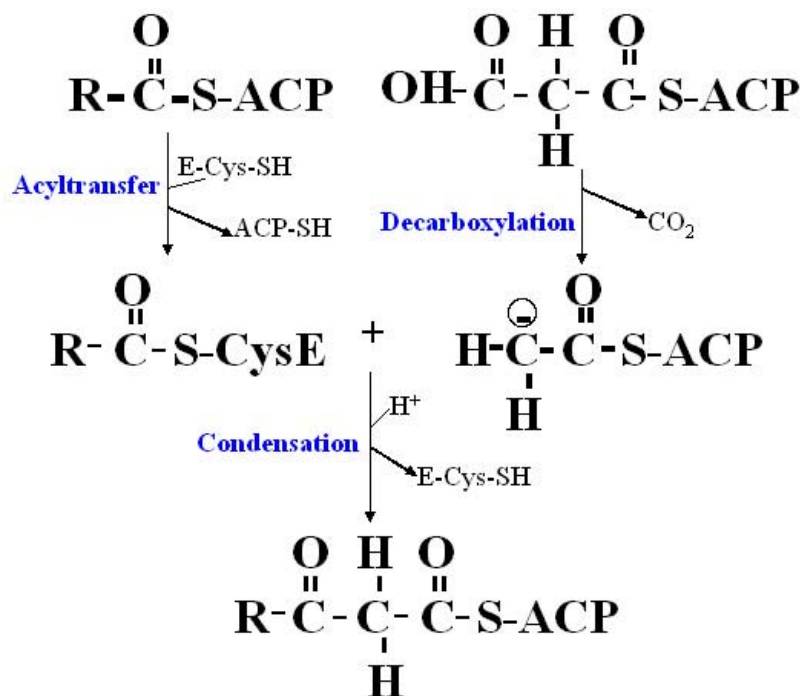


Figure 4. Condensation reaction in fatty acid biosynthesis (modified from Heath *et al.* 2002). **Acyltransfer** - The acyl-ACP is transferred to the active site cysteine of the condensing enzyme, and the reduced ACP is released. For the initiation class of condensing enzyme, the substrate is acetyl-CoA, and CoASH is the by product. **Decarboxylation** - The thioester oxygen group of the malonyl-ACP interacts with the His-His or His-Asn pair of the catalytic triad, decarboxylation occurs, and carbanion is formed at C2. **Condensation** - The condensation reaction occurs, where the carbanion attacks the C2 of the acetyl group attached to Cys, the resulting transition state subsequently breaks down and the product is released from the condensing enzyme.

Microsomal elongase complex for VLCFA biosynthesis

VLCFAs are synthesized through elongation of the C16 or C18 FAs by an endoplasmic reticulum (ER) membrane-bound enzyme system, called the elongase. The enzymatic reactions of FA elongation were originally determined in the microsomal fraction of rat liver [32]. Genes encoding the elongase enzymes were originally identified in the baker's yeast *Saccharomyces cerevisiae*, and later in other organisms. Genes encoding proteins required for condensation and the two reductions have been identified, but the gene encoding the dehydratase component remains unknown. Consistent with early biochemical characterization of FA elongation that suggested the elongase enzymes are organized in a complex [33], the known elongase proteins were reported to co-immunoprecipitate and colocalize with one another [34, 35]. The proteins of the elongase complex that mediates VLCFA synthesis (*green box* in Fig. 10) are described below:

A. Enzymes required for the condensation step, the Elops -

Three genes, *ELO1*, *ELO2*, and *ELO3*, required for FA elongation, were identified in *Saccharomyces cerevisiae*. The strategy for identifying genes required for fatty acid elongation was predicted on the assumption that yeast mutants defective in *de novo* FA synthesis (*e.g.*, *fas2Δ* mutants) would be incapable of growing on medium supplemented with myristate (C₁₄) if they were also defective in fatty acid elongation. Thus, *fas2Δ* cells, which are able to grow in medium supplemented with myristate, were mutagenized and plated on medium containing a mixture of C₁₄, C₁₆, and C₁₈ FAs. The mutagenized colonies were screened by replica plating to identify those that could not grow on medium containing only C₁₄ and the *ELO1* gene was identified as responsible for C₁₄ to C₁₆ elongation [36]. Subsequently, two additional genes (*ELO2* and *ELO3*) with high

identity to *ELO1* were found in the *S. cerevisiae* genome [37]. These were previously known to induce pleiotropic phenotypes and appeared to play a key role in controlling membrane and cytoskeletal functions.

ELO2 was initially cloned by complementation of *GNS1* mutants, which conferred resistance to echinocandins and had defects in β -glucan synthase activities [38]. *ELO2* was also reported as *FEN1*, a mutant allele conferring resistance to various ergosterol biosynthesis inhibitors [39]. *ELO3* was first described under the name *APAI*; the *apa1* mutants were isolated on the basis of their reduced levels of plasma membrane ATPase synthesis [40]. *ELO3* was also isolated as *SUR4*, a gene that when mutated suppressed the reduced viability of the starvation mutant phenotype displayed by the *rvs161* mutant [41]. *ELO3* was also found to complement the *sre1* mutant, which was resistant to an immunosuppressant agent SR 31747 that arrests cell proliferation in *S. cerevisiae* [42]. Once the *ELO1* gene was identified as a component of VLCFA synthesis, the roles of the *ELO2/FEN1* and *ELO3/APAI/SUR4* in FA elongation were investigated.

The lethal phenotype of an *elo2 Δ elo3 Δ* double mutant suggested that the encoded proteins had related and/or overlapping functions [37, 42, 43]. Elo1p, Elo2p and Elo3p showed multiple regions of contiguous identical residues (Fig. 5), and the hydropathy analyses suggested that these proteins contain several membrane-spanning regions. The region with the greatest degree of identity contains 16 conserved residues, a cluster of four consecutive basic residues followed by a conserved histidine rich motif (Fig. 5), present between the predicted transmembrane domains (TMDs) II and III [37]. The HXXHH motif was identified earlier in FA desaturases, ribonucleotide reductase,

hemerithrin, and other iron-containing proteins [33].

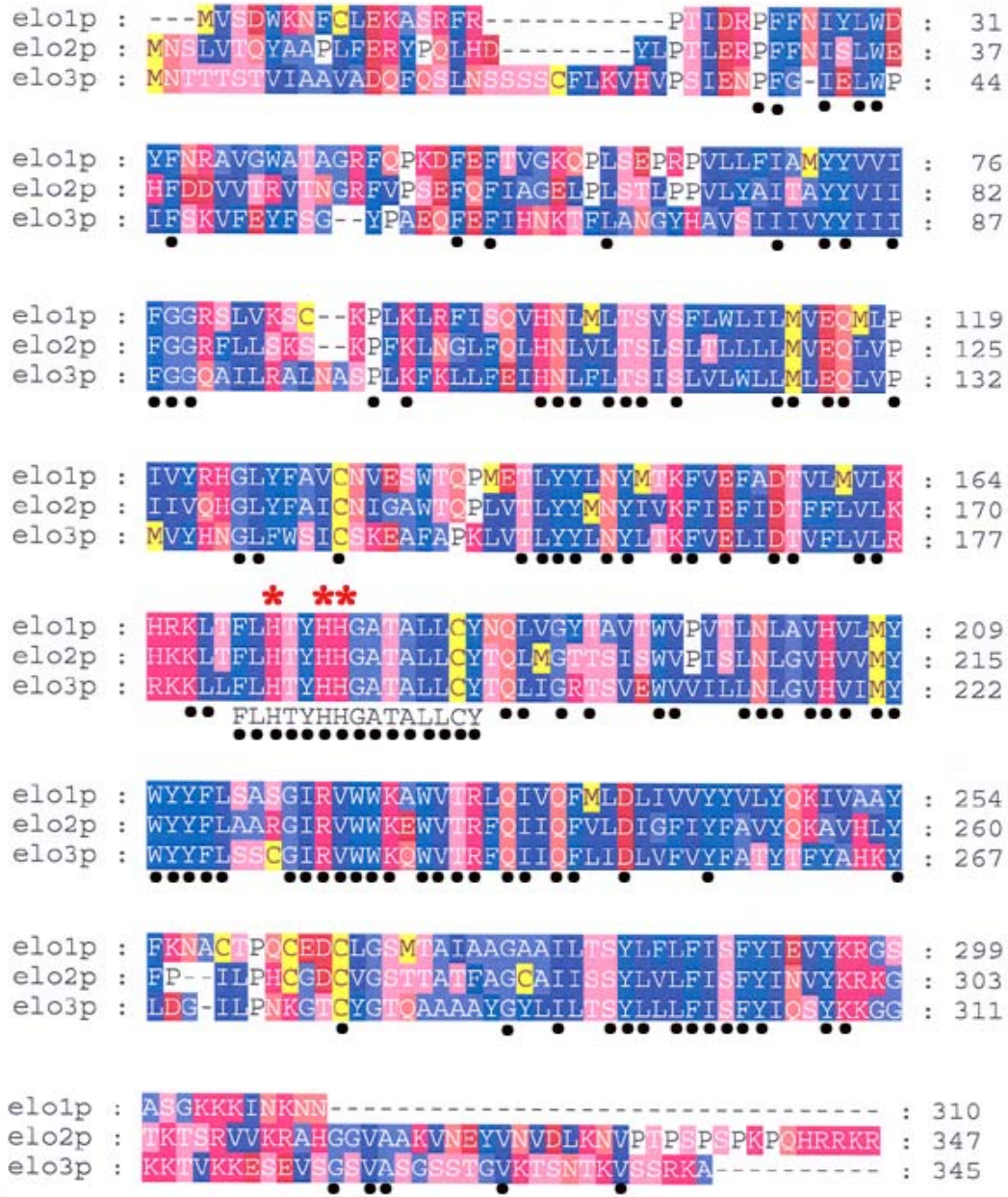


Figure 5. Plot showing protein sequence alignment between the yeast Elops (adapted from Oh *et al.* 1997). The *black dots* indicate the identical residues between the Elops. Residues marked by *red asterisks* indicate the histidine residues of the HXXHH motif common to all three proteins.

The FA content of *elo2Δ* and *elo3Δ* mutants was analyzed by gas

chromatography/mass spectroscopy (GC/MS) and revealed an accumulation of intermediate length FA precursors, suggesting defects in FA elongation. The C₂₆ FA species was present in *elo2Δ* cells but was absent in *elo3Δ* mutant, indicating that Elo3p was required for C₂₄ to C₂₆ elongation. Elo2p showed the highest catalytic specificity for C₂₀ acyl-CoA, whereas Elo3p catalyzed elongation of a broader range of substrates [37].

***ELO* homologs identified in several organisms**

Cig30 (cold-inducible glycoprotein of 30 kDa), also known as *Elovl3*, was the first Elop homolog identified in mammals [44]. It was associated with synthesis of saturated VLCFAs and triglyceride in brown adipose tissue of mice [45]. Based on homology to *Cig30*, two other mouse genes, *Ssc1* and *Ssc2* were identified [46] and later reclassified as members of the *ELOVL* gene family. Complementation studies in yeast indicated that *Ssc1* (*Elovl1*) was functionally equivalent to yeast *ELO3*, and *Cig30* (*Elovl3*) to *ELO2*. High expression of *Ssc2* (*Elovl2*) in testes, a rich source of long-chain polyunsaturated fatty acids (PUFAs), suggested the possibility of its involvement in long-chain PUFA metabolism [46]. PUFAs are FAs of 18 carbons or more in length, containing two or more double bonds that are introduced by specific FA desaturases. The PUFAs can be classified into two groups, *n*-6 or *n*-3, depending on the position (*n*) of the double bond nearest the methyl end of the FA [47, 48]. Heterologous expression of *Elovl2* in *S. cerevisiae* and mouse L cells demonstrated that the encoded protein was involved in the elongation of both C₂₀ and C₂₂ PUFA [49]. Several elongase genes were subsequently identified in human; ELG2 (ELOVL1) [50], ELOVL2 [49], ELOVL3, ELOVL4 [51] and ELG3 (ELOVL5) [52]. ELOVL4 encodes a protein that is 35%

identical to the yeast *ELOs*, and was found by linkage analysis to be associated with two forms of autosomal dominant macular dystrophy [51]. Two elongase genes were identified in rat, rELO1 a homolog of ELOVL5 that elongates C₁₆-C₂₀ mono- and polyunsaturated FA, and rELO2, an ELOVL3 homolog that elongates C₁₆-C₁₈ [53].

Several FA elongase genes were identified from lower eukaryotes, such as MAELO (40% identity with yeast Elo2p) that elongates C₁₆-C₁₈ saturated and monounsaturated FAs in the filamentous fungus *Mortierella alpine* [54, 55]. Using heterologous expression in *S. cerevisiae*, and by addition of different VLCFAs in the growth media, CELO1 from the free-living nematode, *Caenorhabditis elegans* [Cig30 homolog [44]] was reported to specifically elongate C₁₈-PUFAs [54, 56]. Similarly, heterologous expression of an elongase-like sequence, pavELO from a marine microalgae *Pavlova sp.* catalyzed conversion of both n-6 and n-3 C₂₀-PUFAs [57], PSE1 from the moss *Physcomitrella patens* elongated γ -linolenic acid (C₁₈:3n-6) and stearidonic acid (C₁₈:4n-3) [58], IgASE1 from a marine microalga (*Isochrysis galbana*) elongated linoleic acid (C₁₈:2n-6) and α -linolenic acid (C₁₈:3n-3). IgASE1 was the first elongase reported to contain a glutamine instead of the first histidine in the histidine motif [59]. Heterologous expression of SalElo, isolated from Atlantic salmon (*Salmo salar*), in yeast showed broad substrate specificity for PUFAs with the biosynthesis of docosahexaenoic acid (22:6n-3) [60]. Thus, the Elops of various organisms possesses different substrate specificities and generates different chain length FAs.

Elops elongating short chain FAs

Trypanosoma brucei, a eukaryotic human parasite that causes sleeping sickness, encounters diverse environments (gut of tsetse fly and the human bloodstream) during its

life cycle. To evade the immune system of the mammalian host they switch surface coats, composed of 10^7 variant surface glycoprotein (VSG) molecules which are tethered to the plasma membrane by a myristate-containing glycosylphosphatidylinositol (GPI) anchor. Thus, in addition to the usual FAs for making cell membranes they require large amounts of myristate (C_{14}), [61]. Surprisingly, *ELO*-like genes were identified as responsible for synthesizing all the FAs, including the short chain FAs in this parasite. These studies were the first to show that *T. brucei* ELO1 catalyzes conversion of C_4 to C_{10} , *T. brucei* ELO2 elongates C_{10} to C_{14} , and *T. brucei* ELO3 extends C_{14} to C_{18} . Stearate (C_{18}) was required in the tsetse vector form, whereas the bloodstream form used myristate (C_{14}), which was achieved by downregulating ELO3 in blood, thus favoring myristate accumulation [62].

Fatty acid elongase-3 ketoacyl CoA synthases (FAE-3KCSs)

VLCFAs in plants are saturated or monounsaturated, but not polyunsaturated, and are constituents of waxes [63], seed storage lipids [64] and sphingolipids. The membrane-bound β -ketoacyl CoA synthases (KCSs) catalyze the condensation step of VLCFA synthesis. The founding member (FAE1) of this class of enzymes was identified in *Arabidopsis thaliana* [65], and showed seed specific expression [66]. Mutations in FAE1 resulted in reduced levels of seed VLCFAs [67, 68], and a deficiency in acyl chain elongation activities toward C_{18} and C_{20} FAs [69]. FAE1 homologs were identified in several plants, *Brassica oleracea* [70], *Brassica campestris* [71], *Brassica oleacea* [71], *Simmondsia chinensis* [72], *Lesquerella fendleri* [73] and *Limnanthes alba* [74] and also in the green algae, *Dunaliella salina* [75]. In the *Arabidopsis* genome, 20 predicted *FAE1* homologs were found (Fig. 6) [76], and an additional highly homologous gene

(At3g10280) was detected that lacks the conserved active site cysteine and appears to be derived from the duplication of another *KCS* gene (*At2g46720*; *HIC*) [77].

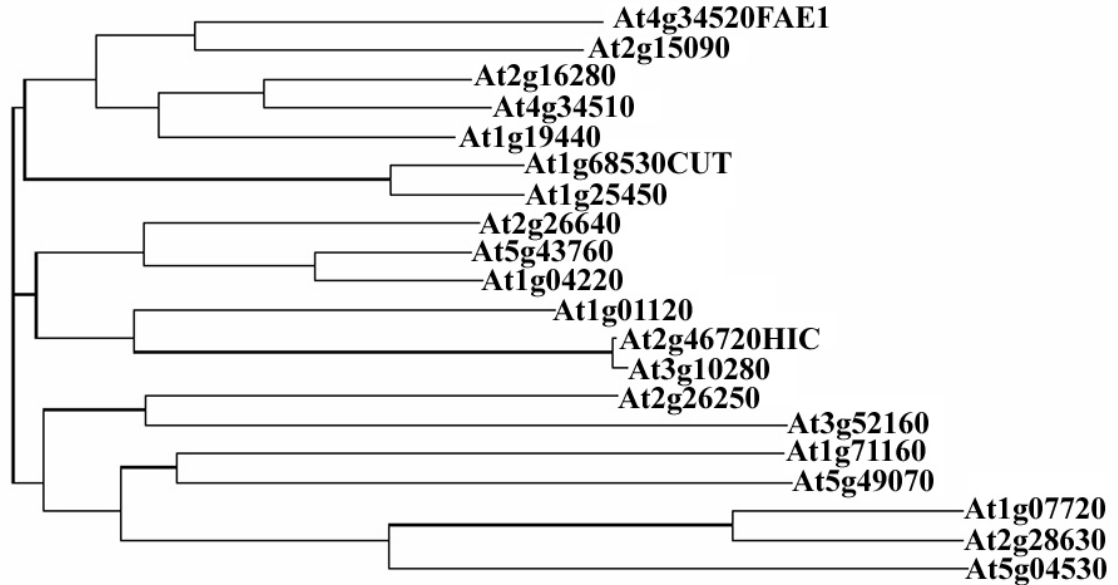


Figure 6. Phylogenetic tree for known and putative *A. thaliana* FAE-KCSs. Putative KCSs are named by the loci designation in the Arabidopsis genome.

Reduced expression of the FAE1 homolog, *CUT1* (At1g68530) in transgenic *Arabidopsis* plants resulted in waxless stems and siliques, conditional male sterility, and the presence of high C₂₄ FA containing wax, which suggested its requirement for elongating C₂₄ FAs [78]. Another FAE1 homolog, *FIDDLEHEAD* (At2g26250), was reported to be required for epidermal cell fusion and epidermal interactions with pollen during vegetative development. The *fdh* mutant showed an organ fusion phenotype and biochemical analyses showed changes in lipid composition of the cell wall, highlighting the role of lipids in epidermal cell adhesion [79-82]. Characterization of waxless (*eciferum*) mutants led to the identification of *CER6* (identical to *CUT1*). These studies also demonstrated that this gene is involved in lipid biosynthesis and is critical for

Arabidopsis pollination. A major reduction of CER6 activity in *Arabidopsis* abolished stem wax accumulation and caused male sterility [83, 84]. Complete loss of *KCSI* (*At1g01120*) expression, which has high sequence identity to *FAE1*, resulted in an 80% reduction in C₂₆ to C₃₀ levels of wax alcohols and aldehydes, but did not show complete loss of any individual wax component or a significant decrease in the total wax load, suggesting redundancy in the KCS activities involved in wax synthesis [85]. *Hic* (*HIC* is similar to *KCSI*) mutant plants showed an increase in stomatal density in response to decreases in carbon dioxide levels, demonstrating a novel role for KCSs in the high carbon dioxide signaling pathway.

Several FAE-KCSs (*FAE1*, *KCSI*, *KCS2*, *At5g43760*, *At1g04220* and *At1g25450*) have been expressed in yeast and GC/MS analysis of the FAs prepared from the yeast showed that these enzymes could elongate endogenous yeast FAs as well as externally supplied unsaturated FAs [86]. Recently, several putative FAE-KCSs(His)₆ fusion proteins were expressed in yeast and purified by metal-affinity chromatography from solubilized yeast microsomes. Elongase assays demonstrated that *At2g26640* elongates both saturated and mono-unsaturated C₁₆ to C₂₀ acyl chains, *KCS1* can utilize C₁₆, C_{16:1}, C₁₈, and C₂₀, and *At4g34510* specifically elongated saturated acyl-CoAs up to C₂₂ [87]. Several structure/function studies of *FAE1* identified an active site cysteine (Fig. 7) that was predicted by alignment of *FAE1* with resveratrol synthase [72, 88], a condensing enzyme involved in the biosynthesis of stilbene- type phytoalexins [89]. The two other residues (His and Asn) of the catalytic triad (Fig. 7) that appear to be important in the decarboxylation of the malonyl substrate [31, 90] were predicted from the alignment of *FAE1* with 3-ketoacyl-ACP synthase [KASIII involved in the condensation of malonyl-

ACP and acetyl-CoA [91, 92], and a chalcone synthase, a plant-specific enzyme involved in polyketide synthesis [90, 93]. *In vitro* and *in vivo* assays of FAE1-KCS from *B. napus* and *Arabidopsis* expressed in yeast indicated that *B. napus* FAE1-KCS enzyme favors longer chain acyl substrates than does the *A. thaliana* enzyme. The differences in substrate specificity of the FAE-KCSs provide an explanation for the variation in the seed oil content of *A. thaliana* (high in 20:1) [64] and *B. napus* (high in 22:1) [94]. The chimeric FAE1-KCS protein containing *A. thaliana* sequence from the N-terminus to residue 114 and *B. napus* sequence from 115 to the C-terminus showed substrate specificity similar to that of *A. thaliana* FAE1-KCS, suggesting that the N-terminal region is involved in substrate specificity [95].

```

CUT1 : TVNIFLSFLLIPIMAIVAVETIMGPPEIILNVN--SLQFDLVQVIC : 69
KCS1 : VTITLSEFLIILPLTGTIVLQITGTFDTFSELISNOAVQLDTATRI : 94
FAE1 : TMAIRFKLCFLPLMVAIVEASISTQDLQNFYLY--LQNNHTSLTM : 59

CUT1 : SSFIVIFISTVYFMSKERTIYLVDYSCYKPEVTCRVPFATFMEHSRI : 116
KCS1 : CLVEISEVLTILYVANRSKPVYLVDYSCYKEEDERKISVDSFLIMTEE : 141
FAE1 : FFLYLALGSTILYLMTRPKPVYLVDYSCYLPESSELKASTORIMQHVRI : 106

CUT1 : ILKD-----KPKSVETCMRILERSGLGETICLPFAIHYIPIPIPIID : 157
KCS1 : NGSF-----TIDTVQFCQRTISMRGLGETIYLPRIITSTPEKINMS : 182
FAE1 : VREAGAWKQESDYLMDFCEKILERSGLGETYVPEGLQTLPLQONLA : 153

CUT1 : ARSEFQMVIFEAMDILEKKTGLKPKVDILIVNCSLFSPTPSLSAM : 204
KCS1 : EARNEAEAVMFGALDSLFEKTGIRPAEVGILIVNCSLFNPTPSLSAM : 229
FAE1 : VSRKLEEVITIGAVLNLFRTIGLSESLIGILVNVSSIFNPFPSSLSI : 200

CUT1 : VINKYKLRNLIKSENLSCMGCSAGLISVDLARDLLQVHENSNAIIVS : 251
KCS1 : IVNHYKMRDIKSYNLSCMGCSAGLISIDLANLLKANTNSYAVVVS : 276
FAE1 : LVNFKLRNLIKSNLSCMGCSAGVIAIDAKSLLOVHNTIYALVVS : 247
C
■

CUT1 : TEITITENYYQGNERAMLIENCLFRMGALATHMSNRRSDRWRAKYKLS : 298
KCS1 : TENITLNWYEGNDRSMLIENCLFRMGGLAILLSNRRQDRKSKYSLV : 323
FAE1 : TENITQNIYMGNNKSMIVTNCIFRGGAILLSNRSIDRKRAKYELV : 294

CUT1 : HIVRIHRGADDKSFYCVYECELKEGHVGINLSHDLMAIAGEALKANI : 345
KCS1 : NVVRIHKGSDDRNINCVYKEDERGTIGVSLARELMSVAGDALKTNI : 370
FAE1 : HIVRVHTGADDRSYECATCEFEEDGIVGVSLSNIPMVAARTIKINT : 341

CUT1 : TITGPIVLPAEQLEFTTSIIGRKIFNPKWKEYIPDFKLAFEHFCIH : 392
KCS1 : TITGPIVLPLSEQLEFTISLVKRMKFKLVKEYIPDFKLAFEHFCIH : 417
FAE1 : ATITGPIVLPISEKFEFVRFVKKKFLNPKLKEYIPDFKLAFEHFCIH : 388
H
■

CUT1 : AGGRAVIDELQKNLQISGEHVEASRMTLHRFGNTSSSSIWYEISYIE : 439
KCS1 : AGGRAVIDEVQKNLQIKDWEHVESRMTLHRFGNTSSSSIWYEMAYTE : 464
FAE1 : ACCRALIDEMKNLEETPLDVLASRMTLHRFGNTSSSSIWYELAYTE : 435
N
■

CUT1 : SKGRVRRGDRVWQIAFGSGFKNSAVWKCNRITIKTPKDG--PWSDCI : 484
KCS1 : AKGRVKAGDRILWQIAFGSGFKNSAVWKALREVSTDEMTGNWAGSI : 511
FAE1 : AKGRVTKGDRINWQIAFGSGFKNSSVWVALRNVKPSINN--PWEQCL : 480

CUT1 : IRYPVFIPVVVL : 497
KCS1 : IQYPVKVYQ---- : 520
FAE1 : HKYPVEIDIDLKE : 493

```

Figure 7. Primary sequence alignment for CUT1, KCS1 and FAE1. Sequences were aligned by the ClustalW algorithm and identical residues are indicated by shaded boxes. Conserved residues in the catalytic triad (Cys, His, and Asn) are indicated by *red squares* below the aligned sequences.

Hydropathy analysis of the Arabidopsis KCS1 and FAE1 proteins predicted that the FAE-KCSs have two membrane-spanning domains close to their N-termini [90]. Heterologous expression of FAE1 with thrombin sites inserted after the putative membrane spanning domains, followed by treatment of microsomes with thrombin, suggested that the C-terminal domain is also membrane associated. However, the thrombin cleaved fragment was solubilized with 2M NaCl, suggesting that the interaction of the C-terminus of FAE1 KCS with the membrane is mainly ionic [90]. These studies led to a topology model for FAE1 that has two N-terminal TMDs followed by a globular portion (Fig. 8) [90].

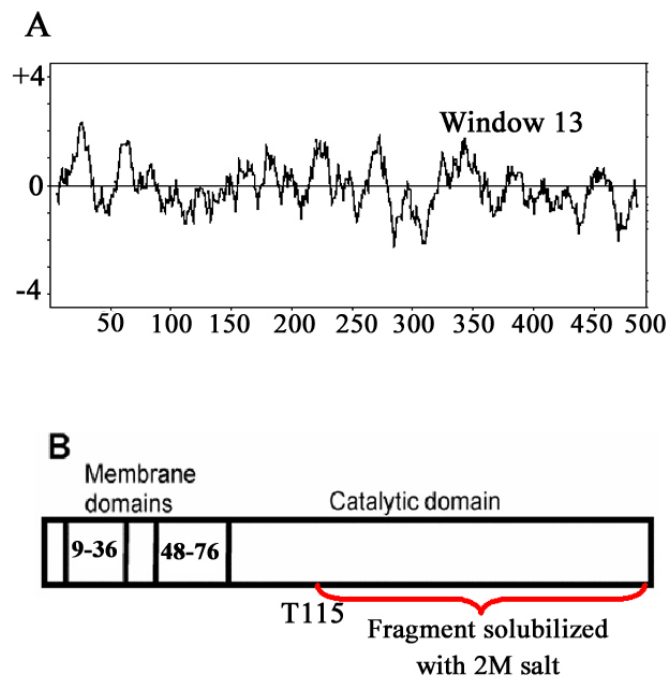


Figure 8. Hydropathy analysis of FAE1 KCS (modified from Ghanevati and Jaworski 2002). (A) Kyte-Doolittle Hydropathy plot of FAE1 indicating the presence of several hydrophobic regions. Hydrophobic regions are indicated above *zero*, and hydrophilic regions are below *zero*. (B) Schematic representation of the putative transmembrane domains of FAE1 amino-acid sequence as predicted by TMAP analysis. Numbers shown inside the *boxes* correspond to the residues of each TMD in FAE1. The thrombin

cleavage site at residue 115 is marked as *T115*. The fragment which is associated with the membrane by ionic interaction is shown in *red*.

F AE-KCS involved in PUFA elongation

Although FAE-KCSs were considered to be unique to plants and some photosynthetic algae, a FAE-KCS condensing enzyme, PmFAE, was recently identified in a marine parasitic protozoon, *Perkinus marinus* and was shown to be involved in arachidonic acid biosynthesis. This is the first example of a member of the FAE-KCS family that is involved in the biosynthesis of PUFAs. Similar to some higher plant KCSs, PmFAE also shows sensitivity to the herbicide flufenacet [96]. Using the PmFAE ORF to search genomic databases, FAE1-like sequences were identified in human pathogens such as the parasitic protozoon *Entamoeba histolytica*, in photosynthetic algae such as *Phaeodactylum tricornutum*, and in the soil-living amoeba *Dictyostelium discoideum* but orthologs are absent in metazoan, yeast and fungal genomes [96].

Difference between Elops and FAE-KCSs

Although the Elops are required for the condensation step of fatty acid elongation, they lack significant homology at the amino acid sequence level with the FAE-KCSs. In addition, the Elops are very hydrophobic with several predicted TMDs spread along their lengths. In contrast, the FAE-KCSs are predicted to have two TMDs at their N-termini (Fig. 8), followed by a cytosolic catalytic domain with high homology to other 3-keto synthases, including the condensing enzymes involved in the synthesis of the polyketides. There are no motifs in the Elops that resemble the catalytic triad, which is conserved in all known condensing enzymes including the FAE-KCSs (Fig. 7). These differences

have led to speculation that the Elop proteins might be auxiliary subunits that act in conjunction with an unidentified catalytic subunit of the elongase system rather than the condensing enzymes per se. On the other hand, there are no homologs of the FAE-KCSs or other 3-keto-CoA synthases in yeast, and it is therefore clear that the condensing enzyme(s) involved in VLCFA synthesis in yeast must be novel enzymes.

Condensation is the rate-limiting step of VLCFA synthesis

Elongase assays with microsomes prepared from rats maintained on a fat-free diet [97] and from brains of quaking and jimpy [severe myelin deficient [98] mouse mutants [99] showed a correlation between a reduction in overall chain elongation rate and a reduction in condensation activity, but no changes in the activities of the other three enzymes of the elongation system [77]. Overexpression of FAE1 (a condensing enzyme) in *Arabidopsis* seeds resulted in higher levels of VLCFA accumulation [100]. These biochemical studies provide indirect evidence suggesting condensation is the rate-limiting step of fatty acid elongation.

B. Enzymes required for the 3-ketoacyl reduction - 3-ketoacyl reductases –

To identify other enzymes of the FA elongation pathway, yeast knockout mutants were screened for loss-of-function of heterologous Pea1p- (PUFA elongase enzyme of *C. elegans*) [101] mediated elongase activity [102]. A previously uncharacterized gene, *YBR159w*, encoding a 347 amino acid protein was identified, which showed limited homology to human estradiol-17 β -hydroxysteroid dehydrogenase (17 β -HSD) (32% similarity), a member of the short-chain alcohol dehydrogenase (SDR) superfamily. Ybr159p orthologs were identified in fission yeast (43% similarity), *Drosophila*

melanogaster (34% similarity), *C.elegans* (30% similarity), and *Arabidopsis* (30% similarity); all these protein sequences contain a diagnostic NADPH binding motif [103] and a Y-X₃-K motif identified as essential for catalysis in 17 β -HSD and in other SDRs (discussed above) [104], as well as several predicted membrane-spanning domains. Both Ybr159p and the *Arabidopsis* ortholog [homolog to maize Glossy8 gene [105]] contain the putative canonical dilysine ER retention motifs at their C-termini. Moreover, the *ybr159* Δ mutant exhibited several phenotypic traits previously observed in mutants deficient in VLCFA synthesis, including the *elo2* Δ , *elo3* Δ and *tsc13-1* mutants. These phenotypes are described next, and the other mutants are discussed further below. The *ybr159* Δ mutants accumulated high levels of long chain bases (LCBs), primarily phytosphingosine (PHS), dihydrosphinganine (DHS) and small amounts of 3-ketosphinganine (3-KS), which are intermediates in the LCB biosynthetic pathway (*yellow box* in Fig. 10). This phenotype possibly reflects reduced partitioning of the LCBs into ceramides and sphingolipids (SPLs) due to the reduced VLCFA synthesis by the *ybr159* Δ mutants [34, 35, 37]. However, it is worth noting that the net levels of ceramides and sphingolipids are not reduced in the mutants, which raises the possibility that either serine palmitoyltransferase (SPT), the rate-limiting enzyme of sphingolipid synthesis is upregulated in the elongase mutants, or the pathways for LCB degradation (including the LCB-kinases and lyase) are downregulated. Regardless of the mechanism, the accumulation of high free LCB levels is a consistent phenotype of the elongase mutants. Compared to wild-type yeast cells that contain α -OH-C₂₆ ceramide, the mutants contained ceramides which migrated with increased hydrophilicity on TLC plates, indicating shorter chain FA-containing ceramide species [34, 35, 37]. This was

confirmed by hydrolyzing the purified ceramide species from the TLC plates and analyzing the methyl esters of the liberated FAs by GC/MS [35, 37]. These short-chain ceramides were confirmed to be hydroxylated by demonstrating that disruption of the *SCS7* gene encoding the enzyme required for the α -hydroxylation (*pink box* in Fig. 10) of the VLCFA [106, 107] reduced the hydrophilicity of the short-chain ceramides relative to that of the short-chain ceramides in the *SCS7⁺elo Δ* yeast strain [35]. GC/MS analysis of FAs from wild-type yeast showed that 26:0 and α -OH 26:0 are the most abundant species, with minor amounts of 22- and 24-carbon-saturated, monounsaturated, and α -OH FAs [108, 109]. In contrast, the *ybr159 Δ* mutants showed greatly reduced levels of 26:0 and accumulation of α -OH-C16:0 FAs and 3-OH FAs of different chain lengths (C₁₆, C₁₈, C₂₀) [34, 35, 37]. In addition to the increased LCB levels and altered FA composition, the *ybr159 Δ* mutant also displayed genetic interactions that were consistent with the conclusion that Ybr159p participates in VLCFA synthesis. For example, similar to the *elo2 Δ elo3 Δ* double mutant, the *elo2 Δ ybr159 Δ* double mutant displayed a synthetic lethal phenotype [34]. Furthermore, deletion of the *YBR159w* gene suppressed the Ca²⁺ sensitivity of the *csg2 Δ* mutant. *CSG2* is required for mannosylation of inositolphosphorylceramide (IPC) to form MIPC (*blue box* in Fig. 10), and previous studies showed that deletion of *CSG2* lead to accumulation of IPC, resulting in calcium sensitivity [110]. Therefore, mutations that reduce FA elongation reduce the level of IPC and thereby suppress the Ca²⁺ sensitivity conferred by *csg2 Δ* .

The FA elongation deficient phenotypes and physical interactions with other elongase mutants, combined with the homology of Ybr159p to members of the oxidoreductase family and the results of the *in vitro* elongase assays with microsomes

prepared from a *ybr159Δ* mutant that revealed a defect in the 3-ketoreductase activity [34], suggesting that *YBR159w* encodes the 3-ketoreductase enzyme of the elongase system. Consistent with this, Ybr159p was detected as an ER-membrane associated protein that co- immunoprecipitated and colocalized with Elo3p and Tsc13p [34]. However, FA elongation is an essential process in yeast, and though the *ybr159Δ* mutant grew slowly it was viable, indicating the presence of another protein with 3-ketoreductase activity that acted in FA elongation. Several ORFs with sequence similarity to *YBR159w* are present in the yeast genome, including Ymr226p (insect short-chain alcohol dehydrogenase homolog), Ayr1p (1-acyl-dihydroxyacetone-phosphate reductase homolog [111], and Yir036p (7β -hydroxysteroid dehydrogenase homolog). Although, individual deletion of these ORFs did not alter the activity of the heterologous PEA1 PUFA elongase activity [101], the *ayr1Δybr159Δ* double mutant showed synthetic lethality, suggesting that Ayr1p possesses the residual 3-ketoreductase activity involved in FA elongation [34]. It is of course possible that the synthetic lethality of the *ayr1Δybr159Δ* double mutant results from another mechanism. For example, Ayr1p was initially identified as a dihydroxyacetone reductase involved in phosphatidic acid biosynthesis [111]. Therefore, altered glycerophospholipid metabolism, along with reduced VLCFA synthesis might result in the synthetic lethal phenotype of the double mutant. However, the *ayr1Δ* mutation is not synthetically lethal in combination with other elongase mutants (*elo2Δ* and *elo3Δ*) and thus it is likely that Ayr1p and Ybr159p are functionally redundant, and that provide the reductase activity that results in the residual VLCFA synthesis in the *ybr159Δ* mutant [34].

C. Enzymes required for the enoyl-CoA reduction - Trans 2,3-enoyl CoA reductases

A screen for mutants with a single mutation that suppressed both the Ca²⁺ sensitivity due to the *csg2Δ* mutation and caused temperature sensitivity, identified twenty-one temperature-sensitive *csg2Δ* suppressor (TSC) complementation groups [112]. Three independent mutations were identified in the TSC13 gene (YDL015c) [35], which proved to be essential [113]. The *tsc13-1* mutant allele (conserved Q81 substituted with lysine) showed similar phenotype to those seen in other elongase mutants, such as high free LCB levels, appearance of short chain FA-containing ceramides, reduced levels of C26 FA, and high levels of hydroxy FAs of different chain length (C16, C18, and C20) [35]. All these phenotype suggested that Tsc13p played a role in FA elongation.

The elongase activities using microsomes prepared from wild-type and *tsc13-1* mutant yeast revealed similar elongase activities in the absence of pyridine nucleotide, suggesting that the condensation activity is not affected in the *tsc13-1* mutant. However, the total elongation activity was 50% reduced in the *tsc13-1* mutant, suggesting that Tsc13p catalyzes a step in elongation subsequent to the condensation step. Moreover, elongase assays with microsomes prepared from wild-type cells showed no accumulation of elongase reaction intermediates. However, the *tsc13-1* mutant microsomes accumulated trans-2,3-stearoyl and 3-hydroxystearoyl intermediates [35]. This led to the hypothesis that the defect in Tsc13p causes reduced activity of the *trans*-2,3-enoyl-CoA reductase leading to accumulation of the *trans*-2,3-stearoyl-CoA. Due to the reversible nature of the dehydratase step [114], accumulation of *trans*-2,3-stearoyl-CoA was expected to result in the accumulation of 3-hydroxystearoyl-CoA [35].

The *TSC13* gene encodes a protein of 310 amino acids with significant homology

(35% identity, 50% similarity) to evolutionarily conserved SC2 proteins. The *SC2* gene, was identified in a screen for cDNAs that encode rat synaptic glycoproteins [115]. Similar to SC2 protein, Tsc13p showed homology in the C-terminal 150 amino acids (29% identical, 45% similar) to steroid-5 α reductase, which catalyzes the reduction of testosterone to dihydrotestosterone. The homology to steroid-5 α reductase, which reduces a double bond that is α,β to a carbonyl group, led to the hypothesis that Tsc13p catalyzes the last step in FA elongation [35].

Tsc13p was found to be an ER-membrane-associated protein that physically and genetically interacts with other elongase components and accumulates at the nucleus-vacuole junctions (NVJ). The intensity of Tsc13p accumulation at the NVJ junctions were enriched during growth on complete medium and as cells entered stationary phase [35]. Studies showed that NVJ were created in the outer nuclear membrane by specific interactions of the vacuolar membrane protein, Vac8p with the nuclear membrane protein, Nvj1p [116]. Recent studies showed that through physical association with Nvj1p, Tsc13p is relocalized from the peripheral ER to NVJ [117].

Several orthologs of *TSC13* were identified from mammals, fungi (*S. pombe*), and *Arabidopsis* [35]. Heterologous expression of *At3g55360* (designated hereafter *AtTSC13* or *ECR*) complemented the temperature-sensitive phenotype of a yeast *tsc13-1elo3 Δ* double mutant, and AtTSC13p was shown to physically interact with the yeast Elo2p and Elo3p proteins [118]. The *ecr* mutant plant showed defects in shoot growth and morphogenesis, an ~60% reduction in total stem cuticular wax, and ~30% reduction of VLCFA content of seed TAG, which indicates that mutations in *ECR* gene affect VLCFA

production. Biochemical and cellular analyses suggested that changes in sphingolipids most likely cause the morphological defects observed in the *ecr* mutants [119].

Towards understanding the structure of the organization of the Elongase Complex

While the biochemical steps of the pathway for FA elongation are known, owing to the difficulties associated with the purification of membrane bound proteins, structural insight of the elongase components are lacking. Since the elongase proteins localize to the ER, behave as integral membrane proteins, and are predicted to have several membrane spanning domains, an important step toward elucidating the organization of the elongase complex is to determine the membrane topology of the elongase proteins. Several tools have been reported to help in mapping the topology of membrane bound proteins. Few well established approaches that will be employed in this study to study the topology of the enoyl-CoA reductases and the 3-ketoreductase of the elongase complex is discussed below:

1. Hydropathy analyses

As a first step toward determining the topology of the elongase proteins, several different programs (HMMTOP, TMHMM, MEMSAT, TOPPRED, TMPRED, and SOSUI) for predicting transmembrane (TM) segments will be compared. Although such hydropathy analyses have proven to be only 60-70% accurate in predicting topological organization [120], they provide a useful starting point for the design of models that can be experimentally tested. The predicted topological models will be used to design the experiments for assigning predicted extramembranous segments as either cytosolic or luminal for these proteins.

2. Epitope Protease Protection

To determine the location of the termini of the proteins epitope tags will be inserted at the both the termini. Yeast strains expressing the dual epitope tagged protein will be used as a source of intact right-side-out membrane vesicles. The integrity of the microsomal preparations will be determined by examining whether the ER luminal Kar2p is accessible to degradation by proteinase K in the absence or presence of detergent. The microsomal membrane fraction will be collected by gentle lysis of the yeast spheroplast expressing the tagged elongase protein. The right-side-out vesicles will be incubated with proteinase K, with and without detergent. The sensitivity of the epitope tags to proteinase K in the presence or absence of detergent will be monitored by immunoblotting with the respective antibodies against the epitope tags. Susceptibility of the epitope tag to proteinase K in the absence of detergent will indicate its cytosolic location, whereas, the ability to detect a protected fragment will indicate a luminal location. This approach has been used to map the topology of Ste14p, an ER membrane protein [121].

3. Glycosylation Scanning.

A well established approach to map the topology of proteins present in the endoplasmic reticulum takes advantage of the lumen specific glycosylation machinery. The oligosacharyl transferase catalyzes the addition of oligosaccharides to the amino group of asparagine residues within the consensus sequence Asn-X-Ser/Thr (NXS/T) in the ER lumen. As addition of the oligosaccharide chain to a single site results in an increase in the apparent molecular mass on SDS-PAGE by about 2.5 kDa, whether the

protein is glycosylated can be monitored by shifted electrophoretic mobility upon treatment with Endoglycosidase H (Endo H), which cleaves the oligosaccharyl chain. The 3-ketoreductase and the enoyl-reductase of the elongase complex possess two potential intrinsic glycosylation sites.

For mapping the topology of these proteins in details a glycosylation reporter cassette (GC) will be inserted. The GC cassette consists of a 53-amino acid domain comprising residues 80-133 of invertase (Suc2p) that contains three NXS/T sites that are glycosylated in the mature Suc2p protein. Importantly, the first and last NXS/T glycosylation acceptor sites are located far enough from the ends of the cassette to insure that if the domain is inserted in a luminal loop of the fusion protein the acceptor sites will be far enough away from the membrane to be efficiently recognized by the glycosylation machinery [122]. The sites of insertion of the tags will be chosen based on the ability to distinguish between the different predicted models and also after alignments of the yeast, plant and mammalian orthologs of the proteins less conserved regions will be identified in order to enhance the chances of creating functional fusion proteins. Function of the proteins will be taken as evidence that the insertion of the GC has not altered the topology. Clearly, the insertion of the 53-amino acid Suc2p glycosylation domain might interfere with the function of the protein, and might also alter the topology of the protein. However, this reporter cassette has been used in determining the topology of other membrane proteins, and its insertion into the luminal loops between membrane-spanning domains has not been observed to interfere with the insertion or orientation of adjacent membrane-spanning domains [34, 121-123].

It is worth pointing out that the strategy for introducing the GC will involve first

inserting a restriction site. The restriction site will be inserted between the two codons that will be separated by the GC and then a PCR-generated GC with compatible ends will be ligated into the restriction site. Since the introduction of the restriction site creates two amino acid insertions, the function of these mutants will be evaluated before inserting the GC cassette. The 2-amino acid insertion will also identify domains that are important for protein stability and functional activity.

4. Factor Xa Protease.

The GC scanning analysis will be confirmed by a different strategy that involves inserting the recognition sequence for a site-specific protease (factor Xa protease) at sites across the protein and monitoring whether or not the fXa protease has access to the cleavage site in sealed right-side-out vesicles. This approach has been used to map the topology of several proteins [121, 123-127]. A cassette containing the fXa protease recognition site (IEGRIEGR, in tandem to increase the probability of recognition and cutting) with compatible ends will be ligated to the restriction sites generated along the gene. Yeast strains expressing the protein will be used as a source of intact right-side-out membrane vesicles and the integrity of the microsomal preparations will be determined as described above. The microsomal membrane fraction will be collected by gentle lysis of the yeast spheroplast expressing the tagged elongase protein with fXa site inserted. The right-side-out vesicles will be incubated with and without the fXa protease, with and without detergent. If the protease is unable to cleave the protein without added detergent, the site will be assigned to the lumen or embedded in the membrane, whereas if it cuts with or without detergent, it will be assigned to the cytosol. Cleavage at the introduced fXa site will be monitored by immunoblotting. It is, of course, important to confirm that

the native proteins lacking the fXa recognition site are not cleaved by the protease.

5. Membrane Based Split-ubiquitin Assay

The membrane-based split-ubiquitin method has been used to study protein-protein interactions between membrane bound proteins. The system utilizes complementation between separable domains of ubiquitin, the N-terminal domain (Nub, amino acids 1-34) and the C-terminal domain (Cub, amino acids 35-76), which is followed by a transcription factor (PLV) that if liberated can activate expression of reporter genes (*HIS3*) [128]. Wild-type Nub (Nub I , with I being isoleucine at position 13) spontaneously assembles with Cub-PLV, resulting in proteolytic cleavage at the C-terminus of Cub-PLV by a ubiquitin-specific protease(s) and subsequent release of the PLV transcription factor. However, a mutant of Nub (Nub G) in which the isoleucine at 13 is changed to glycine has reduced affinity for the Cub-PLV domain and reconstitution of the ubiquitin becomes dependent upon the fusion of the Nub and Cub domains to two interacting proteins that bring the two halves of ubiquitin together. As a result, the interaction between two proteins can be monitored by the cleavage and subsequent activation of the reporter genes (Fig. 9). A prerequisite of the split-ubiquitin system is that Nub and Cub domains must be fused to the membrane protein such that they are oriented in the cytosol because the ubiquitin-specific protease(s) is a cytosolic enzyme. A recent study reported the use of this split-ubiquitin approach to study the topological features of the yeast oligosaccharyl transferase subunits [129]. The known elongase components physically associate with each other and exists in a complex [34, 35]. To investigate the orientation of the C-terminus of the elongase proteins, the Nub G or the Cub-PLV domain will be fused to the C-terminus of all five elongase proteins and

transformed into opposite mating type yeast strains. The diploids will be selected and screened for their ability to grow on plates lacking histidine. If the NubG and Cub-PVL-fused elongase proteins are able to interact, the PLV transcription factor will be liberated and the *HIS3* reporter gene can be expressed, allowing the strain to grow in media lacking histidine. These results will provide additional evidence whether the C-terminus of the elongase proteins are located in the cytoplasm.

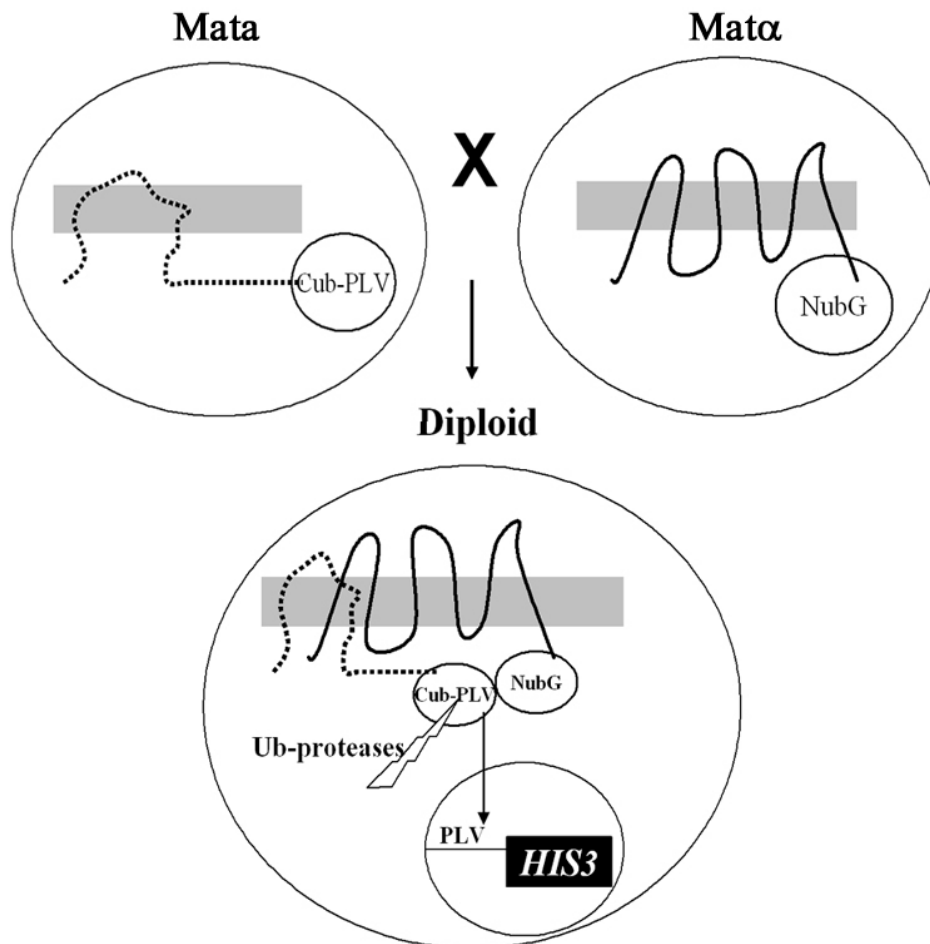


Figure 9 . Schematic representation of the split-ubiquitin assay. The Mata strain expressing the elongase proteins with C-terminally fused Cub-PLV crossed with Mat α strain expressing elongase protein with C-terminally tagged NubG and the diploids selected. If the two proteins interact, the Cub and Nub moieties will come close together and will be recognized and cleaved by the cytosolic ubiquitin-specific proteases. The transcription factor (PLV) released will enter the nucleus and turn on the reporter gene (*HIS3*).

Importance of VLCFAs

1. Organ development and morphogenesis

Plants disrupted for the *ECR* (*AtTSC13*) gene that encodes enoyl CoA reductases were deficient in FA elongation, and displayed an abnormal morphology with reduced size of the aerial organs [119]. The *gl8agl8b* (encode 3-ketoacyl reductase) double mutant in maize [130] and the *acc1* and *acc2* (encoding cytosolic acetyl-CoA carboxylases) mutants in *Arabidopsis* [131] display abnormal embryo development. The *Wax-deficient anther1* (*Wda1*) mutant in rice is severely retarded in microspore development. Biochemical analyses of these plants showed significant defects in FA elongation in their anther walls, highlighting the role of VLCFA containing compounds in organ development [132]. A male-sterile mutation in *Arabidopsis* that disrupts pollen-pistil interactions showed deficiency in long-chain lipids in the mutant pollen, implicating the VLCFAs in proper pollen–stigma signaling and fertilization [133]. Silencing the *NbECR* gene (encoding enoyl-CoA reductase in *Nicotiana benthamiana*) produced cell death in leaves, disorganization of the cellular membrane structure, and a reduction in VLCFA, demonstrating the role of VLCFA in membrane biogenesis [134]. The *Elovl3*-ablated mice displayed a sparse hair coat and the hair lipid content was disturbed, which resulted in severe water repulsion defects and increased trans-epidermal water loss [135]. Mutation in the human gene *ELOVL4* has been linked with Stargardt-like macular dystrophy and autosomal dominant macular dystrophy, which are inherited forms of macular degeneration characterized by decreased visual acuity, macular atrophy and extensive fundus flecks [51]. This implicates the biosynthesis of VLCFAs in the normal development of the retina. Long chain FA containing lipids are the primary structural

component of the adult brain, making up 50% to 60% of the brain dry weight. DHA is the most abundant FA in the phospholipids of the cerebral gray matter, mostly concentrated in neuronal membranes of the cerebral cortex and synaptosomes. DHA-enriched diets have been reported to lower the risk of Alzheimer disease in humans [136].

2. Lipids, wax and seed oil synthesis

In higher plants, VLCFAs serve as components or precursors of waxes in the tryphine layer of the extracellular pollen coat [137], and suberin and cutin of the leaf cuticle and cell wall, which permits selective release of volatiles, limits diffusion of water and solutes, provides protection from attack by herbivores, pathogens and environmental stresses [63]. VLCFAs also accumulate as storage lipids in the seed oil of some plants, in which they are incorporated into triacylglycerols (TAGs) or wax esters [138]. Mutations in the FAE-KCSs, including *FDH*, *CUT1* and *FAE1*, result in waxless phenotypes (changes in cell wall lipid composition and cuticular permeability) and additionally, epidermal cell fusion [80], conditional male sterility [78] and changes in seed oil content [65], respectively. VLCFAs with multiple methyl branches were found as major components of the *Mycobacterium tuberculosis* cell wall lipids that play crucial roles in the host-pathogen interaction and pathogenesis [139, 140].

3. Industrial applications

VLCFAs like erucic acid (22:1) and its derivatives are used in industry for the production of high-temperature lubricants, cosmetics, pharmaceuticals, as important renewable raw materials used in plastic film manufacture and in the synthesis of nylon [141]. Since mammals cannot synthesize PUFAs *de novo*, and due to their several

beneficial effects on human health, such as cardiovascular function, improved performance of skeletal muscle [142] and memory, PUFAs have attracted considerable interest as pharmaceutical and nutraceutical compounds [48]. For example, studies with aged rodents on diets deficient in docosahexaenoic acid (DHA), showed 90% more synaptic loss and inferior memory performance [143] than for rodents fed with diets supplemented with DHA. Several lines of evidence indicate that dietary supplementation of PUFAs (such as fish oil) reduces the risk of primary cardiac arrest as a result of incorporation of the DHA into heart phospholipids; PUFAs also appear to exert anti-thrombotic and anti-arrhythmic activities. Furthermore, various cardiovascular diseases have been associated with aberrant PUFA synthesis. Riemersma *et al.* [144] demonstrated that there exists a correlation between the increased mortality from coronary heart disease and low levels of linoleic acid, dihomo-gamma-linoleic acid (20:3n-6) and arachidonic acid (20:4n-6) in adipose tissue. Defects in elongation of the n-3 and n-6 FAs have been reported in patients suffering from hypertension [145]. Thus, several PUFA rich oil-producing organisms, including the fungus *Mortierella alpine*, fish and marine algae are used in industry to generate PUFA.

4. Ceramide and sphingolipid synthesis

VLCFAs are a major acyl component of SPLs in all organisms from yeast to humans. SPLs in yeast, as shown in Fig. 10, is composed of a long-chain sphingoid base, typically 18 carbons long, which is amide-linked to a VLCFA through the C2-amino group, and a polar head group, generally a sugar residue, present at the C1 carbon [146]. SPLs are an important class of lipids most abundant in the plasma membrane, but also found in the *trans*-Golgi network and in recycling endosomes [147]. SPLs also play a

vital role in vesicle transport of glycosylphosphatidylinositol (GPI)-anchored proteins [148]. In yeast [149], mammalian cells [150], and possibly in plants [151], SPLs interact with sterols to trigger the formation of highly ordered, detergent-resistant plasma membrane microdomains known as lipid rafts [152]. Lipid rafts are involved in cellular trafficking of proteins [such as delivery of proteins to plasma membrane in yeast [149] and GPI-anchored proteins [153]] and in endocytosis [154]. The presence of a variety of cell signaling proteins within lipid rafts has led to the consensus that these lipid domains play an important role in the process of signal transduction [155, 156].

Ceramides, a SPL precursor that is formed from the direct condensation of VLCFAs with a long chain base by ceramide synthase, are reported to play role in apoptosis, growth arrest, endocytosis and stress response [157-162].

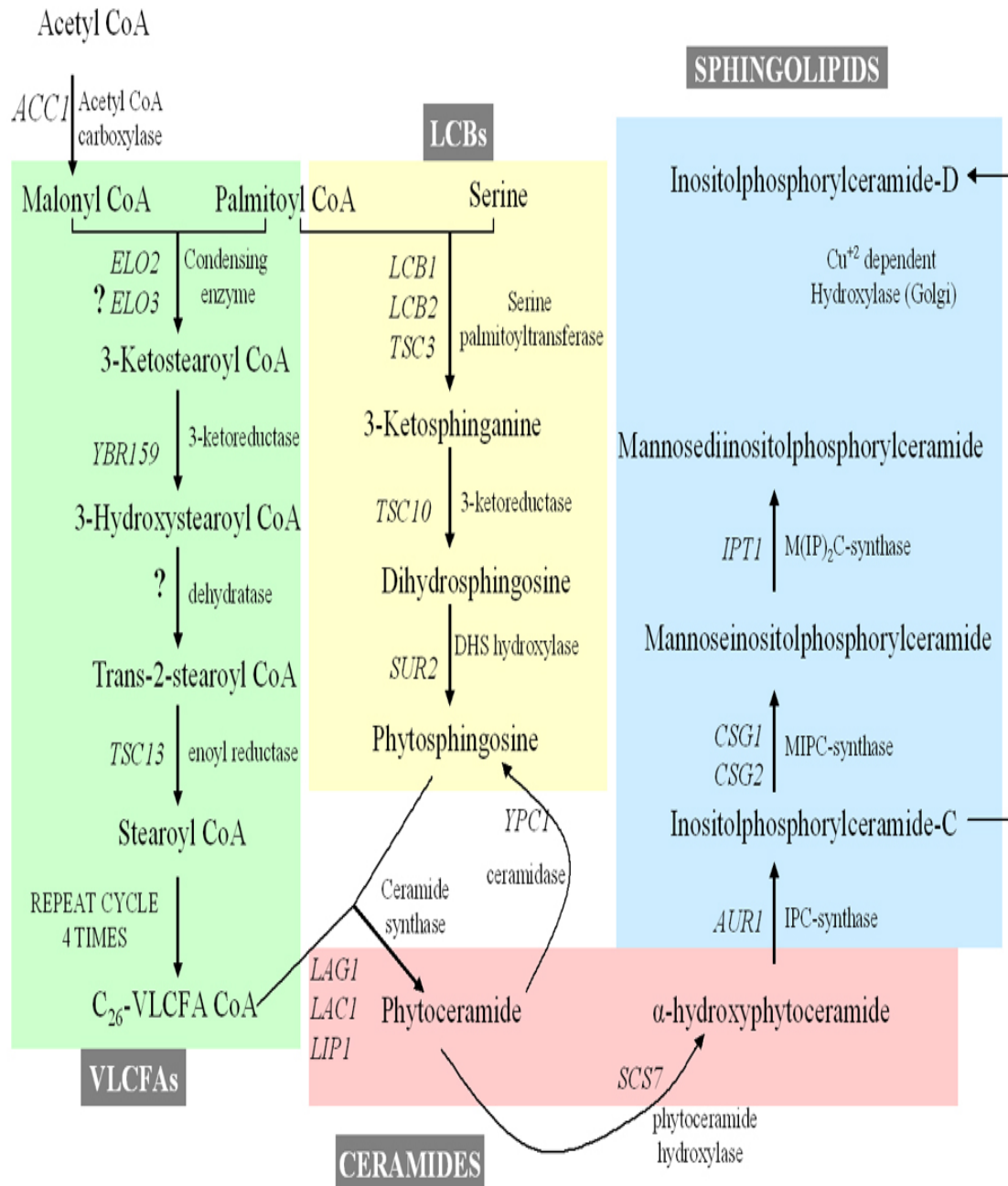


Figure 10. Pathways of fatty acid elongation (green box), LCB (yellow box), ceramide (pink box) and sphingolipid (blue box) synthesis in *S. cerevisiae*. The genes encoding the enzymes required for catalysis are mentioned (adapted from Kohlwein *et al.* 2001).

SPECIFIC GOALS OF THIS STUDY

AIM1. The condensation step of fatty acid elongation in animals and in fungi appears to be mediated by Elop homologs, which bear no resemblance to the well-characterized condensing enzymes (including the FAE-KCSs). In fact, it has not been conclusively shown that Elops directly catalyze condensation.

The objective of this aim was to study whether the FAE-KCSs could fulfill the essential functions of the yeast Elo2p/Elo3p proteins. By performing a cDNA library screen we identified several FAE-KCSs from *A. thaliana* that were able to rescue the lethality associated with *elo2Δelo3Δ* yeast double mutant. The Elops were shown previously to act in conjunction with Ybr159p and Tsc13p, the reductases of FA elongation, and also to coimmunoprecipitate with these reductases. Surprisingly, our genetic data provides evidence that in spite of the lack of sequence similarity between the FAE-KCSs and the Elops, the FAE-KCSs depend on the same reductases for VLCFA synthesis. We investigated whether physical interactions exist between the FAE-KCSs and the elongase components by performing coimmunoprecipitation experiments. Since the majority of VLCFAs are incorporated into SPLs in yeast, we investigated whether the FAE-KCS-derived VLCFAs could be channeled to the ceramide synthase and thereby restore synthesis of the SPLs to the yeast mutants that lacked Elops.

AIM2. Despite much evidence that VLCFAs are important in cellular physiology, the enzymes required for their synthesis are still not well characterized. It is important to unravel the molecular details of the elongase enzymes for several reasons. For example, the elongase enzymes can be new drug targets against tuberculosis, because

the VLCFA containing lipids in the cell wall of *M. tuberculosis* are unique to this pathogen, and play a crucial role in host-pathogen interaction and attack [163]. The structural knowledge might help in designing crosslinking experiments for studies intended to identify other components of the elongase complex, like the dehydratase component as well as other potential subunits. The lack of structural information for these enzymes prevents understanding of how the catalytic centers of these enzymes are organized with respect to the membrane and to each other, and also of how the intermediates of FA elongation are transferred from one reaction center to the next. The intrinsic hydrophobicity of these enzymes has hindered previous attempts to purify and characterize these membrane-bound elongase enzymes. In the absence of high-resolution structural data, good topology models provide necessary background for the design of structure-function studies of these proteins. The hydropathy analysis of these proteins predicts that each has several transmembrane domains. However, while all programs predict multiple membrane-spanning domains, the number varies depending on the algorithm used, indicating the need for experimental determination of their topology.

The objective of this aim was to map the membrane topology of the 3-ketoreductase and the enoyl-reductase of the elongase complex. The topologies of yeast and Arabidopsis Tsc13p were delineated using biochemical techniques. Several functionally important residues of Tsc13p were also identified and their positions with respect to the membrane were determined. We also used similar techniques to determine the membrane topology of the major 3-keto reductase, Ybr159p of the elongase complex. The topologies of both reductases were further confirmed by the split-ubiquitin experiments performed to identify protein-protein interactions.

**MEMBERS OF THE ARABIDOPSIS FAE1-LIKE 3-KETOACYL-CoA
SYNTHASE GENE FAMILY SUBSTITUTE FOR THE Elop PROTEINS OF
SACCHAROMYCES CEREVISIAE.**

**Shilpi Paul¹, Kenneth Gable¹, Frédéric Beaudoin², Edgar Cahoon³, Jan Jaworski⁴,
Johnathan A. Napier² and Teresa M. Dunn¹.**

**¹Department of Biochemistry and Molecular Biology, Uniformed Services
University of the Health Sciences, 4301 Jones Bridge Road, Bethesda, MD 20184**

**²Crop Performance and Improvement (CPI), Rothamsted Research, Harpenden Herts
AL5 2JQ, UK.**

**³ USDA-ARS Plant Genetics Research Unit, Donald Danforth Plant Science Center, 975 N.
Warson Rd. , St. Louis, MO 63132**

⁴Donald Danforth Plant Science Center, 975 N. Warson Rd., St. Louis, MO 63132

Running Title: FAE-KCSs Substitute for Elop Proteins

Address Correspondence To: Teresa Dunn, ¹Department of Biochemistry and Molecular Biology, Uniformed Services University of the Health Sciences, 4301 Jones Bridge Road, Bethesda, MD 20184, tdunn@usuhs.mil, Phone: 301-295-3592, FAX: 301-295-3512

Several 3-keto-synthases have been studied including the soluble fatty acid synthases, those involved in polyketide synthesis, and the FAE1-like 3-keto-CoA synthases. All of these condensing enzymes have a common ancestor and an enzymatic mechanism that involves a catalytic triad consisting of Cys, His and His/Asn. In contrast to the FAE1-like family of enzymes that mediate plant microsomal fatty acid elongation, the condensation step of elongation in animals and in fungi appears to be mediated by the Elop homologs. Curiously these proteins bear no resemblance to the well-characterized 3-keto-synthases. There are three *ELO* genes in yeast that encode the homologous Elo1p, Elo2p and Elo3p proteins. Elo2p and Elo3p are required for synthesis of the very long chain fatty acids, and mutants lacking both Elo2p and Elo3p are inviable confirming that the very long chain fatty acids are

essential for cellular functions. In this study we show that heterologous expression of several Arabidopsis FAE1-like genes rescues the lethality of an *elo2Δelo3Δ* yeast mutant. We further demonstrate that Fae1p acts in conjunction with the 3-keto and trans-2,3,-enoyl reductases of the elongase system. These studies indicate that even though the plant-specific Fae1p family of condensing enzymes evolved independently of the Elop family of condensing enzymes, they utilize the same reductases and presumably dehydratase that the Elop proteins rely upon.

INTRODUCTION

Cytosolic fatty acid synthases catalyze the *de novo* synthesis of the majority of cellular fatty acids, which have 16 or 18 carbons. However, there are many other types of fatty acids in the cellular lipids, including the very long chain fatty

acids (VLCFA) that are synthesized through elongation of the C16 or C18 fatty acid by a microsomal enzyme system. The VLCFA have been implicated in a number of cellular processes including the formation of nuclear pores, trafficking of lipids and proteins, and the formation of membrane domains that organize signaling proteins. In higher plants, VLCFA are critical components of the waxes found in the pollen coat and in leaves, and they are also found in the storage triacylglycerols of some seeds. Very long-chain polyunsaturated fatty acids including arachidonic acid, eicosapentaenoic acid, and docosahexaenoic acid are abundant in the membranes of brain and retina and they also serve as precursors of the biologically active eicosanoids. Despite mounting evidence that the VLCFA are important in cellular physiology, many aspects of their synthesis and function remain to be resolved.

In yeast the saturated VLCFA are present in the sphingolipids, which are essential for cell viability. Interestingly, a mutation that leads to the synthesis of C26-containing phosphatidylinositol can bypass the requirement for sphingolipids (though the mutant strains grow poorly) highlighting the importance of the VLCFA (1,2). It is now well established that the Elop proteins are components of the membrane-associated elongase system that mediates VLCFA synthesis. Elo1p is involved in the elongation of medium-chain fatty acids, whereas Elo2p and Elo3p participate in the elongation of C16 to C24, and Elo3p is required for elongating C24 to C26 (3-6). Yeast transformed with foreign ELO homologs synthesize novel (e.g., mono- and polyunsaturated)

elongated fatty acids demonstrating that the Elop proteins are responsible for selection of the acyl-CoA substrates for elongation (7-13). Although this implicates the Elop proteins as condensing enzymes, conclusive evidence that they directly catalyze the condensation reaction is lacking.

In plants the condensation step of fatty acid elongation is catalyzed by the FAE1-KCSs. For example FAE1, the founding member of the Arabidopsis FAE1-KCS gene family, is involved in the synthesis of the 22-carbon monounsaturated fatty acid (14). Lassner et al (15) demonstrated that the FAE1 homolog from jojoba encodes the condensing enzyme, 3-ketoacyl-CoA synthase (KCS) and Millar and Kunst (16) showed that KCS regulates the substrate specificity and activity of the elongation process. All 3-keto synthases characterized to date, including the FAE1-KCSs, the soluble fatty acid synthases, and those involved in polyketide synthesis catalyze a Claisen condensation by essentially the same mechanism (17). In these systems, studies of the mechanism, analysis of essential catalytic residues, sequence homology and, when available, the 3-D structure reveal that all of these condensing enzymes have a common ancestor.

In contrast, the Elop proteins provide an exception to the notion that all condensing enzymes involved in fatty acid elongation arose from a common origin. The hallmarks of all condensing enzymes studied to date are missing from the ELO gene family. For example, all condensing enzymes contain a conserved cysteine, which is the acyl acceptor in the first step of the mechanism. While there are two conserved cysteines among the Elop homologs, there is no

evidence of the catalytic triad that is found in other 3-keto synthases. A highly conserved feature of the Elop sequences is a histidine box, suggestive of a metal binding site, yet no other condensing enzymes contain such a domain. The FAE-KCSs are membrane-bound condensing enzymes with two membrane spanning domains at the N-terminus (18). In contrast, hydropathy analyses of the Elop homologs predict the presence of 5-7 transmembrane domains spread between the N- and C-terminus.

In addition to the Elop proteins, there are several other proteins that are required for fatty acid elongation. Each C₂ elongation is a four-step process consisting of a condensation-reduction-dehydration-reduction cycle (Figure 1). The yeast *YBR159w* and *TSC13* genes encode the 3-keto and 2,3-enoyl reductases of the elongation cycle (19-21). Consistent with early biochemical characterization of fatty acid elongation that suggested the elongase enzymes are organized in a complex (22), the Elop, Ybr159p and Tsc13p elongase proteins co-immunoprecipitate with one another (20,21). The dehydratase component of the elongase system has yet to be identified, and whether there are other proteins required is also not yet known.

Although yeast have no FAE-KCS homologs, several Arabidopsis FAE-KCSs have been expressed in yeast and these heterologously-expressed enzymes are able to direct the synthesis of novel fatty acids (23). For example, expression of FAE1 in yeast leads to accumulation of monounsaturated C22 erucic acid (18,23-25). That the FAE-KCSs in yeast lead to the synthesis of novel elongated fatty acids raises several

questions. For example, can the FAE-KCSs substitute for the yeast Elop proteins? Does the conversion of the 3-keto intermediates generated by the FAE-KCSs into elongated fatty acids depend on the other enzymatic activities of the elongase complex? If so, do the FAE-KCSs physically associate with the reductases? In the studies reported here, we have addressed these questions.

EXPERIMENTAL PROCEDURES

Media, Strains and Genetic Manipulations - Yeast media were prepared and cells were grown according to standard procedures (26). The yeast strains used in this study are listed in Table I.

Disrupting the ELO1, ELO2 and ELO3 Genes - The construction of the disruption alleles with *TRP1* replacing parts of the coding sequences of *ELO2* and *ELO3* was described previously (21). The *elo2::KAN* disrupting allele was PCR-amplified using genomic DNA prepared from the yeast knock out collection (Invitrogen) and primers, ELO2F and ELO2R (Table 2). To construct the *elo1::KAN* disrupting allele, a PCR fragment extending from 400 base pairs upstream from the start codon to 300 base pairs downstream of the stop codon of *ELO1* was generated using the primer pair ELO1F and ELO1R (Table 2) and genomic DNA prepared from wild-type yeast (TDY2037, Table I). The PCR fragment was digested with *Bam*H1 and *Sal*I and ligated between the *Bam*H1 and *Xho*I sites of a bluescript

plasmid to create pBS-ELO1. The *SpeI/SalI* fragment from pFA6a-KanMX6 (27) was substituted for the *XhoI/NheI* fragment of pBS-ELO1, thereby replacing codons 10 – 183 of *ELO1* with the kanamycin resistance marker. The pBS-ELO1::KAN plasmid was digested with *BamHI* and *KpnI* to liberate the *elo1::KAN* fragment that was used to disrupt the *ELO1* gene.

Construction and Screening of an Arabidopsis Yeast Expression Library - Inflorescences along with small amounts of stems, leaves, and newly initiated siliques were collected from *Arabidopsis thaliana* Columbia-0 plants and used immediately for the construction of a cDNA library in a yeast expression vector. Total RNA was initially isolated from the plant material by using Trizol reagent (Invitrogen), and polyA⁺ RNA was enriched by two successive passes of the total RNA through oligo-dT cellulose columns (Amersham Biosciences), according to protocols provided by the manufacturers. cDNA inserts with *EcoRI* and *XhoI* restriction sites on the 5' and 3' ends, respectively, were generated from 5 µg of polyA⁺-enriched RNA by using a Uni-ZAP cDNA synthesis kit (Stratagene), essentially as described in the manufacturer's protocol, except that Superscript II reverse transcriptase (Invitrogen) was used for synthesis of first strand cDNA. Enrichment for cDNAs of between approximately 700 and 3,000 bp was conducted with Sephacryl cDNA size fractionation columns (Invitrogen). Size selected-cDNAs with flanking *EcoRI* and *XhoI* restriction sites were ligated into the *EcoRI* and *SalI* restriction sites of a modified form of the pADH yeast expression vector (21). Prior to its

use, an *EcoRI* site was introduced into the multicloning site of the pADH vector by mutation of the *HindIII* site immediately adjacent to the *ADH* promoter. Following incubation at 14°C for 24 h, the ligation reaction was drop dialyzed against water for 15 min on 0.025 µm pore size VSWP filter discs (Millipore) and transformed into *E. coli* DH10B cells (Invitrogen) by electroporation. Transformed cells were grown with shaking (250 rpm) for one hour at 37°C in 5 ml of LB media without selection. The cells were grown for an additional 5 h with ampicillin (100 µg/ml) selection and were then inoculated into 250 ml of LB media with ampicillin selection. Following growth at 37°C with shaking for 8 h, plasmid was isolated from harvested cells and used for yeast complementation studies. The plasmid library was transformed into strain TDY7005 (*elo2Δ elo3Δ/pELO3*, see Table I) and *LEU2*⁺ prototrophic transformants were selected. The transformants (254,000) were screened for growth on FOA and fifteen were identified that were able to lose the *URA3*⁺-marked plasmid that carried the *ELO3* gene. The *LEU2*⁺-marked plasmids from these strains were recovered and their ability to rescue the *elo2Δ elo3Δ* double mutant was confirmed. Sequence analysis revealed that nine carried the At5g43760 FAE-KCS cDNA, 5 carried the At2g16280 FAE-KCS cDNA and one carried the At1g04220 FAE-KCS gene.

Construction of the FAE1-KCS Expression Plasmid, the HA-FAE-KCS Expression Plasmids, and the MYC-Tagged Yeast and Arabidopsis Ybr159p - FAE1-KCS was PCR-amplified from a

cDNA kindly provided by Dr. Ljerka Kunst (15) using primers FAE1-PvuF and FAE1-PvuR. The amplified fragment was restricted with *PvuII* and ligated into a *HindIII* cut pADH plasmid after filling the 5' protruding ends with DNA Polymerase I. For HA-tagging of the FAE-KCSs, *XhoI*-ended or *SalI*-ended PCR products were generated that extended from codon 2 through to the stop codon for each gene. The primers used are listed in Table 2 with the Arabidopsis At gene designator and either -HAF (for HA-tagging primer, forward) or -HAR (for HA-tagging primer, reverse). The PCR-generated fragments were restricted with either *XhoI* or *SalI* and ligated into the *SalI* site of plasmid pADH-3X-HA (21) resulting in an in-frame fusion of the N-terminal triple-HA tag to each of the FAE-KCS. For tagging of the yeast Ybr159p and the Arabidopsis homolog of Ybr159p (encoded by At1g67730 and hereafter referred to as AtYbr159p), a triple-MYC epitope tag was introduced at the amino terminus of the pESC-Ybr159 and pESC-AtYbr159 constructs described before (17). For this an *AvrII* site was first introduced after the start codon in both constructs by QuikChange PCR mutagenesis (Stratagene, La Jolla, Calif.), using the complementary mutagenic primers 159AvrF and 159AvrR or At159AvrF and At159AvrR, respectively. A *SpeI*-ended fragment carrying the triple-MYC cassette was generated by PCR using a Bluescript-based 3X-MYC-containing plasmid (19) and ligated into the *AvrII* site.

Elongase Assays –Microsomes were prepared from exponentially growing cells. Cells were pelleted at 5000 x g, washed with water and

repelleted. The cell pellets were resuspended in TEGM (0.05M Tris (7.5), 1mM EGTA, 1mM BME, 1mM PMSF, 1ug/ml Leupeptin, 1ug/ml Pepstatin A, 1ug/ml Aprotinin) buffer at 1 ml/50 OD cells and glass beads (0.5 mm diameter) were added to the meniscus. Cells were disrupted by four cycles of vortexing for 1 min followed by cooling on ice for 1 min, and pelleted at 8000 x g for 10 min. The supernatant was transferred to a fresh tube and spun at 135,000 x g for 30 min. The resulting pellet was resuspended by dounce homogenization in at least a 10 x volume of TEGM buffer and repelleted at 135,000 x g. The final membrane pellet was resuspended in TEGM buffer containing 33% glycerol and stored at -80°C.

Total elongase activity was measured in a volume of 200 µl containing 50 mM Tris, pH 7.5, 1mM MgCl₂, 150 µM triton X-100, 1 mM NADPH, 1 mM NADH, 10 mM β-mercaptoethanol, 1mM dithiothreitol, 40 µM acyl-CoA acceptor and 60 µM 2[¹⁴C]-malonyl-CoA (0.05 µCi/ml) at 37°C. The reaction was initiated by the addition of 0.2 mg of microsomal protein. Protein concentrations were determined using the Biorad protein assay reagent (Bio-Rad Laboratories, Hercules, CA). For assays of the condensing activity, the NADPH/NADH were omitted. The reaction was terminated after 10 min by adding 200 µl of 5 M KOH/10 % MeOH and heating at 80°C for 1 h. Following addition of 200 µl of 10 N H₂SO₄, free fatty acids were recovered by two 1.5 ml extractions into hexane. Following evaporation of hexane, the fatty acid methyl esters (FAMES) were generated by dissolving in 1 ml of 1 M methanolic HCl and heating at 80°C for 1 h.

An equal volume of 0.15 M NaCl was added, the FAMES were extracted into hexane and resolved by reverse phase C18-silica gel TLC using $\text{CHCl}_3\text{:MeOH:H}_2\text{O}$ (5:15:1) as the developing solvent. The radiolabeled fatty acids were detected and quantified using the Cyclone Storage Phosphor System (Packard Instrument Company, Inc, Meriden, CT).

Immunoblotting and Immunoprecipitation -

Microsomes were prepared from strains containing HA-tagged FAE1-KCS and the yeast MYC-tagged Tsc13p or the Arabidopsis homolog of Tsc13p (encoded by At3g55360 and hereafter referred to as AtTsc13p) (21,28) or the yeast and the Arabidopsis MYC-Ybr159p (described above).

The microsomes were solubilized at 1 mg/ml with 0.1% sucrose monolaurate (SML) (Roche Diagnostics, Indianapolis, IN) for 10 min, and the high speed (135,000 x g, 30 min) supernatant was collected. The supernatant (100 μl) was incubated with 3 μl of the precipitating antibody for 1 h and then with 25 μl of protein A-Sepharose (125 mg/ml from Sigma) for 1 h. The precipitates were washed three times with 1 ml of TEGM buffer containing 0.1% SML, resuspended in 100 μl SDS loading buffer, and a 10- μl sample was subjected to SDS-PAGE on a 4-12% gradient gel. Following transfer of the separated proteins to nitrocellulose, the blots were blocked in 0.1 M Tris, 7.5, 0.15 M NaCl, 0.1% Tween 20, 5% dry milk. The MYC-Tsc13p was detected with HRP-conjugated monoclonal anti-MYC antibodies (Sigma) at 1/2500. HA-FAE1-KCS was detected using HRP-conjugated monoclonal anti-HA antibodies (from Boehringer Mannheim) at 1/1000. The bound

antibodies were detected by the ECL Western blotting detection system (Amersham Pharmacia Biotech).

Fatty Acid Analysis - Cells (5×10^8) in mid-logarithmic growth were harvested and resuspended in 100 μl distilled H_2O along with C21 and C23 fatty acids as internal standards. Fatty acids were extracted and the fatty acid methyl esters were prepared as previously described (21). Gas chromatography/mass spectrometry (GCMS) was performed using an HP 6890 Series GC system with a Supelcowax 10 column, coupled to an HP 5973 Mass Selective Detector.

IPC Analysis - Cells were grown in SD medium without inositol overnight and harvested during exponential growth phase. The cells were resuspended to 10 $\text{OD}_{600}/\text{ml}$ in SD without inositol, and 50 $\mu\text{Ci}/\text{ml}$ myo-[2- ^3H]-Inositol (16 Ci/mmol, Amersham) was added. After a 10 minute labeling, the cells were diluted to 2 $\text{OD}_{600}/\text{ml}$ with SD media containing 30 μM unlabeled inositol and incubated for an additional 90 minutes. Sodium Azide (4mM final) was added and the lipids were extracted by bead beating in $\text{CHCl}_3\text{:MeOH}$ (1:1). The extraction was repeated and the extracted material was combined, clarified by centrifugation, dried and desalted using water saturated butanol. 250,000 cpm were spotted on TLC and developed using $\text{CHCl}_3\text{:MeOH:H}_2\text{O:AcOH}$ (16:4:1.6:4). The TLC was dried, sprayed with EN 3 HANCE (NEN) and visualized using Kodak XAR film.

RESULTS

The elo Mutants are Affected in the Condensation Step of Fatty Acid Elongation - A number of studies are consistent with the conclusion that the Elo proteins participate specifically in the condensation step of fatty acid elongation. For example, many previous studies of the Elo family of proteins have shown that they control the substrate specificity of fatty acid elongation (reviewed in (29)). To address this question further, the condensation step of fatty acid elongation was assayed *in vitro* using microsomes prepared from wild-type and *elo1Δ*, *elo2Δ*, and *elo3Δ* mutant yeast cells. The ability of the mutant microsomes to direct the elongation of various acyl-CoA acceptors was assessed by measuring incorporation of label from ¹⁴C-malonyl-CoA into elongated fatty acids. By omitting NADPH from the assay, the condensation reaction can be assayed (Figure 1).

As shown in Figure 2, microsomes prepared from wild-type cells form the 3-keto condensation products by condensing malonyl-CoA with each of the acyl-CoA substrates when NADPH is omitted. For example, with the C14-CoA substrate the C16-3-keto product accumulates, with the C16-CoA substrate the C18-3-keto product accumulates, etc. (Figure 2A). In contrast, when NADPH is included in the *in vitro* assay, the whole series of elongated fatty acids with chain lengths up to C26 are generated (Figure 2A). Assays of the condensation reaction using the microsomes from the *elo* mutants confirm that the Elo proteins participate in the condensation

step of elongation. Previous *in vivo* studies have shown that Elo1p is required for elongation of myristate to palmitate (3,5,6). The *in vitro* assays reveal that the condensation step is specifically affected since microsomes prepared from cells lacking Elo1p are unable to form the C16-3-keto product when C14-CoA is used as a substrate for the condensation reaction (Figure 2B). With the *elo1Δ* mutant microsomes, the longer substrates (C16-CoA to C24-CoA) are converted to the 3-keto products by Elo2p and/or Elo3p. The *elo2Δ* mutant microsomes have low condensation activity toward the C16 and C18-CoA substrates (Figure 2C). Finally, the *elo3Δ* mutant microsomes form very little C24-3-keto product with the C22-CoA substrate, and no C26-3-keto product with the C24-CoA substrate (Figure 2D). These data provide additional evidence that the Elo proteins are required for the condensation step of elongation.

The Arabidopsis FAE1 Gene and Other FAE-KCS Genes Rescue the Lethality of an elo2Δelo3Δ Mutant - The yeast *elo2Δelo3Δ* double mutant is inviable, reflecting that the VLCFA have essential functions for cell growth. Whereas the Elo proteins are needed for the condensation step of fatty acid elongation in yeast, members of the FAE1-like family of enzymes, hereafter referred to as the FAE-KCSs, catalyze the condensation step of fatty acid elongation in plants. As discussed above, there is no significant homology between the FAE-KCS proteins and the Elo proteins. Although previous studies have clearly demonstrated that FAE1-KCS expression in yeast leads to the synthesis of novel fatty acids

(16,18,19,23,25), whether the FAE-KCSs can substitute for the yeast Elo2p/Elo3p proteins had not been tested. Therefore, it was of interest to test whether the Arabidopsis FAE1-KCS condensing enzyme could rescue the lethality of the *elo2Δelo3Δ* double mutant.

To address this question, a yeast mutant with chromosomal disruption of both the *ELO2* and *ELO3* genes that carried a wild-type *ELO3* gene on a *URA3*-marked, and therefore FOA-counterselectable, plasmid was used (TDY7005, *elo2Δ::KAN elo3Δ::TRP1/pELO3*, Table I). The *FAE1-KCS* cDNA was PCR-amplified and subcloned into a *LEU2*⁺-marked yeast expression plasmid (Experimental Procedures). Following transformation of the *FAE1-KCS*-encoding plasmid, the *elo2Δelo3Δ* double mutant was able to lose the *URA3*-marked *ELO3*-rescuing plasmid (Figure 3A). Consistent with the *in vitro* assays discussed above, knowledge that the *FAE1-KCS* condensing enzyme can rescue the *elo2Δelo3Δ* double mutant provides additional evidence that the Elops are required specifically for the condensation step of elongation.

Whether other members of the Arabidopsis FAE-KCS gene family are able to restore viability to the *elo2Δelo3Δ* double mutant was investigated by screening an Arabidopsis cDNA library. A yeast expression library was constructed by ligating Arabidopsis cDNAs behind the constitutively expressed yeast pADH1 promoter in a *LEU2*-marked plasmid (Experimental Procedures). The library was transformed into the *elo2Δelo3Δ* double mutant carrying the wild-type *ELO3* gene on a *URA3*-marked plasmid (TDY7005, Table I), and leucine prototrophic

transformants were selected. Those transformants that were able to lose the *ELO3*-containing *URA3*-marked plasmid were identified by screening for growth on 5-fluoroorotic acid (FOA). The cDNA-containing plasmids were recovered from the FOA-resistant transformants and retested to confirm that they were able to rescue the lethality of the *elo2Δelo3Δ* double mutant. Three additional FAE-KCS genes, At2g16280, At5g43760, and At1g04220, were identified that rescue the *elo2Δelo3Δ* mutant (Figure 3A). It is likely that other members of the Arabidopsis FAE-KCS gene family can also substitute for the yeast Elo2p/3p proteins but that they are not as highly represented in this cDNA expression library. It is worth noting that five additional FAE-KCSs were PCR-amplified from the expression library, cloned into the 3X-HA expression vector, and confirmed to be expressed. However, they were not able to rescue the *elo2Δelo3Δ* double mutant suggesting that they are unable to elongate the endogenous substrates to provide the saturated VLCFA required for yeast viability (see Discussion).

Because Elo1p is involved in synthesizing C16 and C18 fatty acids, it was assumed that it was not required for the rescue of the *elo2Δelo3Δ* double mutant by the FAE-KCSs. This was confirmed by demonstrating that an *elo1Δelo2Δelo3Δ* triple mutant (TDY7006, Table I) harboring the FAE-KCS expression plasmids grew similarly to the rescued *elo2Δelo3Δ* double mutant (Figure 3B).

Characterization of the in vivo and in vitro Activities of the FAE-KCSs - The elongated fatty acids that accumulated in the *elo2Δelo3Δ* mutant

rescued by the FAE-KCSs were analyzed by GCMS (Figure 4A). The segment of the GCMS trace from 8 to 20 minutes profiling the elongated (>C18) and α -hydroxylated C16-C22 fatty acids is shown. Though these are the fatty acids relevant to this study, they represent a minor fraction (<5%) of the total fatty acids, with C16, C18 and C18:1 comprising the majority of the yeast fatty acids. In Figure 4B the relative abundance of each of the elongated (>C18) and α -hydroxylated C16-C22 fatty acids fatty acid species is indicated.

Consistent with previous characterizations (14,19,23), the predominant elongated saturated fatty acid in the FAE1-KCS rescued mutant is C20. In contrast to wild-type yeast, there are also significant levels of C20:1 and C22:1 in the *elo2 Δ elo3 Δ* mutant rescued by FAE1-KCS. This demonstrates that unlike Elo2p and Elo3p, FAE1-KCS is able to elongate the C18:1 fatty acid that is present in yeast. The fatty acid profiles of the At5g43760- and At1g04220-rescued *elo2 Δ elo3 Δ* mutants are very similar, with the major VLCFA in these strains being C22. Overall, these rescued mutants have an *in vivo* fatty acid composition that is very similar to that of the *elo3 Δ* mutant. The previously reported fatty acid profiles of yeast expressing these two FAE-KCSs (23) are somewhat different from the results reported here. In that study the genes were expressed in wild-type yeast and thus the fatty acid profiles reflect the combined activities of the endogenous yeast Elo1/2/3 proteins and the heterologously-expressed FAE-KCSs (see Discussion). The *elo2 Δ elo3 Δ* mutant rescued by At2g16280 FAE-KCS accumulates significant levels of C24 VLCFA, making it the most similar to wild-type

yeast.

Although they restored viability to the *elo2 Δ elo3 Δ* mutant, none of the heterologously-expressed FAE-KCS genes restored wild-type VLCFA profiles. As mentioned above, the fatty acid profiles of the rescued mutants are similar to the fatty acid profiles observed in some of the yeast elongase mutants. For example, α -hydroxylated fatty acids with chain lengths of C16, C18, C20 and C22 accumulate, whereas in wild-type yeast the only α -hydroxylated fatty acid is the C26 species (Figure 4B). From our previous studies (19-21), it is clear that the shorter α -hydroxylated fatty acids arise because phytosphingosine is acylated with shorter fatty acids in the VLCFA-deficient mutants and the resulting C16-C22 ceramides are substrates for the Scs7p hydroxylase (30) (see Discussion).

In addition to the altered VLCFA profiles, the FAE-KCS rescued *elo2 Δ elo3 Δ* mutants display other phenotypes that are characteristic of mutants with deficiencies in VLCFA synthesis. Similar to the *elo2 Δ* and *elo3 Δ* mutants, and in contrast to wild-type cells (20,21), the rescued *elo2 Δ elo3 Δ* double mutants have high levels of the free long-chain bases (data not shown). These rescued strains also display temperature sensitivity, another common phenotype of the mutants with reduced VLCFA synthesis (Figure 4C). The temperature sensitive growth phenotype is most severe for the FAE1-KCS-rescued *elo2 Δ elo3 Δ* double mutant, which is not able to grow at or above 30°C.

The analysis of the fatty acids that accumulate in the rescued mutants provides information about which of the endogenous yeast

fatty acids can be elongated by the FAE-KCSs. To further investigate the activities of the FAE-KCSs, *in vitro* elongase assays were conducted using microsomes prepared from yeast lacking the endogenous Elo1p/2p/3p proteins and rescued by each of the four *FAE-KCS* genes. Using a variety of different acyl-CoA acceptors, the substrate specificities of the FAE-KCS proteins were addressed. All four of these HA-tagged FAE-KCSs were expressed well in yeast, and similar amounts of the FAE-KCS proteins were present in the microsomal protein preparations used for these *in vitro* assays (Figure 5A). The indicated acyl-CoAs were used at 40 μ M in the standard elongation assay (Experimental Procedures). The elongase reactions were initiated by adding 14 C-malonyl-CoA along with NADPH, allowing overall elongation to be measured. The products were extracted and converted to the fatty acid methyl esters (FAMES) as previously described, and the FAMES were resolved by reverse phase TLC (Figure 5B-E). In the reactions without added NADPH, substrates that could be elongated showed the expected 3-Keto products (data not shown).

FAE1-KCS elongated the saturated C16 and C18-CoA substrates well, and also elongated the C20-CoA to C22, albeit less well. The monounsaturated C16:1 and C18:1-CoA substrates were efficiently elongated, but FAE1-KCS had little or no activity toward the C22 and C24-CoAs or the C24:1-CoA. It also elongated the C18:2 substrate, forming C20:2 and small amounts of C22:2. The At5g43760 FAE-KCS displayed a strong preference for the C18 and C20-CoA substrates and also had activity toward the C16-

CoA and the C16:1-CoA and very low activity with the C18:1-CoA (Figure 5C). The At1g04220 FAE-KCS was similar to At5g43760 with activity toward the C16, C18 and C20-CoA substrates, but also had low activity toward C22-CoA. It also elongated the C16:1, C18:1 and C18:2-CoA substrates (Figure 5D). The At2g16280 FAE-KCS utilized the C16-C22-CoAs and showed a strong preference for generating the C24 product, with very little of the intermediate C20 and C22 fatty acids accumulating (Figure 5E). Interestingly, this FAE-KCS elongated the monounsaturated C24:1-CoA but displayed little activity toward the C16:1, C18:1 or C18:2 substrates. The spots above fully elongated products (especially apparent from the At2g16280 catalyzed reactions with the C20 and C22-CoA substrates) are most likely the 3-keto (seen in the reactions run without NADPH) and possibly the 3-hydroxy elongation intermediates.

The FAE-KCSs Coimmunoprecipitate with Ybr159p and Tsc13p, the Reductases of the Elongase Complex - The ability of the FAE-KCS enzymes to direct VLCFA synthesis in yeast raised questions as to whether this elongation pathway is dependent upon the other characterized components of the yeast Elo_p-containing elongase system. We have shown that Ybr159p is the major 3-keto reductase (19,20) and that Tsc13p is the trans-2,3-enoyl reductase required for fatty acid elongation (21,28). Furthermore, immunoprecipitation experiments have shown that these reductases, along with the Elo_p proteins, are organized in a complex. Since the FAE-KCSs are not homologous to the Elo_ps, it was questionable whether they could associate with the other

elongase proteins. However, the activity of FAE1 in yeast is dependent on Ybr159p (19), arguing that this component of the elongase is responsible for reducing the 3-keto intermediate generated by the FAE-KCSs. In addition, expression of the FAE-KCSs did not bypass the slow growth phenotype of the *ybr159Δ* mutant or the lethality of the *tsc13Δ* mutant (data not shown).

Whether the FAE-KCSs physically associate with the reductases was tested directly by immunoprecipitation experiments. Membranes were prepared from cells co-expressing HA-tagged FAE1 with either MYC-tagged yeast or MYC-tagged Arabidopsis Tsc13p (Figure 6A). Membranes were also prepared from cells co-expressing HA-tagged FAE1 with either MYC-tagged yeast or MYC-tagged Arabidopsis Ybr159p (Figure 6B). Following solubilization, the microsomal proteins were immunoprecipitated with either HA or MYC antibodies. Samples of the solubilized membranes (Tot), along with the supernatants (Sup) and pellets (Pel) from the immunoprecipitations were immunoblotted with anti-HA or anti-MYC antibodies. The HA antibodies immunoprecipitated the MYC-tagged yeast Tsc13p and MYC-tagged Arabidopsis Tsc13p proteins along with the HA-tagged FAE1. Conversely, the MYC antibodies pulled down HA-tagged FAE1 along with the MYC-tagged yeast and Arabidopsis Tsc13p. The HA-tagged FAE1 also coimmunoprecipitated with MYC-tagged Ybr159p from Arabidopsis and to a lesser extent with MYC-tagged yeast Ybr159p (Figure 6B). The weak interaction between FAE1 and yeast Ybr159p compared to its interaction with the Arabidopsis Ybr159p homolog is discussed further

below (Discussion). Coimmunoprecipitation experiments using the HA-tagged At2g16280 FAE-KCS and MYC-tagged yeast and Arabidopsis Tsc13p confirmed that this FAE-KCS also associates with Tsc13p (Figure 6C). These results demonstrate that the FAE-KCSs physically associate with the Tsc13p trans-2,3-enoyl reductase and the Ybr159p 3-keto reductase of the elongase system.

To determine whether FAE-KCSs and Elops can interact with the same elongase complexes, we also tested whether Elo3p coimmunoprecipitated with HA-FAE1 (Figure 6D). The HA-FAE1 was expressed in wild-type yeast cells, and solubilized microsomal protein was immunoprecipitated with anti-HA conjugated sephadex beads. The failure to see any Elo3p (which migrates as three discrete bands due to differential glycosylation) coimmunoprecipitated with the HA-tagged FAE1 suggests that elongase complexes can form with either an Elop protein or a FAE-KCS protein, but not with both. The failure of Elo3p to coimmunoprecipitate with HA-FAE1 also demonstrates the specificity of the interactions of the FAE-KCSs with the reductases. It is important to note that the level of endogenously expressed Elo3p is higher than the levels of the HA-FAE-KCSs. This is evident from Figure 5A which shows that HA-Elo3p (expressed from its own promoter and thus reflecting endogenous Elo3p levels) is more abundant than the HA-tagged FAE-KCSs. It is also significant that an HA-tagged Arabidopsis Elop-like protein (At3g06460) failed to coimmunoprecipitate with MYC-tagged Arabidopsis or yeast Tsc13p (Figure 6E). Finally,

HA-tagged FAE1 did not coimmunoprecipitate with the ER localized Lcb1p protein providing additional evidence for the specificity of the coimmunoprecipitations (data not shown). Taken together, these results strongly suggest that the FAE-KCSs associate specifically with the reductases of the elongase complex.

The VLCFA Synthesized by the Heterologously-expressed FAE-KCSs are Incorporated into Inositolphosphoceramides - The experiments above demonstrate that the FAE-KCSs interact with the yeast elongase complex and direct the synthesis of sufficient VLCFA to rescue the lethality of an *elo2Δelo3Δ* double mutant. In yeast, the majority of the VLCFA are found in the sphingolipids, primarily the inositolphosphoceramides (IPCs). The IPCs are synthesized from the ceramides, which are in turn generated by joining the VLCFA in amide linkage with phytosphingosine in a reaction catalyzed by ceramide synthase (Figure 7A). Because sphingolipids are essential for yeast cell viability, it appears that ceramide synthase is capable of using the VLCFA derived from the FAE-KCSs to acylate phytosphingosine, creating ceramides that can be converted to IPCs. The appearance of the α -OH C16-C22 fatty acids in the rescued mutants provides indirect evidence that the VLCFA produced by the FAE-KCSs are incorporated into ceramides since Scs7p hydroxylates the fatty acid in ceramides. To directly test whether the FAE-KCS derived VLCFA are incorporated into sphingolipids, the FAE-KCS rescued *elo1Δelo2Δelo3Δ* triple mutant cells were labeled with inositol and the extracted IPCs were analyzed

by thin layer chromatography. As shown in Figure 7B, each of the FAE-KCS-rescued *elo1Δelo2Δelo3Δ* triple mutants synthesized IPCs. Whereas the IPC in wild-type yeast contains exclusively α -OH C26 fatty acid (labeled as 26 Figure 7B), mutants lacking Elo3p accumulate C22 IPC-C. The reduced hydrophobicity of the C22 IPC-C relative to the C26 PC-C is reflected in its lower mobility in the thin layer chromatographic analysis. Interestingly, the C22 IPC-C that accumulates in the *elo3Δ* mutant is not mannosylated; like the *csg* mutants that fail to convert IPC to MIPC (31,32), the *elo3Δ* mutant makes IPC but no MIPC or M(IP)₂C (Figure 7B). With the exception of the strain expressing At2g16280, the IPCs that are synthesized by the FAE-KCS-rescued *elo1Δelo2Δelo3Δ* triple mutants are relatively hydrophilic and, like the C22 IPC-C that accumulates in the *elo3Δ* mutant, they are not mannosylated. The data are consistent with the fatty acid analyses (Figures 4). For example, in the FAE1-rescued mutant, C20 is the major VLCFA in the cells and C20-IPC-C accumulates. Similarly, the At5g43760 and At1g04420 rescued mutants, C22 is the predominant fatty acid and C22 IPC-C accumulates. The At2g16280-rescued mutant accumulates C24 and thus C24-IPC-C; unlike the IPCs with shorter fatty acids, this IPC species is mannosylated (note the appearance of MIPC). The spots above the indicated IPC-C species (and below PI) are IPC-B species that lack the α -hydroxylation on the fatty acids (30). The appearance of these IPC-B species in the mutants that accumulate the C20 and C-22 IPCs suggests that the fatty acid chain length of the IPCs affects

their hydroxylation by Scs7p.

DISCUSSION

The large number of different FAE-KCS isozymes (22 in *Arabidopsis*) is believed to reflect their activities toward different acyl-CoA substrates as well as the fact that some of the genes display tissue specific expression. There are no FAE-KCS homologs in the yeast genome. Rather, the Elop family of proteins is believed to catalyze the condensation step of fatty acid elongation in yeast, as well as in other eukaryotes, including mammals. The evidence that the Elop proteins are responsible for condensation relies in part upon the finding that heterologously-expressed Elop homologs can direct the synthesis of novel fatty acids in yeast. Since the Elop proteins have none of the hallmarks of the well characterized 3-ketoacyl-CoA synthases, they either represent a completely novel type of condensing enzyme or they could be a regulatory subunit that confers acyl-CoA substrate recognition to an as yet unidentified condensing enzyme. In this regard, it should be noted that the dehydratase activity of the elongase system has not been identified, so it is entirely possible that additional elongase proteins will be identified.

We have recently reported that Ybr159p is the major 3-ketoreductase, and that Tsc13p is the trans-2,3-enoyl reductase of the yeast elongase system (19-21). Furthermore, we found that these enzymes coimmunoprecipitate with one another and with the Elop proteins, a result that is consistent with early biochemical characterizations

that suggested that the elongase enzymes are organized in a complex (33). Despite the lack of sequence homology between the Elop and FAE-KCS proteins, the data presented here demonstrate that the FAE-KCSs act in conjunction with the reductases of the elongase complex. The coimmunoprecipitation data strongly suggests that the FAE-KCSs physically associate in a complex with the Ybr159p and Tsc13p reductases. This raises the intriguing possibility that the Elop and FAE-KCS proteins evolved independently as distinct 3-keto-CoA synthases and yet are able to interact with the other components of the elongase complex. Although the significance is unclear, we previously observed that all of the known components of the yeast elongase complex (Elo1p/2p/3p, Ybr159p, and Tsc13p) have a high pI (> 10), and we note that the FAE-KCSs also have high pIs (> 9.2). The coimmunoprecipitation results indicate that FAE1 interacts more strongly with the *Arabidopsis* Ybr159p homolog than with yeast Ybr159p. While it is tempting to speculate that this reflects differences between the Ybr159p proteins that affect their association with FAE1, there is currently no information as to which proteins of the elongase complex are in direct contact.

In addition to the large FAE-KCS gene family, there are also several Elop homologs in *Arabidopsis*, the roles of which have not been defined. On the other hand, there is a single homolog of Tsc13p, the trans-2,3-enoyl reductase in *Arabidopsis* that functionally complements a yeast *tsc13Δ* mutant (28). Kunst and coworkers recently reported the characterization of an *Arabidopsis* mutant lacking the Tsc13p homolog,

referred to in that study as ECR (34). The mutant displayed reduced synthesis of VLCFA, and decreased cuticular wax, storage lipid, and VLCFA-containing sphingolipids. Although the plants displayed morphological abnormalities that could be specifically attributed to the sphingolipid deficiency, the plants were viable and accumulated some VLCFA, indicating that there is at least one other reductase that can reduce the trans-2,3-CoA intermediates in Arabidopsis (34). It is unclear whether the residual fatty acid elongation that is occurring in the mutant plants is dependent on the FAE-KCSs, or whether it might be mediated by the Arabidopsis Elo homologs.

In this study four Arabidopsis FAE-KCSs that are able to substitute for the yeast Elo2p/Elo3p proteins by directing the synthesis of saturated VLCFA is reported. It is likely that additional members of the Arabidopsis FAE-KCSs will also functionally complement the *elo2Δelo3Δ* double mutant, but that they were not recovered because they are either not present or are poorly represented in the Arabidopsis yeast expression library. For example, despite the fact that FAE1 does complement and that we were able to PCR amplify it from the expression library, it was not found in the complementation screening. The characterization of the complementing FAE-KCSs confirms that yeast require saturated VLCFA with a minimal chain length of C20 for viability. As mentioned in “Results”, five additional FAE-KCSs (At2g26250, At1g01120, At2g26640, At1g19440, and At1g25450) were PCR amplified from the library and expressed in yeast, but were unable to rescue the *elo2Δelo3Δ* double mutant. Thus, they apparently cannot elongate the available substrates

(mainly C16 in the *elo2Δelo3Δ* mutant) to produce the required VLCFA. It will be interesting to characterize their substrate specificities using the *in vitro* elongase assays.

The heterologous expression of several FAE-KCSs in wild type yeast was recently reported (23) including several that were also characterized in this study. Three of the six that were found to be enzymatically active in that study (FAE1, At5g43760, and At1g04220) were among those that were found to be capable of complementing the *elo2Δelo3Δ* double mutant. Expression of At1g01120 was reported to result in the accumulation of C22, 24 and 26 VLCFA and expression of At1g25450 in the accumulation of C26, 28 and 30 (23), but we found that neither was able to rescue the *elo2Δelo3Δ* double mutant. This may reflect the difference in expressing the genes in wild type yeast instead of in the *elo2Δelo3Δ* double mutant. For example, if these FAE-KCSs elongate fatty acids with chain lengths greater than C18, these substrates would have been available (produced by Elo2p/Elo3p) in a wild type background, but not in the *elo2Δelo3Δ* double mutant background. Previous studies of yeast expressing the At1g01120 (*KCSI*) gene suggested that it does elongate C18, 20, 22 and 24 fatty acids (35). It is possible that the coexpression of some of these non-complementing *FAE-KCSs* together with *FAE1* in the *elo2Δelo3Δ* mutant will result in the ability to grow at 37°C, a nonpermissive temperature for the FAE1- rescued mutant (Figure 4B). For example, a FAE-KCS that elongates C20 substrates, along with FAE1 that elongates the C16 produced by *de novo* fatty acid synthesis to C20, would restore synthesis of VLCFA >C22 and

thereby would likely restore growth at 37°C.

While this study confirms that the VLCFA produced by the FAE-KCSs fulfills the essential function missing in the *elo2Δelo3Δ* mutant, the rescued strains are not completely normal. For example, the *FAE1-KCS*-rescued mutant is unable to grow at temperatures above 30°C, a phenotype shared by a large number of mutants with reduced sphingolipid synthesis (36,37). This may reflect a role of the VLCFA-containing sphingolipids in reducing membrane fluidity at elevated temperatures. Furthermore, while only C26 ceramides are produced in wild type yeast, the mutants accumulate ceramides with shorter chain lengths. Interestingly, the shorter ceramides are inositolphosphorylated by Aur1p, but the IPCs with fatty acids shorter than C24 are not substrates for mannosylation as no MIPC or M(IP)₂C is generated.

In summary, we present here the finding that FAE-KCS proteins can substitute for the yeast Elop proteins. Surprisingly, although yeast have no FAE-KCS homologs, the FAE-KCS proteins apparently associate with the other components of the yeast elongase complex.

REFERENCES

1. Nagiec, M. M., Wells, G. B., Lester, R. L., and Dickson, R. C. (1993) *J Biol Chem* **268**, 22156-22163
2. Lester, R. L., Wells, G. B., Oxford, G., and Dickson, R. C. (1993) *J Biol Chem* **268**, 845-856
3. Dittrich, F., Zajonc, D., Huhne, K., Hoja, U., Ekici, A., Greiner, E., Klein, H., Hofmann, J., Bessoule, J. J., Sperling, P., and Schweizer, E. (1998) *Eur J Biochem* **252**, 477-485
4. Oh, C. S., Toke, D. A., Mandala, S., and Martin, C. E. (1997) *J Biol Chem* **272**, 17376-17384.
5. Toke, D. A., and Martin, C. E. (1996) *J Biol Chem* **271**, 18413-18422
6. Schneiter, R., Tatzer, V., Gogg, G., Leitner, E., and Kohlwein, S. D. (2000) *J Bacteriol* **182**, 3655-3660
7. Leonard, A. E., Bobik, E. G., Dorado, J., Kroeger, P. E., Chuang, L. T., Thurmond, J. M., Parker-Barnes, J. M., Das, T., Huang, Y. S., and Mukerji, P. (2000) *Biochem J* **350 Pt 3**, 765-770.
8. Parker-Barnes, J. M., Das, T., Bobik, E., Leonard, A. E., Thurmond, J. M., Chaung, L. T., Huang, Y. S., and Mukerji, P. (2000) *Proc Natl Acad Sci U S A* **97**, 8284-8289
9. Zank, T. K., Zahringer, U., Lerchl, J., and Heinz, E. (2000) *Biochem Soc Trans* **28**, 654-658.
10. Zank, T. K., Zahringer, U., Beckmann, C., Pohnert, G., Boland, W., Holtorf, H., Reski, R., Lerchl, J., and Heinz, E. (2002) *Plant J* **31**, 255-268.
11. Beaudoin, F., Michaelson, L. V., Hey, S. J., Lewis, M. J., Shewry, P. R., Sayanova, O., and Napier, J. A. (2000) *Proc Natl Acad Sci U S A* **97**, 6421-6426.
12. Beaudoin, F., Michaelson, L. V., Lewis, M. J., Shewry, P. R., Sayanova, O., and Napier, J. A. (2000) *Biochem Soc Trans* **28**, 661-663.
13. Agaba, M., Tocher, D. R., Dickson, C. A., Dick, J. R., and Teale, A. J. (2004) *Mar Biotechnol (NY)*

14. James, D. W., Jr., Lim, E., Keller, J., Plooy, I., Ralston, E., and Dooner, H. K. (1995) *Plant Cell* **7**, 309-319
15. Lassner, M. W., Lardizabal, K., and Metz, J. G. (1996) *Plant Cell* **8**, 281-292
16. Millar, A. A., and Kunst, L. (1997) *Plant J* **12**, 121-131
17. White, S. W., Zheng, J., Zhang, Y. M., and Rock, C. O. (2005) *Annu Rev Biochem* **74**, 791-831
18. Blacklock, B. J., and Jaworski, J. G. (2002) *Eur J Biochem* **269**, 4789-4798.
19. Beaudoin, F., Gable, K., Sayanova, O., Dunn, T., and Napier, J. A. (2002) *J Biol Chem* **277**, 11481-11488.
20. Han, G., Gable, K., Kohlwein, S. D., Beaudoin, F., Napier, J. A., and Dunn, T. M. (2002) *J Biol Chem* **277**, 35440-35449.
21. Kohlwein, S. D., Eder, S., Oh, C. S., Martin, C. E., Gable, K., Bacikova, D., and Dunn, T. (2001) *Mol Cell Biol* **21**, 109-125.
22. Cinti, D. L., Cook, L., Nagi, M. N., and Suneja, S. J. (1992) *Prog. Lipid Res.* **31**, 1-51
23. Trenkamp, S., Martin, W., and Tietjen, K. (2004) *Proc Natl Acad Sci U S A* **101**, 11903-11908
24. Ghanevati, M., and Jaworski, J. G. (2001) *Biochim Biophys Acta* **1530**, 77-85.
25. Ghanevati, M., and Jaworski, J. G. (2002) *Eur J Biochem* **269**, 3531-3539.
26. Sherman, F., Fink, G. R., and Hicks, J. B. (1986) *Methods in Yeast Genetics*, Cold Spring Harbor Laboratory, Cold Spring Harbor
27. Wach, A. (1996) *Yeast* **12**, 259-265
28. Gable, K., Garton, S., Napier, J. A., and Dunn, T. M. (2004) *J Exp Bot* **55**, 543-545
29. Leonard, A. E., Pereira, S. L., Sprecher, H., and Huang, Y. S. (2004) *Prog Lipid Res* **43**, 36-54
30. Haak, D., Gable, K., Beeler, T., and Dunn, T. (1997) *J Biol Chem* **272**, 29704-29710
31. Zhao, C., Beeler, T., and Dunn, T. (1994) *J Biol Chem* **269**, 21480-21488

32. Beeler, T. J., Fu, D., Rivera, J., Monaghan, E., Gable, K., and Dunn, T. M. (1997) *Mol Gen Genet* **255**, 570-579
33. Poulos, A. (1995) *Lipids* **30**, 1-14
34. Zheng, H., Rowland, O., and Kunst, L. (2005) *Plant Cell* **17**, 1467-1481
35. Todd, J., Post-Beittenmiller, D., and Jaworski, J. G. (1999) *Plant J* **17**, 119-130.
36. Dunn, T. M., Gable, K., Monaghan, E., and Bacikova, D. (2000) *Methods Enzymol.* **312**, 317-330
37. Beeler, T., Bacikova, D., Gable, K., Hopkins, L., Johnson, C., Slife, H., and Dunn, T. (1998) *J Biol Chem* **273**, 30688-30694
38. Bernert, J. T., Jr., and Sprecher, H. (1977) *J Biol Chem* **252**, 6736-6744

FOOTNOTES

This work was supported by an NSF 2010 Collaborative grant to TMD, JJ, and EC.

Abbreviations – VLCFA, very long chain fatty acids; KCS, 3-ketoacyl-CoA synthase; FAE-KCS, FAE1-like 3-ketoacyl-CoA synthase; FAMES, fatty acid methyl esters; TLC, thin layer chromatography; LCB, long chain bases; IPCs, inositolphosphoceramides; MIPCs, mannosylinositolphosphoceramides; M(IP)₂Cs, mannosyldiinositolphosphoceramides.

FIGURE LEGENDS

Figure 1. Fatty Acid Elongation in *Saccharomyces cerevisiae*. Palmitoyl-CoA is elongated to a C26-VLCFA by the membrane-associated elongase enzymes. Each cycle of elongation involves four successive reactions, the condensation of malonyl-CoA with the acyl-CoA substrate, reduction of the 3-keto acyl-CoA, dehydration of the 3-hydroxy acyl-CoA, and reduction of the trans-2,3 acyl-CoA.

Figure 2. The altered VLCFA composition of the *elo* mutants result from defects in the condensation step of fatty acid elongation. Fatty acid elongation activity in wild-type (A), *elo1Δ* (B), *elo2Δ* (C), and *elo3Δ* (D) mutant microsomes was compared using C14-, C16-, C18, C20, C22, and C24-CoAs as substrates. The assays were conducted in the absence of NADPH (-) to measure condensation activity, and in the presence of NADPH (+) to measure overall elongation. The reaction products were converted to methyl esters, extracted and separated by reverse phase TLC. The chain lengths of the elongated products are indicated on the left of each panel. In the absence of NADPH, the 3-keto intermediate formed by the condensation of malonyl-CoA with the acyl-CoA acceptor accumulates. The radiolabeled spots present in the – NADPH lanes of the TLC are actually the 2-ketones that arise from decarboxylation of the 3-keto intermediates during the preparation of the FAMES [97]. The small amount of C16 and C18 that forms in the absence of any added acyl-CoA (shown for the wt, labeled “None” in panel A) results from contaminating fatty acid synthase that purifies with the microsomes, as it is eliminated by including cerulenin in the assays or by deleting the *FAS2* gene.

Figure 3. Several FAE-KCSs rescue the lethality of the yeast *elo2Δelo3Δ* double mutant. A. The *elo2Δelo3Δ* double mutant is unable to lose the *URA3*-marked plasmid that carries the wild type *ELO3* gene, and is therefore unable to grow on FOA. Introduction of the indicated *FAE-KCS* genes on a *LEU2*-marked yeast expression plasmid (but not the “vector” alone) allows the mutant strain to lose the *URA3*-marked *ELO3*-containing plasmid, demonstrating that the *FAE-KCS* genes can substitute for the *ELO3* gene. B. The *FAE-KCS* genes also rescue the *elo1Δelo2Δelo3Δ* triple mutant.

Figure 4. The FAE-KCSs restore VLCFA synthesis to the rescued *elo1Δelo2Δelo3Δ* triple mutants but do not completely reverse the phenotypes associated with VLCFA synthesis defects. A. Fatty acids were extracted from wild-type, *elo1Δ*, *elo2Δ*, *elo3Δ*, and FAE-KCS-rescued *elo1Δelo2Δelo3Δ* triple mutant cells, converted to methyl esters, and analyzed by GCMS. C21/23 fatty acids were added to the cells as internal standards prior to extraction of the fatty acids and were used for normalization, but are not shown in the traces. The majority of the intracellular fatty acids are saturated and monounsaturated C16 and C18 (not shown in these traces) with the elongated (>C18) saturated fatty acids representing only about 5% of the total fatty acids [164]. In wild-type yeast a high proportion (>50%) of the C26 is α -hydroxylated, also not shown in these traces. The insets identify the α -OH-C16, C20:0, and the C20:1 species. B. The relative abundance of the unhydroxylated saturated and monounsaturated C20-C26 and hydroxylated C16-C26 fatty acids is presented. C. The indicated strains were grown to an OD₆₀₀ of 0.5, and were diluted (1/5000) into the wells of a microtiter plate. The cells were transferred to plates containing YPD medium and the plates were incubated at 26 °C, 30 °C, 33 °C or 37 °C for 3 days prior to photographing.

Figure 5. *In vitro* elongase activities were measured using microsomes prepared from the FAE-KCS-rescued *elo1Δelo2Δelo3Δ* triple mutants. A. The FAE-KCS proteins were expressed at similar levels. Microsomal protein (10μg) was prepared from the FAE-KCS-rescued

elo1Δelo2Δelo3Δ triple mutant and resolved by SDS-PAGE. The amino-terminally 3X-HA-tagged FAE-KCSs proteins (lane 2, HA-FAE1; lane3, HA-At2g16280; lane 4, HA-At5g43760; lane 5, HA-At1g04220) were detected by immunoblotting with anti-HA antibody. The electrophoretic mobilities of the tagged FAE-KCSs were consistent with their predicted molecular weights (60-62 kDa). Lane 1 contains protein from the mutant expressing no HA-tagged protein and lane 6 contains 3X-HA-tagged Elo3p (MW of 43.7 kDa). B-D. Fatty acid elongation activity was assayed using microsomes prepared from each of the FAE-KCS-rescued *elo1Δelo2Δelo3Δ* triple mutants. Microsomes were incubated with the indicated acyl-CoAs in the presence of NADPH, and the reaction products were analyzed by reverse phase TLC as described in Figure 2. The chain lengths of the elongated products are indicated on the right side of each panel.

Figure 6A. FAE1 coimmunoprecipitates with the reductase components of the elongase complex. A. HA-tagged FAE1 was co-expressed with MYC-tagged yeast Tsc13p (top) or MYC-tagged AtTsc13p encoded by the At3g55360 gene (bottom). Microsomes were prepared, solubilized, and immunoprecipitated with anti-HA antibodies, anti-MYC antibodies, or unconjugated sephadex beads. The total soluble protein (Tot), supernatant (Sup), and pellet (Pell) from each immunoprecipitation was detected by immunoblotting with anti-HA (left) or anti-MYC (right). B. As in A, except that the HA-tagged FAE1 was coexpressed with MYC-tagged yeast Ybr159p (top) or MYC-tagged AtYbr159p encoded by the At1g67730 gene (bottom). The proteins migrate as predicted by their molecular weights, 41.4 kDa for yeast MYC-Tsc13p, 40.4 kDa for MYC-AtTsc13p, 38.7 kDa for yeast MYC-Ybr159p, 40.4 kDa for MYC-AtYbr159p and 60 kDa for HA-FAE1. C. HA-tagged At2g16280 (62.2 kDa) was coexpressed with MYC-tagged yeast Tsc13p (top) or with MYC-tagged Arabidopsis Tsc13p (bottom). Microsomal protein (Tot) was solubilized (Sol) and immunoprecipitated with anti-HA or anti-MYC antibodies or with unconjugated sephadex beads. The immunoprecipitates were immunoblotted with anti-HA antibodies. D. HA-tagged FAE1 was expressed in a wild-type yeast, and immunoprecipitated with anti-HA antibodies or unconjugated sephadex beads. Total microsomal protein (Tot) solubilized protein (Sol) and the pellets from the immunoprecipitations (unconjugated beads or anti-HA antibodies) were immunoblotted with anti-HA (left) or with anti-Elo3p (right). Elo3p, with a predicted MW of 39.5 kDa, runs as a broad band due to glycosylation. E. The HA-tagged Arabidopsis Elop-like protein (At3g06460, 38.2 kDa) was coexpressed with MYC-tagged yeast Tsc13p (top) or with MYC-tagged Arabidopsis Tsc13p (bottom) and the solubilized proteins were immunoprecipitated with anti-HA or anti-MYC antibodies. The immunoprecipitates were immunoblotted with anti-HA (left) or anti-MYC (right) antibodies.

Figure 7. The FAE-KCS-derived VLCFA are incorporated into Inositolphosphoceramides. A. The pathway for synthesis of the IPC, MIPC and MIP₂C sphingolipids in *Saccharomyces cerevisiae*. B. Wild-type, *elo3Δ*, and the FAE-KCS- rescued *elo1Δelo2Δ elo3Δ* triple mutant cells were incubated with ³H-inositol and the inositol-containing lipids were visualized by autoradiography following separation by TLC. Whereas the ceramide backbone of the IPC-C species in wild-type cells is comprised exclusively of PHS and an α-OH-C26 fatty acid, in the FAE-KCS-rescued mutants, IPCs with shorter chain lengths (C20-C24) are seen. The ceramides of the relatively hydrophobic IPC-Bs contain an unhydroxylated fatty acid. In addition to the inositolphosphoceramides, phosphatidylinositol (PI) as well as lyso-PI are present.

Table I. Yeast Strains used in this Study

Strain Name	Relevant Genotype	Complete Genotype
TDY2037	wild-type	<i>Mata lys2 ura3-52 trp1Δ leu2Δ</i>
TDY7000	<i>elo1Δ</i>	<i>Mata lys2 ura3-52 trp1Δ leu2Δ elo1::KAN</i>
TDY7001	<i>elo2Δ</i>	<i>Mata lys2 his4 ura3-52 trp1Δ leu2Δ elo2::URA3</i>
TDY7002	<i>elo3Δ</i>	<i>Mata ura3-52 trp1Δ leu2Δ elo3::TRP1</i>
TDY7005	<i>elo2Δ elo3Δ</i> /pELO3	<i>Mata lys2 ura3-52 trp1Δ leu2Δ elo2::KAN elo3::TRP1</i> /pRS316-ELO3
TDY7006	<i>elo1Δ elo2Δ elo3Δ</i> /pELO3	<i>Mata lys2 ura3-52 trp1Δ leu2Δ elo1::KAN elo2::TRP1 elo3::TRP1</i> /pRS316-ELO3
TDY7007	<i>elo1Δ elo2Δ elo3Δ</i> /pFAE1	<i>Mata lys2 ura3-52 trp1Δ leu2Δ elo1::KAN elo2::TRP1 elo3::TRP1</i> /pFAE1
TDY7010	<i>elo1Δ elo2Δ elo3Δ</i> /pAt1g04220	<i>Mata lys2 ura3-52 trp1Δ leu2Δ elo1::KAN elo2::TRP1 elo3::TRP1</i> /pAt1g04220
TDY7009	<i>elo1Δ elo2Δ elo3Δ</i> /pAt5g43760	<i>Mata lys2 ura3-52 trp1Δ leu2Δ elo1::KAN elo2::TRP1 elo3::TRP1</i> /pAt5g43760
TDY7008	<i>elo1Δ elo2Δ elo3Δ</i> /pAt16280	<i>Mata lys2 ura3-52 trp1Δ leu2Δ elo1::KAN elo2::TRP1 elo3::TRP1</i> /pAt2g16280

Table 2. PCR Primers used in this Study.

Primer Name	Sequence
Elo2F	5'- GGCCGGATCCGTACGTATTCACATGTCCTG
Elo2R	5'- GGCCGGATCCTAGACATGACTGTCGAAAGG
Elo1F	5'- GGCATATGGGATCCTTCTGCCAGCCAACTCAAT
Elo1R	5'- GGCATATGGTCGACGTGTGACACTAGAATCGC
FAE1-PvuF	5'-CCGGCAGCTGATGACGTCCGTTAACGTTAAGCTCCTTTAC
FAE1-PvuR	5'-CCGGCAGCTGTTAGGACCGACCGTTTTGGACATG
FAE1-HAF	5'-GGGCCCCTCGAGCACGTCCGTTAACGTTAAG
FAE1-HAR	5'-GGGCCCCTCGAGTTAGGACCGACCGTTTTG
At2g16280-HAF	5'-CCCGGGCTCGAGCGAAGCTGCTAATGAGCCT
At2g16280-HAR	5'- CCCGGGCTCGAGTCAGAAGTCGAGCTTAAC
At5g43760-HAF	5'-CCCGGGCTCGAGCAGCCATAACCAAAACCAA
At5g43760-HAR	5'-CCCGGGCTCGAGCTACGACGATGTAATGGG
At1g04220-HAF	5'-CCCGGGCTCGAGCAATGAGAATCACATTCAA
At1g04220-HAR	5'-CCCGGGCTCGAGCTATCGAGATTCCGAGGA
At2g26250-HAF	5'CCCGGGGTCGACCGGTAGATCCAACGAGCAA
At2g26250-HAR	5'CCCGGGGTCGACTTAGAGAGGCACAGGGTA
At1g01120-HAF	5'-CCCGGGCTCGAGCGAGAGAAACAAACAGCATT
At1g01120-HAR	5'-CCCGGGCTCGAGTCATTGCACAACCTTTAAC
At2g26640-HAF	5'-CCCGGGGTCGACCGATGTAGAGCAAAAGAAA
At2g26640-HAR	5'-CCCGGGGTCGACCTAGATTGTGGAGACCTT
At1g19440-HAF	5'-CCCGGGGTCGACCGACGGTGCCGGAGAATCA
At1g19440-HAR	5'-CCCGGGGTCGACCTAATAACTTAAAGTTAC
At1g25450-HAF	5'-CCCGGGGTCGACCTCTGATTTCTCGAGCTCC
At1g25450-HAR	5'-CCCGGGGTCGACTCATAGTTTAACAACCTTC
159AvrF	5'-GGATCCACCATGCCTAGGACTTTTATGCAA
159AvrR	5'-TTGCATAAAAGTCCTAGGCATGGTGGATCC
At159AvrF	5'-GGATCCACCATGCCTAGGGAGATCTGCACT
At159AvrR	5'-AGTGCAGATCTCCCTAGGCATGGTGGATCC

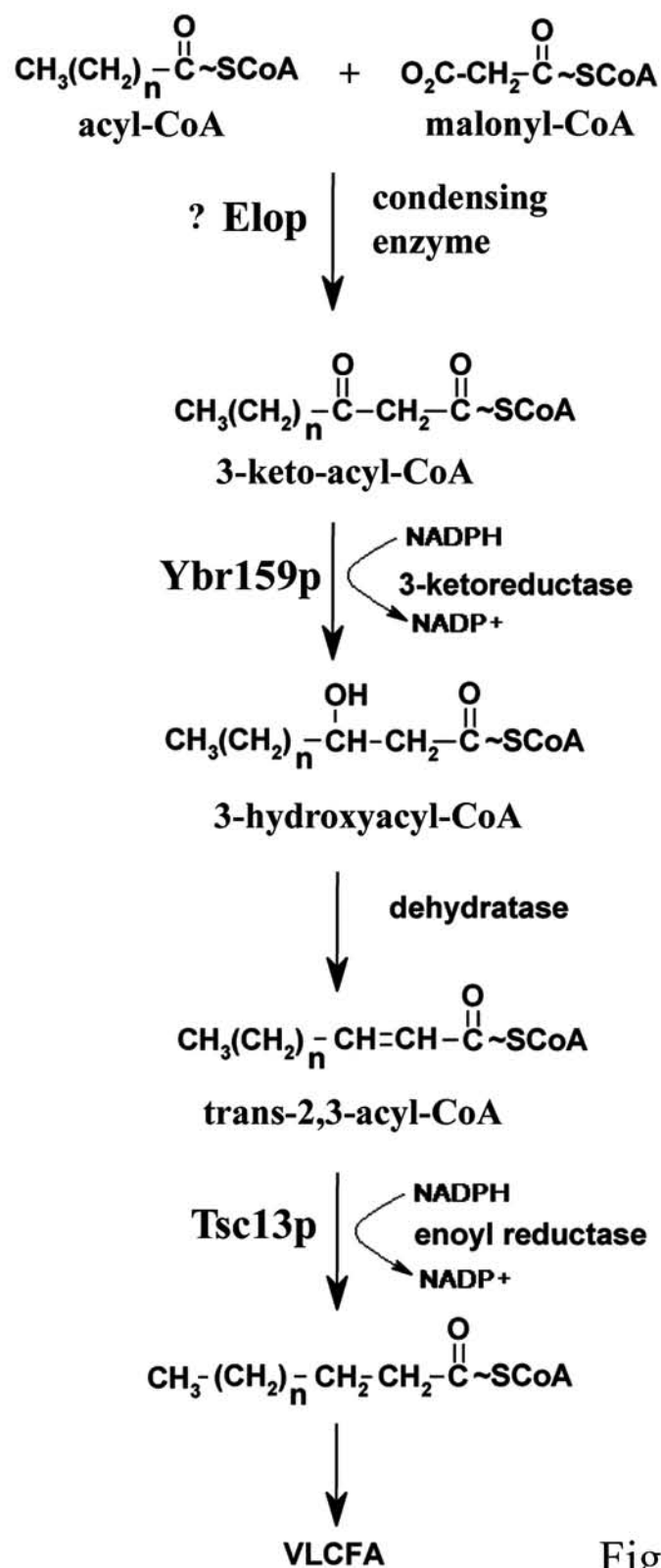


Fig 1

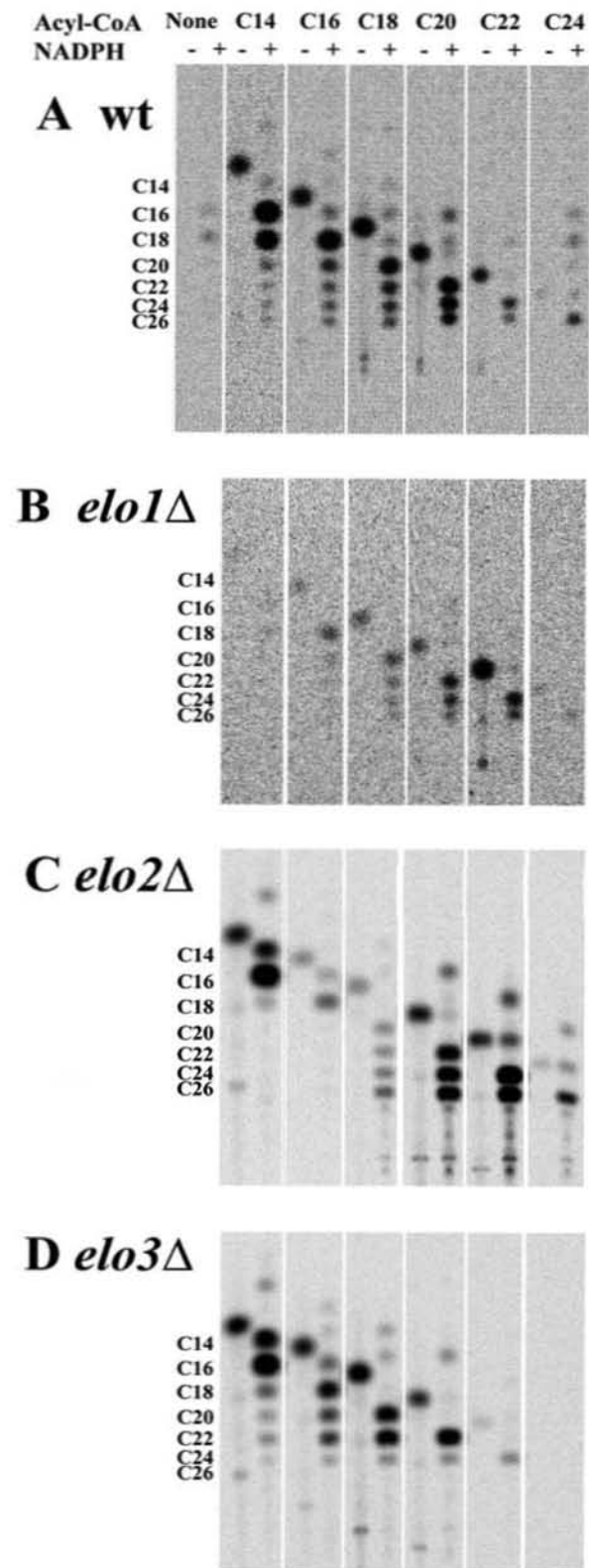


Fig 2

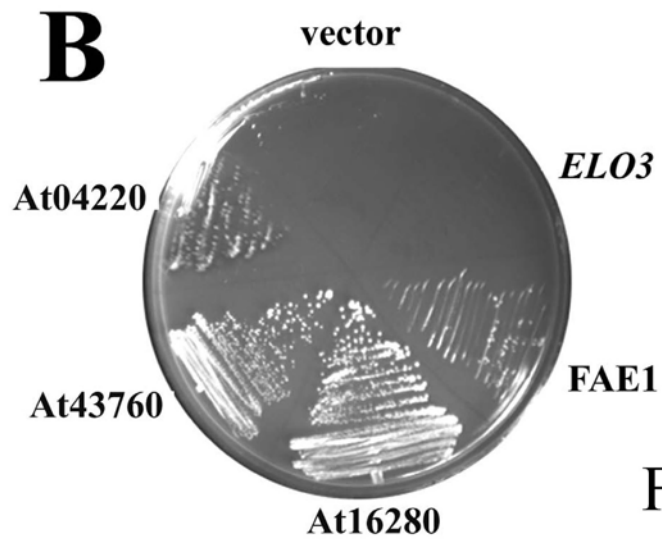
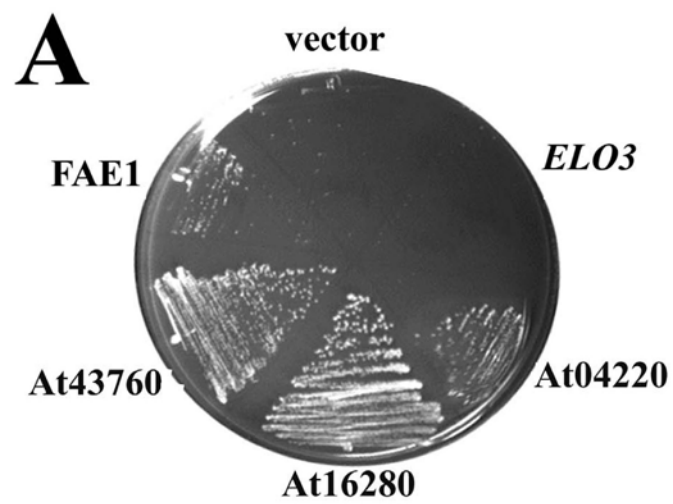


Fig 3

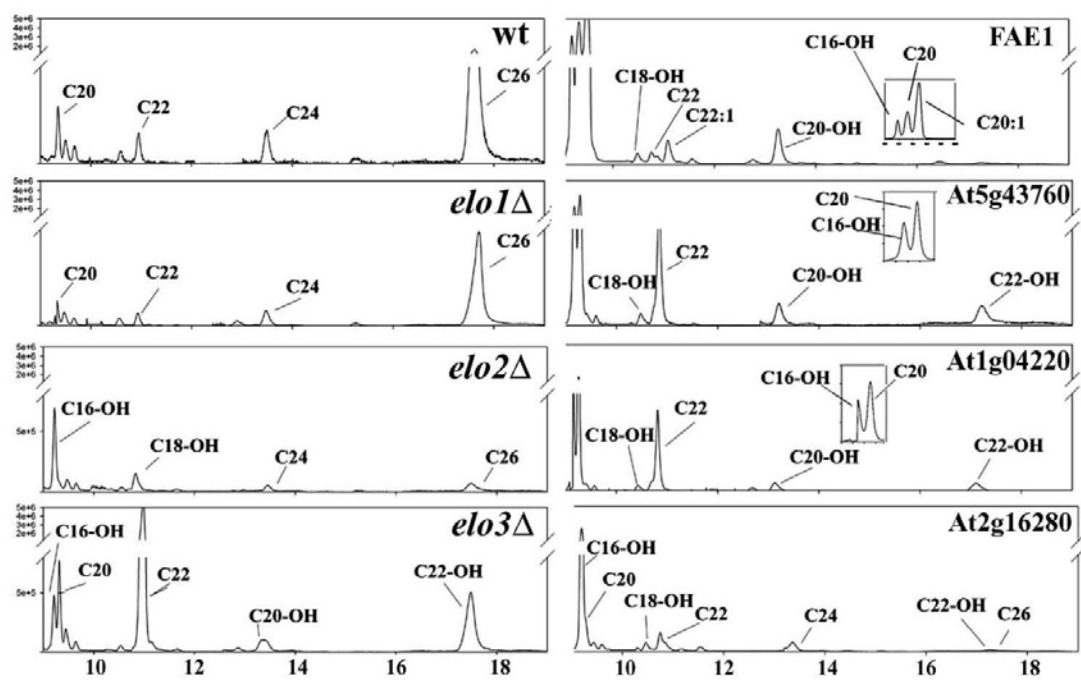


Fig 4A

Relative Abundance of α -OH and VLCFAs

	C16-OH	C20	C20:1	C18-OH	C22	C22:1	C20-OH	C24	C22-OH	C26	C24-OH	C26-OH
wt		5.2			3.2			6.7		62.2		22.7
<i>elo1</i> Δ		3.4			2.6			4.9		60.2		28.9
<i>elo2</i> Δ	32.9			17.2				5.5		13		31.5
<i>elo3</i> Δ	4.9	7.8		1.9	61.3			3.7	17.2		3.0	
FAE1	13.1	27.8	54.6	0.5	0.3	1.3	2.8					
At5g43760	26.8	38.5		3.1	22.1		3.1		6.4			
At1g04220	26.9	38.5		4.2	17.1		6.7		6.6			
Atg2g16280	75.3	6.0		11.4			1.3	4.9		1.0		

Fig 4B

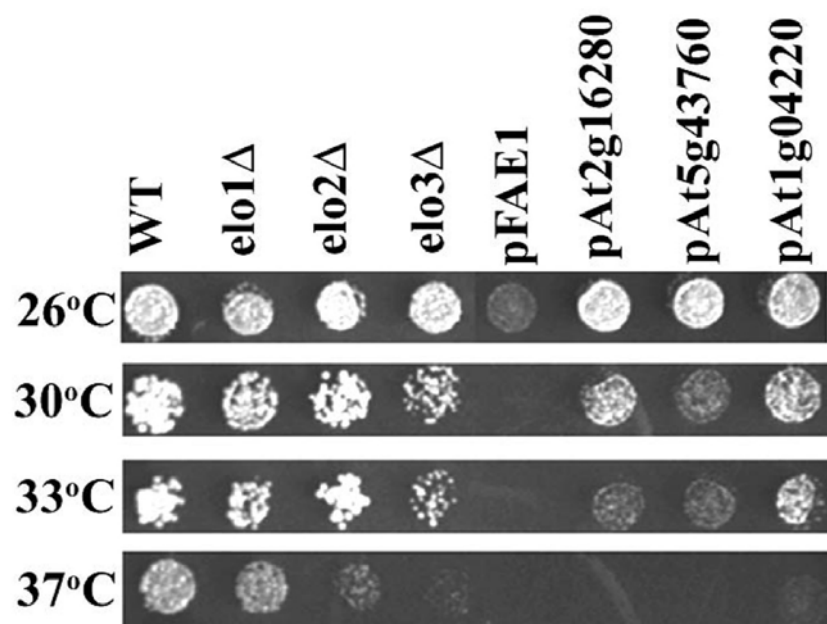


Fig 4C

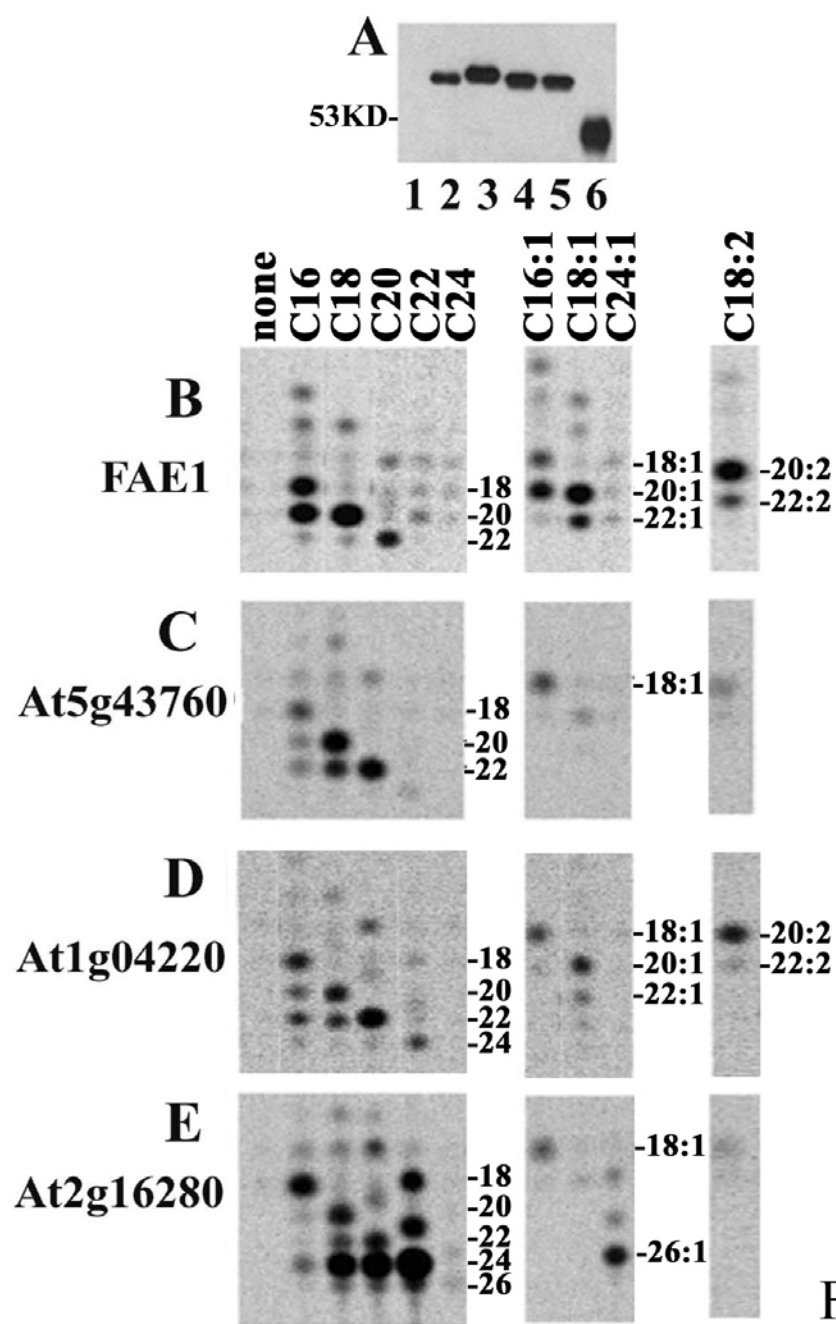


Fig 5

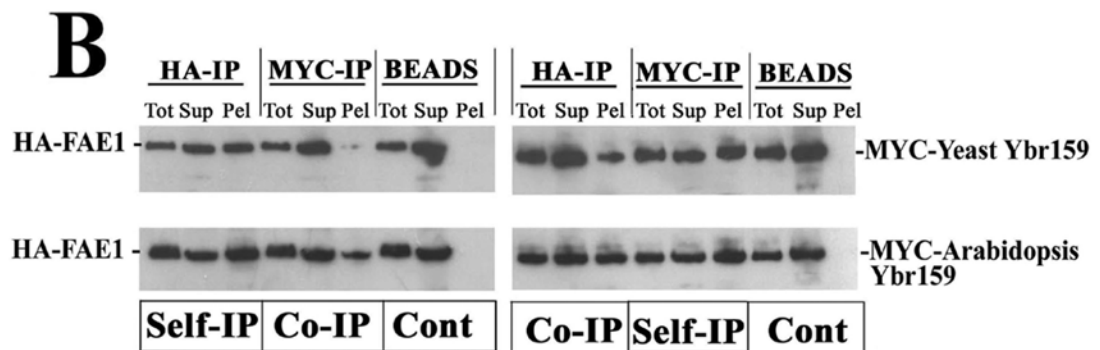
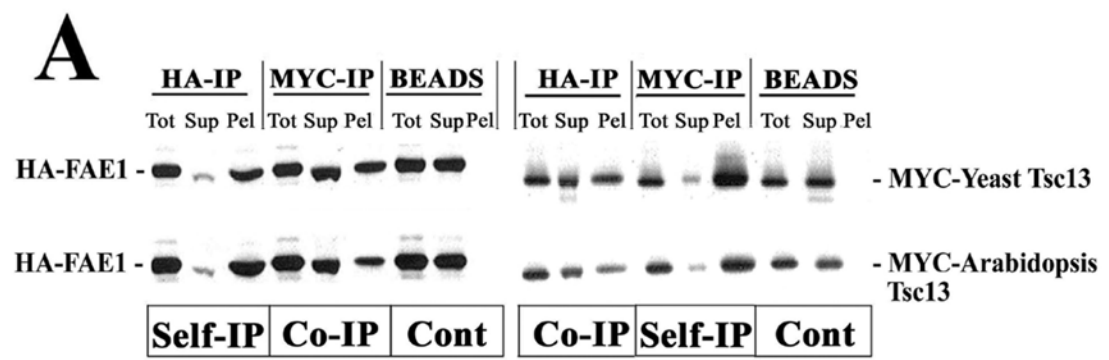


Fig 6A & B

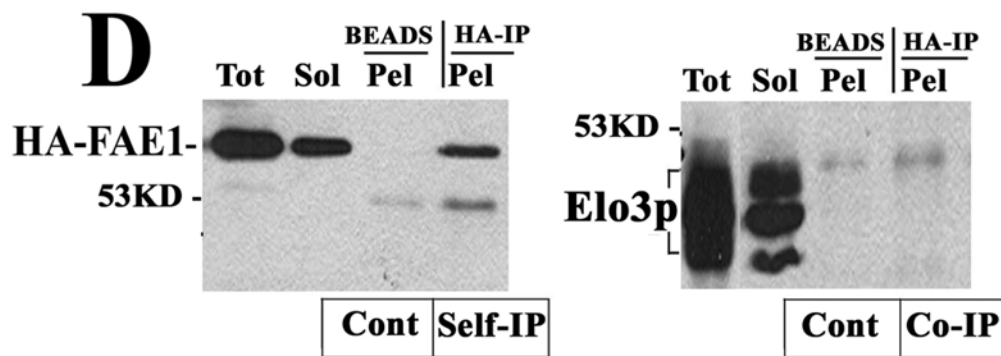
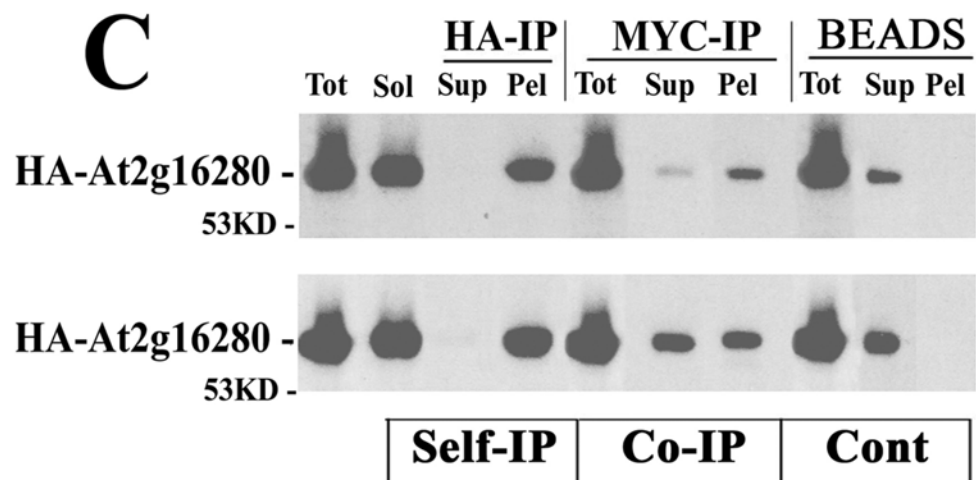


Fig 6C & D

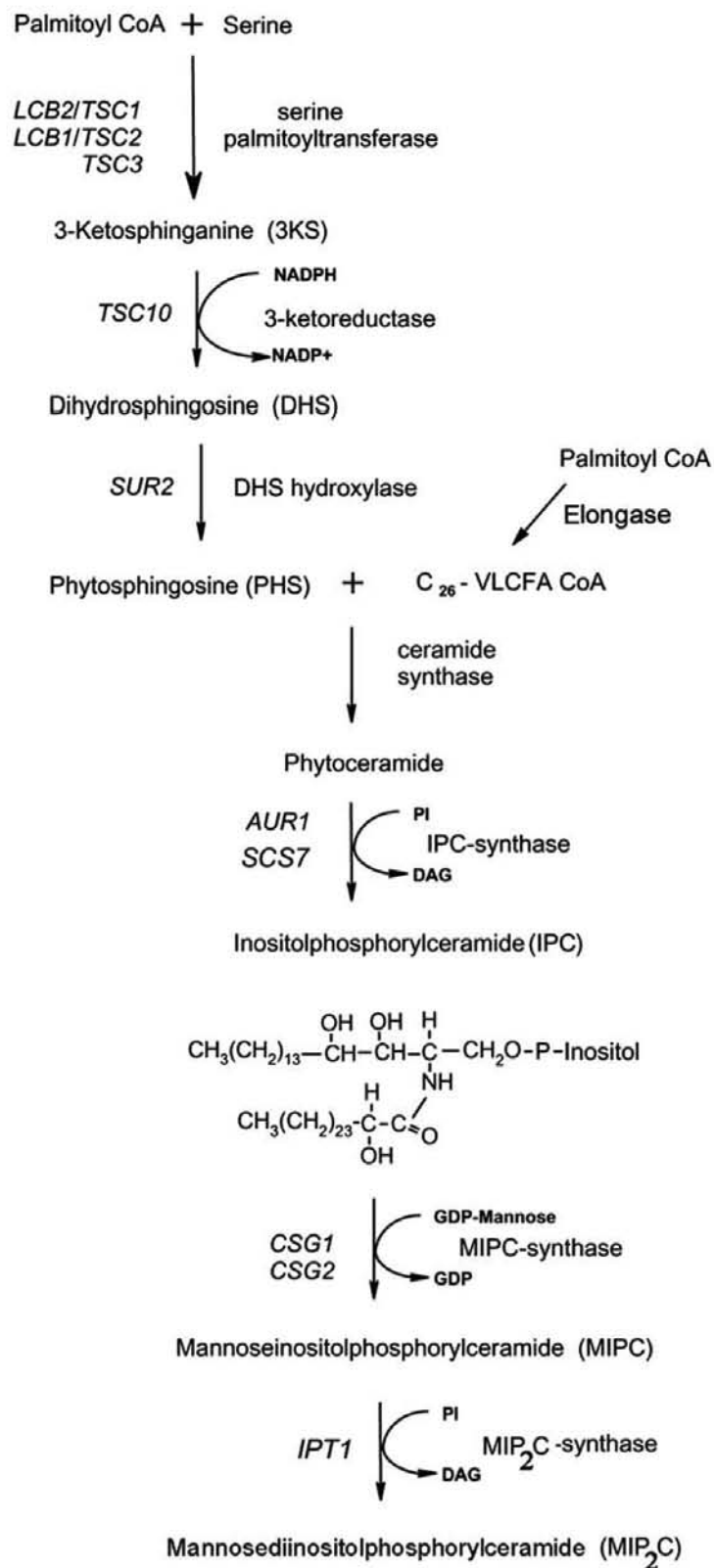


Fig 7A

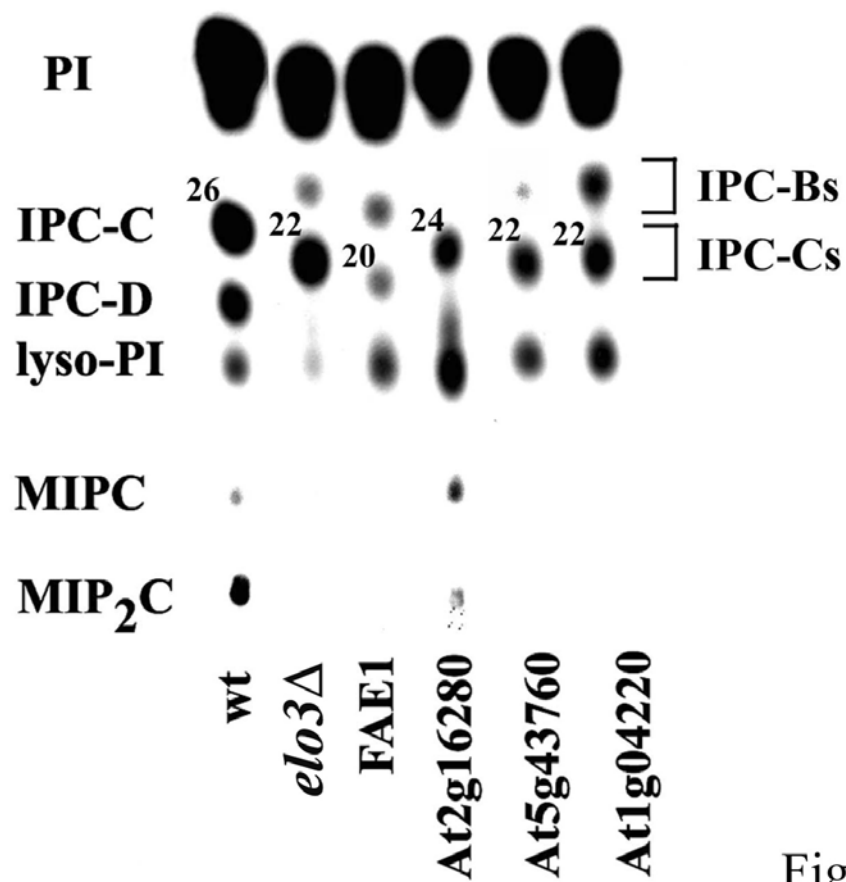


Fig 7B

A Six-Membrane-Spanning Topology for Yeast and Arabidopsis Tsc13p, the Enoyl Reductases of the the Microsomal Fatty Acid Elongating System.

Shilpi Paul, Kenneth Gable and Teresa M. Dunn¹

Department of Biochemistry and Molecular Biology, Uniformed Services University of the Health Sciences, 4301 Jones Bridge Road, Bethesda, MD 20184

Running Title: Transmembrane topology of Tsc13p

Address Correspondence To: Teresa Dunn, ¹Department of Biochemistry and Molecular Biology, Uniformed Services University of the Health Sciences, 4301 Jones Bridge Road, Bethesda, MD 20184, tdunn@usuhs.mil, Phone: 301-295-3592, FAX: 301-295-3512

SUMMARY

The very long chain fatty acids are crucial building blocks of essential lipids, most notably the sphingolipids. These elongated fatty acids are synthesized by a system of enzymes that are organized in a complex within the endoplasmic reticulum membrane. Although several of the components of the elongase complex have recently been identified, little is known about how these proteins are organized within the membrane or about how they interact with one another during fatty acid elongation. In the present study, the topology of the yeast Tsc13p protein, the enoyl reductase of the elongase system, was investigated. The N- and C-termini of Tsc13p are in the cytoplasm and six putative membrane-spanning domains were identified by insertion of glycosylation and factor Xa cleavage sites at various positions. The N-terminal domain including the first membrane spanning segment contains sufficient information for targeting to the endoplasmic reticulum membrane. Studies of the Arabidopsis Tsc13p protein revealed a similar topology. Highly conserved domains of the Tsc13p proteins that are likely to be important for enzymatic activity lie on the cytosolic face of the ER, possibly partially embedded within the membrane.

INTRODUCTION

Cytosolic fatty acid synthases (FAS) catalyze the *de novo* synthesis of the 16 or 18 carbons containing fatty acids (FAs), that are further elongated to very long chain fatty acids (VLCFAs) by a microsomal enzyme system, the elongase. VLCFAs are essential components of cuticular waxes, seed triacylglycerols in plants and several classes of lipids, including the sphingolipids. Sphingolipids function in eukaryotic cells as membrane structural components, in cell interactions with surroundings, and as bioactive molecules involved in signaling and cell regulation. Sphingolipids also interact with sterols to form lipid rafts, which are involved in trafficking of plasma membrane proteins, endocytosis, and protein stability at the cell surface (1-3).

The endoplasmic reticulum (ER) associated elongase system is comprised of four distinct enzymes that sequentially catalyze condensation between a CoA-esterified fatty acyl substrate and malonyl-CoA, a 3-ketoacyl-CoA reduction, a 3-hydroxyacyl-CoA dehydration, and a final enoyl-CoA reduction to yield a fatty acid that is two carbon units longer than the primer (4). Several of the genes encoding components of the elongase system were first identified in *Saccharomyces cerevisiae* (5-9) and later in plants and mammals (10-16). Several studies indicate that the elongase proteins are organized in a complex within the ER (5,7,17). A complete understanding of the

molecular mechanism and organization of the elongase complex will require structural analysis, a challenging prospect owing to the intrinsic technical difficulties associated with the purification and crystallization of membrane proteins. However, in the absence of high-resolution structural data, detailed topology models are important for the design and interpretation of structure-function studies of membrane proteins. Thus, as a first step toward elucidating the organization of the elongase complex we have undertaken the topological mapping of the component proteins. Here we present our studies on the topological organization of the *Saccharomyces cerevisiae* and *Arabidopsis thaliana* Tsc13p proteins, the enoyl-CoA reductases of the elongase complex.

TSC13 was identified in a screen for mutants that suppress the Ca^{2+} sensitivity of *csg2Δ* cells (18). Csg2p is required for conversion of inositolphosphoceramide (IPC) to mannosylinositolphosphoceramide (MIPC) and we discovered several years ago that the overaccumulation of IPC in the *csg2Δ* cells results in calcium sensitivity (18,19). Furthermore, mutations that reduce the overaccumulation of IPC were found to suppress the Ca^{2+} sensitivity, including mutations in the genes required for the VLCFA component of IPC (18,19). The mammalian (14) and plant (10,15) orthologs of Tsc13p have also been identified and characterized.

In the present study, we provide evidence that the N- and C-termini of both the yeast and *Arabidopsis* Tsc13p proteins reside in the cytosol and that these proteins contain six membrane spanning domains. Based on this model, two highly conserved and functionally critical residues are found to be associated with the membrane, raising the possibility that the active site of the enzyme is partially embedded within the lipid bilayer.

EXPERIMENTAL PROCEDURES

Yeast Strains and Media - Yeast media were prepared, and cells were grown according to standard procedures (20). The yeast *Mata*

ura3-52 ade his4 trp1Δ leu2Δ tsc13::TRP/pTSC13-316 strain was used in this study.

Disruption of TSC13 gene and construction of tagged yeast and Arabidopsis TSC13 -

Construction of the *tsc13Δ* mutant and the pTSC13-316 and pMYC-TSC13-426 plasmids were described previously (7). The plasmid expressing the dual epitope-tagged Myc-Tsc13p-HA was generated by moving the 3X-MYC-TSC13 cassette from pMYC-TSC13-426 to pRS425, introducing an in-frame *SpeI* site between codon 309 and the stop codon of the *TSC13* gene by QuikChange mutagenesis (Stratagene), and ligating a *SpeI*-ended 3X-HA cassette into the *SpeI* site.

To generate the 1-117-GFP fusion protein, the MYC-TSC13-425 plasmid containing the *SpeI* at position 309 was digested with *SpeI* and *NheI* to remove the fragment encoding amino acids 117-309 of Tsc13p. The remaining vector fragment was ligated with an *XbaI*-ended fragment encoding GFP (5) and the construct was verified by DNA sequencing.

A yeast plasmid constitutively expressing the 3X-HA-N-terminally tagged *Arabidopsis* gene, At3g55360 (designated hereafter as *AtTSC13*) under control of the *ADH* promoter was generated as described previously (15).

TSC13-GC Topology Reporter Plasmids -

The *TSC13* gene fusion alleles with the invertase glycosylation cassette (Suc2A or GC) inserted were constructed in two steps. In the first step, in-frame *SpeI* restriction sites (encoding Threonine and Serine) were introduced at 12 positions (indicated in Fig. 1) within the *TSC13* gene. For each mutagenesis reaction, the MYC-TSC13-425 plasmid was used as template and a pair of mutagenic primers containing the *SpeI* site flanked by 12 nucleotides of homology to *TSC13* was used. Following mutagenesis and transformation into *E. coli*, plasmids were isolated and screened for the presence of the *SpeI* site. In the second step, a *SpeI*-ended GC (the 53-amino acid domain from the Suc2p protein that has 3 sites for N-linked glycosylation) was inserted into the *SpeI* sites as well as into

an in-frame *NheI* site at position 117. The DNA sequences of all the constructs were verified by sequencing. The GC cassette was inserted at 7 different locations along the *AtTSC13* gene (Fig. 1) using the same strategy.

Construction of TSC13-fXa Fusion Alleles - fXa cleavage sites were inserted using a pair of oligonucleotides encoding a repeat of the fXa protease recognition site (IEGR) that would anneal to leave overhanging ends compatible for ligation into the *SpeI* sites of pMYC-TSC13-425 (described above). The oligonucleotides were annealed by mixing, heating at 95°C for 5 min and cooling on ice. The *TSC13*-fXa fusion alleles were verified by DNA sequencing.

Site-directed Mutagenesis - The *tsc13* mutant alleles with charged residues substituted by alanine were generated by QuikChange mutagenesis (Stratagene). All mutants were confirmed by DNA sequencing.

Complementation Assay - The various Tsc13p-GC, Tsc13p-fXa, alanine substitution mutant, and epitope-tagged Tsc13p proteins were assessed for function by determining whether their expression would complement the lethality of the *tsc13Δ* mutant. Plasmids expressing the modified *TSC13* alleles were introduced into pTSC13-316-rescued *tsc13Δ* mutant cells and the transformants were tested for ability to lose the *URA3*⁺-marked pTSC13-316 rescuing plasmid. Transformants containing plasmids expressing functional Tsc13p proteins were able to lose the *URA3*⁺-marked plasmid and were therefore able to grow on 5-FOA plates.

Determination of the Glycosylation Status of the Tsc13p-GC Fusion Proteins - For analysis of the glycosylation status of the Tsc13p-GC proteins, microsomes were prepared from cells grown in minimal medium (minus leucine) to insure maintenance of the plasmid. The cells, were pelleted, washed with water, resuspended at 2 ml/g wet cell weight and lysed by bead beating in 50 mM Tris, 7.5, 1 mM EGTA,

1 mM β-mercaptoethanol, 1 μM aprotinin, 1 μM phenylmethylsulfonyl fluoride, and 1 μM leupeptin. Glass beads were added to just below the meniscus, and cells were lysed by four cycles (60 s each) of vortexing with cooling on ice between cycles. Unbroken cells, beads, and debris were removed by centrifugation (5000 × g for 10 min), and the low speed supernatant was centrifuged at 100,000 × g for 30 min at 4°C, to provide the microsomal pellet. The pellet was resuspended in the same buffer, repelleted at 100,000 × g for 30 min at 4°C and resuspended at ~10 mg/ml protein in the same buffer containing 33% glycerol. The glycosylation status of the Tsc13p-GC proteins was analyzed as described previously (21,22) with slight modifications. In brief, 100 μg of microsomal protein was suspended in 54 μl of 20 mM Tris-HCl, pH 7.5, containing 5 mM Na₂EDTA, and 50 mM NaCl. Six μl of 10X denaturing buffer (5% SDS, 10% β-mercaptoethanol) were added, and the samples were incubated at 70 °C for 10 min. Ten μl of 0.5 M sodium citrate, pH 5.5 were added to the heated samples to bring the volume to 70 μl, and the samples were split into two aliquots. One aliquot was treated with 5000 units of EndoH (New England Biolabs), and the other aliquot was incubated with buffer. Samples were incubated at 37°C for 60 min., and then further incubated at 70°C for 10 min with denaturing buffer (5% SDS, 10% β-mercaptoethanol). Following resolution by 12% SDS-PAGE, the proteins were analyzed by immunoblotting.

Right-side-out Microsomal Vesicle Preparation and Cleavage with Factor Xa Protease - Preparation of microsomes for analyzing the fusion proteins containing the fXa cleavage sites was performed essentially as described previously (21,22) with minor modifications. Spheroplasts were generated, lysed with lysis buffer, and the homogenates were cleared of debris. The microsomal membrane fraction were recovered by centrifugation at 100,000 × g for 30 min at 4 °C, washed once with storage buffer (20 mM Tris-HCl, pH 7.5, containing 250 mM sorbitol, 50 mM potassium acetate, and 1 mM β-

mercaptoethanol), resuspended in storage buffer at 4 mg/ml protein, and stored at -80 °C. The fXa protease cleavage assay was performed as described (22) and the products were separated by SDS-PAGE and detected by immunoblotting.

Protease Protection Assay - Right-side-out microsomes were prepared from yeast expressing the HA-TSC13-MYC fusion protein. Protease protection assays were performed as described (23) and the samples were resolved by SDS-PAGE and analyzed by immunoblotting.

Cell Fractionation - Microsomes were prepared by bead beating (17) and incubated on ice for 1h with an equal volume of buffer containing either 1M sodium chloride, 0.4M sodium carbonate or 2% Triton X-100. After centrifugation of the samples at $100,000 \times g$ for 30 min at 4°C, the supernatant (S) and the pellet (P) fractions were collected and subjected to SDS-PAGE and immunoblotting.

Immunoblotting - Proteins were resolved using 12 % SDS-PAGE, transferred to nitrocellulose and the blots were blocked in 0.1 M Tris, 7.5, 0.15 M NaCl, 0.1% Tween 20, 5% dry milk. Myc-Tsc13p was detected with horseradish peroxidase-conjugated monoclonal anti-Myc antibodies (Sigma) at 1/2500, the HA-tagged proteins were detected with horseradish peroxidase-conjugated monoclonal anti-HA antibodies (Roche Molecular Biochemicals) at 1/1000, and Kar2p was detected using anti-Kar2p (1:10,000) as the primary antibody followed by incubation with horseradish peroxidase-conjugated goat anti-rabbit antibody (Bio-Rad). The bound antibodies were detected using the ECL detection system (Amersham Biosciences).

Immunofluorescence and Fluorescence Microscopy - Immunostaining of Myc-Tsc13p and fluorescence microscopy of the 1-117-GFP fusion protein were performed as described (5). For detecting Myc-Tsc13p, cells were incubated with a monoclonal anti-Myc antibody (from Invitrogen; 1:200

dilution) followed by the Cy3-conjugated anti-mouse IgG secondary antibody (Sigma; 1:5000).

RESULTS

Membrane Topology Predictions for Tsc13p - Tsc13p, the enoyl reductase of the fatty acid elongation system, is an integral ER membrane protein. Determination of the topology of Tsc13p is an important step toward understanding both its mechanism and its organization within the elongase complex. As is often the case, various algorithms for predicting membrane-spanning segments suggested several possible topologies for Tsc13p. SOSUI, a program that takes into account the Kyte Doolittle hydrophathy, amphiphilicity, amino acid charge, and the length of the protein (24) predicted a single transmembrane domain (TMD) located between amino acids 262-283. In contrast, six TMDs were predicted by both Localizome (86-105, 125-143, 164-184, 204-226, 247-266 and 272-291) and HMMTOP (88-112, 145-162, 169-186, 203-220, 251-269 and 274-291). Localizome uses hmmpfam to detect the presence of Pfam domains (25) and a prediction algorithm, Phobius, to predict the TM helices. The results are combined and checked against the TM topology rules stored in a protein domain database called LocaloDom (26). HMMTOP (Hidden Markov Model for Topology Prediction) is based on the principle that topology of TM proteins is determined by the difference in amino acid distribution in various structural parts of these proteins rather than by specific amino acid composition (27,28). TMHMM, which is also based on a hidden Markov Model (29) predicts four TMDs (166-188, 202-222, 243-265 and 269-291). In the experiments described below, these different models for Tsc13p topology were experimentally evaluated.

Mapping the Orientation of the Tsc13p Termini by Protease Protection - To determine the orientation of the N and C terminal ends of Tsc13p, the N-terminus was tagged by inserting a Myc epitope after the start codon, and the C-terminus was tagged by

inserting an HA epitope before the stop codon. To ascertain that insertion of the epitope tags did not alter the structure of Tsc13p, the function of the epitope-tagged protein was tested. A plasmid expressing the Myc-Tsc13p-HA protein was transformed into *tsc13Δ* cells carrying the wild-type *TSC13* gene on a *URA3*-marked and therefore 5-fluoroorotic acid (5-FOA)-counterselectable plasmid. *TSC13* is an essential gene in *S. cerevisiae* (7) and thus the plasmid carrying the wild-type *TSC13* gene is required for survival of the haploid deletion strain. A *LEU2*-marked plasmid expressing Myc-Tsc13p-HA was transformed into the rescued *tsc13Δ*. 5-FOA resistant colonies that had lost the *URA3*-marked *TSC13* plasmid were recovered indicating that insertion of the N- and C-terminal epitope tags did not disrupt the function of Tsc13p (Fig. 2A). In addition, immunofluorescence localization of the Myc-Tsc13p-HA protein revealed perinuclear and peripheral ER staining (Fig. 2B) similar to that previously observed for wild-type Tsc13p (7).

To localize the N and C termini of Tsc13p with respect to the ER membrane, protease protection assays were conducted. Sealed right-side-out membrane vesicles were isolated by gently lysing yeast spheroplasts prepared from cells expressing Myc-Tsc13p-HA, and sensitivity of the protein to proteinase K in the presence or absence of detergent was examined. The microsomes were digested with proteinase K in the presence or absence of detergent and the Myc-Tsc13p-HA was analyzed by immunoblotting with either anti-Myc or anti-HA antibodies. The immunoblots indicated that both the N-terminal Myc-tag and the C-terminal HA-tag were sensitive to proteinase K even in the absence of detergent as no protected immunoreactive protein fragments were detected in either case (Fig. 3). If the N-terminus had been luminal, a protected Myc fragment should have been observed and similarly if the C-terminus were in the ER lumen, a protected HA-tagged fragment would have been seen. This indicates that both the N- and C-termini of Tsc13p are cytosolically oriented, and that Tsc13p has an even number of membrane spanning domains. The integrity of the sealed

right-side-out vesicles was confirmed by the observation that the ER luminal Kar2p protein was insensitive to proteinase K until the vesicles were disrupted with detergent (Fig. 3). As has been previously reported, in the presence of detergent, proteinase K clipped Kar2p to a smaller size but did not completely degrade it (23). The sidedness of the vesicles was confirmed by demonstrating that fXa protease cleavage sites inserted into the luminal domains of the integral membrane protein, Lcb1p, were inaccessible to the fXa protease unless the vesicles were disrupted with detergent (22).

The Native Glycosylation Sites at Residues 38 and 255 of Tsc13p are not Modified - A well established approach to map the topology of proteins present in the ER takes advantage of the lumen specific glycosylation machinery. The glycosylation status of the two potential N-linked glycosylation sites (NXS/T) at residues 38 and 255 of Tsc13p was evaluated. As shown in Fig. 4A, treatment with endoglycosidase H (EndoH) did not alter the electrophoretic mobility of Myc-Tsc13p and thus the potential N-linked glycosylation sites in the native Tsc13p sequence are not glycosylated. The first predicted TMD lies between residues 86-110; therefore, the lack of modification of the potential glycosylation site at 38 is consistent with the protease sensitivity results and provides further evidence that the N-terminus of Tsc13p is cytosolic. The lack of glycosylation at 255 indicates that this residue is also not in a luminal loop that is accessible to the glycosylation machinery. Several of the hydropathy algorithms (discussed above) place residue 255 within a TMD; this would explain the lack of modification of this potential glycosylation site.

Analysis of Tsc13p-GC Fusion Proteins Reveals Several Membrane-associated Domains - To further investigate the topology of Tsc13p, a set of fusion proteins containing a glycosylation reporter cassette (GC) inserted in-frame at 13 positions along the length of the protein was constructed (Fig. 4A). The cassette consists of a 53-amino acid domain

comprising residues 80-133 of invertase (Suc2p) that contains three NXS/T sites for N-linked glycosylation. These sites are located far enough from the N- and C-terminal ends of the cassette to insure that if the GC is inserted anywhere in the luminal loop of a fusion protein, the acceptor sites will be sufficiently far from the membrane to be efficiently recognized by the glycosylation machinery (21). The locations within Tsc13p into which the cassettes were inserted were chosen based on their ability to distinguish the different topological models predicted by the hydropathy analyses. In addition, alignments of Tsc13p proteins from different species were used in an attempt to identify sites with low conservation across evolution that might be sufficiently flexible to tolerate an insertion without disrupting function (Fig. 1). It is important to point out that this reporter cassette has been successfully used in determining the topology of other membrane proteins (21,22,30) and that its insertion into luminal loops between membrane-spanning domains has not been observed to interfere with their insertion or orientation.

The Tsc13p-GC fusion proteins were evaluated for function by testing their ability to restore viability to the *tsc13Δ* mutant. Tsc13p-GC fusions with the Suc2p domain inserted at 8 different locations were functional (Fig. 4A) indicating that these proteins retained their native conformation. Tsc13p-GC fusions with the cassette inserted at position 135 or 166 resulted in unstable proteins. Although insertion of the cassette at position 159 or 170 resulted in stable proteins, these fusion proteins were not functional (Fig. 4A). Furthermore, indirect immunofluorescence revealed that these two fusion proteins failed to localize to the ER (data not shown). The Tsc13p-GC fusion protein with the cassette at position 273, was also not functional (Fig. 4A), but this protein displayed normal ER localization (data not shown).

The Tsc13p-GC fusion proteins with the cassette inserted at 117, 126, 198 or 273 were glycosylated as indicated by increased electrophoretic mobility following EndoH treatment, and therefore these regions of Tsc13p are localized in the lumen of the ER.

Moreover, the electrophoretic mobilities of the fusion proteins with the GC located at position 7, 69, 226, 236 or 309 were not altered after treatment with EndoH, demonstrating that these regions of Tsc13p are located in the cytosol (Fig. 4A). Although the fusion proteins with the GC at 159 and 170 were not glycosylated, because they were not functional and did not localize properly, it is not possible to definitively conclude that they are normally cytosolic. While these analyses clearly reveal the presence of at least two luminal loops in Tsc13p, it is not clear from these data whether the segment between 126 and 198 forms a single large luminal loop or whether there are additional membrane associated domains within this region of Tsc13p.

Analysis of Tsc13p Topology by fXa Insertion

- To further investigate the topology of Tsc13p, tandem fXa protease cleavage sites (IEGRIEGR) were inserted at several positions (31) and their accessibility to fXa protease in sealed right-side-out membrane vesicles was assessed. A tandem recognition sequence was inserted to increase the probability of cleavage by the fXa protease, which cuts on the C-terminal side of the arginine in the IEGR tetrapeptide. The Tsc13p-fXa fusion proteins were expressed in *tsc13Δ* mutant cells, sealed right-side-out vesicles were prepared, and the sensitivity to fXa protease cleavage was assayed in the absence or presence of detergent. The integrity of the vesicle preparations was verified by showing that the luminal ER protein, Kar2p, was accessible to proteinase K only in the presence of detergent (discussed above). The fXa sites inserted at positions 69, 226 or 236 were accessible to fXa protease whether or not Triton X-100 was present (Fig 4B). This result is consistent with the lack of glycosylation of the GC cassettes inserted at the same positions and confirms the cytoplasmic orientation of these regions of the protein. Furthermore, the protease recognition sites at 117, 198 or 273 were only accessible to the protease when Triton X-100 was present (Fig. 4B), a result that is also consistent with the glycosylation experiments. Taken together, the glycosylation and fXa protease

cleavage results suggest that Tsc13p contains at least four membrane spanning domains located between amino acids 69-117, 198-226, 236-273, and 273-309, and that the N- and C-termini are cytosolic (Fig. 4C). This agrees with the hydrophobicity data and the Localizome and HMMTOP algorithms, which predicted the presence of TMDs between amino acids 88-108, 204-224, 248-268, and 270-290. It is likely that there are two additional TMDs located between 126 and 198, but this could not be demonstrated using these methods because the insertion of GC and fXa recognition sequences into this region of Tsc13p resulted in unstable, nonfunctional and/or mislocalized proteins. The possibility that there are additional membrane domains between 126 and 198 is addressed below.

Evidence for Additional TMDs between Residues 126 and 198 of Tsc13p - To determine whether the segment of Tsc13p between residues 126 and 198 is a large luminal domain or whether it contains additional membrane associated segments, fXa cleavage sites were inserted after residue 117 and after residue 200 such that this fragment could be cut out of Tsc13p and its membrane association could be assessed. The fXa-flanked segment of Tsc13p also had an HA tag inserted at 198 for immunodetection (Fig. 5A). This HA-tagged Tsc13p with the two fXa cleavage sites retained the ability to rescue the *tsc13Δ* mutant and therefore it was assumed to adopt its native topology. Microsomes were prepared from the *tsc13Δ* mutant cells expressing the tagged Tsc13p using a bead beating procedure that generates inverted vesicles. The segment between residues 117 and 200 was liberated from the protein with fXa protease, the microsomes were subjected to high speed centrifugation, and the pellets and supernatants were analyzed for the presence of the HA-tagged fragment (Fig. 5B). Four distinct bands were detected with the anti-HA antibody, the sizes of which were consistent with the full-length tagged Tsc13p, the products from cleavage at one or the other of the fXa sites, and the 117-200 amino acid fragment derived from cleavage of both fXa sites. In samples incubated with buffer alone,

the 117-200 fragment of Tsc13p was found exclusively in the pellet. Furthermore, the 117-200 fragment of Tsc13p was found to be integrally associated with the membrane because 1% Triton X-100, but neither 0.5 M NaCl nor 0.1 M sodium carbonate, solubilized it (Fig. 5B). These results clearly showed that the 117-200 fragment of Tsc13p is not a luminal loop but rather that it contains additional membrane associated domains. Taken together, the data are therefore most consistent with the presence of six-membrane-spanning domains in Tsc13p (Fig. 5C).

The N-terminal Membrane Spanning Domain of Tsc13p is Sufficient for ER Localization - Polytopic membrane proteins are initially targeted to the ER by a signal sequence that may include the first TMD, and subsequent TMDs often contain information that directs insertion and contributes to the topogenesis (32). To determine whether the first hydrophobic segment of Tsc13p contains sufficient information to direct membrane association, a chimeric protein with the N-terminus including TMD1 of Tsc13p (amino acids 1-117, with a Myc tag after the first codon) was fused to GFP. When expressed in yeast, this chimera showed a typical ER localization pattern (Fig. 6A), similar to that of wild-type Tsc13p (Fig 2D). The Tsc13p1-117-GFP chimeric protein fractionated with membranes and behaved as an integral membrane protein in that it could only be solubilized with detergent (Fig. 6B). Taken together, the fluorescence localization and solubilization studies show that the N-terminal 117 amino acids of Tsc13p, which contains the first TMD, has sufficient information to direct ER membrane targeting and association.

The Arabidopsis Tsc13p is also a Six-membrane Spanning Protein - Comparison of the hydropathy predictions of the *S. cerevisiae* Tsc13p with the *A. thaliana* orthologue, AtTSC13 encoded by the At3g55360 gene that was previously shown to complement the yeast *tsc13Δ* mutant and to be involved in VLCFA synthesis in plants (10,15), suggested that the proteins are likely to have the same topologies. To investigate the topology of the

AtTSC13 protein, HA-AtTSC13 and several HA-AtTSC13-GC fusion proteins were expressed in yeast and their glycosylation was investigated. Neither of the two endogenous glycosylation sites located at N76 and N244 were glycosylated, nor were the GCs inserted after amino acid 80, 159, 218 or 310. On the other hand, the GCs inserted after amino acid 122, 182 and 258 were glycosylated since their electrophoretic mobilities increased following EndoH treatment (Fig. 7A). These results are entirely consistent with the presence of six membrane spanning domains in AtTSC13, and thus indicate that the Arabidopsis and yeast proteins have similar topologies (Fig. 1, 5C & 7B).

Alanine Substitutions of Conserved Charged Residues in or near the TMDs of Tsc13p - A comparison of the amino acid sequences of Tsc13p homologs from Arabidopsis, H. sapiens and S. cerevisiae revealed the presence of several highly conserved amino acids including several charged residues near or within the predicted TMDs (Fig. 1 & Fig. 5C). To examine the physiological significance of several of these amino acids, alanine substitution mutants were generated and tested for their ability to complement tsc13Δ.

Despite their high conservation, several of these residues were not critical for function since the alanine substitution mutants, K76A, D77A, Y103A, H137A, E144A, H149A and E259A (Fig. 8A) and E91A (data not shown), were able to complement the *tsc13Δ* mutant. On the other hand, the Y138A, K140A and R141A mutants were not functional (Fig. 8A). Immunoblot analysis revealed that the Y138A mutant protein was unstable, but the K140A and R141A mutant proteins were present at similar levels to wild-type Tsc13p (data not shown).

The K140, R141 residues are predicted to lie in or near the cytosolic end of TMD2 (Fig. 5). It was therefore of interest to determine whether their mutation altered the topology of Tsc13p. This was investigated by introducing the K140A and R141A mutations into the Tsc13p-GC reporter proteins with the GC at 117, 198 and 226. The results indicated that

these mutations did not alter the membrane topology of Tsc13p (Fig. 8B). Thus, it appears that although the K140 and R141 residues are critical for function, they are not required for proper topogenesis of Tsc13p.

Tsc13p has three cysteine residues at 90, 165 and 220, of which C165 is conserved. Individual substitution of each cysteine to serine did not disrupt function, nor did the simultaneous substitution of all three residues since the triple cysteineless mutant was also able to complement *tsc13Δ* (data not shown).

DISCUSSION

The topology of Tsc13p, the enoyl-CoA reductase of the ER-associated elongase system was investigated by several approaches. Since the exact features of membrane proteins that dictate how they insert into membranes are not fully understood, the available algorithms for predicting membrane topologies can only serve as heuristic guides for the actual topology. Various programs predicted different numbers of membrane-spanning domains (1, 4 or 6) for Tsc13p. Our results are most consistent with a six membrane-spanning model which places both the N and the C-termini of Tsc13p in the cytosol. We also evaluated the topology of the Arabidopsis Tsc13p ortholog and find that it has a similar membrane topology to that of the yeast Tsc13p.

The accessibility of the epitope tags at both ends of Tsc13p to proteinase K in sealed right-side out vesicles together with the absence of any protected epitope-tagged fragments suggested that both ends are cytosolically oriented. The absence of glycosylation at N38, which is a potential site for glycosylation, provided further evidence that the N-terminus is cytosolic. However, glycosylation sites can be obscured by their proximity to the membrane or by association with other proteins (33), so to rule out the possibility that N38 might reside in the lumen but escape glycosylation, we utilized the Suc2p glycosylation cassette. This 53-amino acid domain contains three N-linked glycosylation sites that are located far enough from the N- and C-terminal ends of the

cassette to insure their recognition by the glycosylation machinery. Cassettes inserted at the N- (positions 7 and 69) and C- (position 309) termini were not glycosylated confirming the conclusion from the protease protection studies. Assignment of the C-terminus to the cytosol is also consistent with two other studies. In an effort to determine the topology of the *S. cerevisiae* membrane proteome (30), a topological reporter cassette (Suc2p/His4C) was fused at the C-terminus of many membrane proteins, including Tsc13p. The lack of glycosylation, along with catalytic activity of the His4Cp domain, indicated that the reporter at the C-terminus of Tsc13p was cytosolic. In another study aimed at identifying interactions between yeast membrane proteins (34), Tsc13p with a split ubiquitin domain fused at the C-terminus was found to interact with other appropriately tagged elongase proteins. Such an interaction is reflected by cleavage of the reconstituted ubiquitin by a cytosolic protease and therefore further confirms that the C-terminus of Tsc13p is in the cytosol.

Our glycosylation and factor Xa results provide strong evidence that the regions of Tsc13p comprised of amino acids 85-110, 202- 222, 243-269 and 274-291 contain membrane spanning domains. Since the majority of the topological reporter cassette-containing fusion proteins were capable of complementing the *tsc13Δ* mutant, it is likely that these proteins are adopting the native Tsc13p topology. Moreover, the cytosolically-oriented N-terminal 85-amino acid tail together with the first predicted membrane spanning domain located between residues 85 and 110 contains sufficient information to target a cytosolic GFP to the ER providing clear evidence for the presence of a transmembrane domain, TMD 1, in this region.

Because all insertions between residues 126 and 198 resulted in mislocalization and/or disruption of function, it was unclear whether this segment of Tsc13p represented a long luminal domain or whether, as predicted by several algorithms, there were additional membrane spanning domains in this region. Since there is one TMD before residue 126

and three after residue 198 and both ends of Tsc13p are cytosolic, the presence of any additional TMDs in this region would require an even number, most likely two. We provided evidence for additional membrane associated segments within this region by proteolytically cleaving it from the full length Tsc13p and showing that the released fragment remained associated with the membrane fraction. The membrane association of this liberated fragment is apparently not a result of interaction with other membrane proteins because it was stable to high salt and pH, but could be solubilized with detergent.

The inability to detect a luminal loop between residues 126 and 198 leaves open the possibility that there are membrane embedded rather than membrane spanning domains in this region of Tsc13p. However, because the analysis of the Arabidopsis ortholog of Tsc13p provides evidence for the presence of a luminal loop in the region analogous to the yeast 126 to 198 segment (discussed below), we favor a topological model with six membrane spanning domains (Fig. 5C). This topology is consistent with the predictions of the Localizome and HMMTOP prediction programs, although these programs differ in their prediction of the precise location of TMD2. Localizome places it between residues 125-143 and HMMTOP places it between residues 145-162. We have indicated the uncertainty about the location of TMD2 using the *dashed line* in Fig. 5C. However, it seems likely that TMD2 is located between 125 and 143 because the corresponding regions of the plant and mammalian orthologs are also predicted to contain a membrane spanning domain. Furthermore, this topology would place the highly conserved domain that contains the functionally important K140 and R141 residues identified in this study near the cytosolic face of TMD2 where it could act in conjunction with the conserved cytosolic domain immediately preceding TMD1. This later domain contains the Q81 residue that when mutated to lysine reduces enoyl-reductase activity (7).

The plant and mammalian Tsc13p orthologs have hydrophilicity profiles that are

similar to that of the yeast protein. As mentioned above, HMMTOP predicts six TMDs in Arabidopsis Tsc13p located in similar relative positions and with the same orientation as those in yeast except that the fifth predicted TMD of AtTSC13 is more N-terminal suggesting that the third cytoplasmic loop is shorter and the third luminal loop longer in comparison to yeast Tsc13p. Our topological analysis of the AtTSC13 protein expressed in yeast is fully consistent with this model. HMMTOP also predicts six TMDs and a very similar overall topology for the human Tsc13p ortholog.

Several recent studies have indicated that membrane spanning segments of proteins are often flanked by tryptophan residues because of their propensity to localize to the interface between the polar and hydrophobic layers of the phospholipid bilayer (35). It is therefore of interest to note that several of the predicted transmembrane domains of Tsc13p are flanked by tryptophan residues (*purple circles*, Fig. 5C). While in many cases the arabidopsis and mammalian Tsc13p orthologs lack a similarly positioned tryptophan residue (Fig. 1), there are often either tyrosines or phenylalanines (which also often flank membrane spanning domains) located in equivalent positions near the ends of the predicted membrane spanning domains.

Based on our topology model of Tsc13p, the three cysteine residues in the protein all lay near the cytosolic side of the membrane (*yellow circles*, Fig. 5C). Since cysteines often serve as covalent binding sites for acyl-CoAs, we tested whether any of the cysteines were critical for function by substituting them with serine. Each of the single mutants and the triple cysteineless mutant was functional suggesting that these

residues do not participate directly in catalysis. However, it should be emphasized that the assay for function was the ability to complement the *tsc13Δ* mutant and thus we cannot conclude that these residues are not required for optimal activity of Tsc13p.

There is nothing known about the mechanism of Tsc13p or about its active site and it bears no similarity with the well characterized enoyl-ACP reductase of the soluble FAS system. Furthermore, although the C-terminus of Tsc13p shares significant homology with steroid-5 α reductase and both enzymes catalyze the reduction of a double bond that is α,β to a carbonyl group, Tsc13p lacks the predicted NADPH binding site that is present in steroid-5 α reductase. In this study, several conserved charged residues present in highly conserved regions (*blue shading* in Fig. 5C) as well as some conserved charged residues that are predicted to lie in the TMDs were substituted with alanine. We identified two residues, K140 and R141, which are critical for function but not for stability or topogenesis, while the Y138A mutation rendered Tsc13p unstable. Our topology studies suggest that these residues lie in or at the cytosolic face of TMD2. It is also worth pointing out that several of the insertions into the 126 to 198 region of Tsc13p abolished function. Although it is tempting to speculate that these two highly conserved domains contribute to the formation of an active site at the cytosolic face of the ER membrane or possibly extending into the membrane, the precise functions of these highly conserved domains of the *trans*-2,3-enoyl CoA reductases remain to be determined. In conclusion, our topology study has established the foundation for further structure-function studies on Tsc13p.

REFERENCES

1. Wang, Q., and Chang, A. (2002) *Proc Natl Acad Sci U S A* **99**, 12853-12858
2. Simons, K., and Toomre, D. (2000) *Nat Rev Mol Cell Biol* **1**, 31-39
3. Ikonen, E. (2001) *Curr Opin Cell Biol* **13**, 470-477.
4. Poulos, A. (1995) *Lipids* **30**, 1-14
5. Han, G., Gable, K., Kohlwein, S. D., Beaudoin, F., Napier, J. A., and Dunn, T. M. (2002) *J Biol Chem* **277**, 35440-35449.
6. Beaudoin, F., Gable, K., Sayanova, O., Dunn, T., and Napier, J. A. (2002) *J Biol Chem* **277**, 11481-11488.
7. Kohlwein, S. D., Eder, S., Oh, C. S., Martin, C. E., Gable, K., Bacikova, D., and Dunn, T. (2001) *Mol Cell Biol* **21**, 109-125.
8. Oh, C. S., Toke, D. A., Mandala, S., and Martin, C. E. (1997) *J Biol Chem* **272**, 17376-17384.
9. Toke, D. A., and Martin, C. E. (1996) *J Biol Chem* **271**, 18413-18422
10. Zheng, H., Rowland, O., and Kunst, L. (2005) *Plant Cell* **17**, 1467-1481
11. Zhang, X. M., Yang, Z., Karan, G., Hashimoto, T., Baehr, W., Yang, X. J., and Zhang, K. (2003) *Mol Vis* **9**, 301-307
12. Xu, X., Dietrich, C. R., Lessire, R., Nikolau, B. J., and Schnable, P. S. (2002) *Plant Physiol* **128**, 924-934.
13. Tvrdik, P., Westerberg, R., Silve, S., Asadi, A., Jakobsson, A., Cannon, B., Loison, G., and Jacobsson, A. (2000) *J Cell Biol* **149**, 707-718
14. Moon, Y.-A., and Horton, J. D. (2003) *J. Biol. Chem.* **278**, 7335-7343
15. Gable, K., Garton, S., Napier, J. A., and Dunn, T. M. (2004) *J Exp Bot* **55**, 543-545
16. Beaudoin, F., Michaelson, L. V., Hey, S. J., Lewis, M. J., Shewry, P. R., Sayanova, O., and Napier, J. A. (2000) *Proc Natl Acad Sci U S A* **97**, 6421-6426.
17. Paul, S., Gable, K., Beaudoin, F., Cahoon, E., Jaworski, J., Napier, J. A., and Dunn, T. M. (2006) *J Biol Chem* **281**, 9018-9029
18. Beeler, T., Bacikova, D., Gable, K., Hopkins, L., Johnson, C., Slife, H., and Dunn, T. (1998) *J Biol Chem* **273**, 30688-30694
19. Zhao, C., Beeler, T., and Dunn, T. (1994) *J Biol Chem* **269**, 21480-21488
20. Sherman, F., Fink, G. R., and Hicks, J. B. (1986) *Methods in Yeast Genetics*, Cold Spring Harbor Laboratory, Cold Spring Harbor
21. Gilstring, C. F., and Ljungdahl, P. O. (2000) *J Biol Chem* **275**, 31488-31495
22. Han, G., Gable, K., Yan, L., Natarajan, M., Krishnamurthy, J., Gupta, S. D., Borovitskaya, A., Harmon, J. M., and Dunn, T. M. (2004) *J Biol Chem* **279**, 53707-53716
23. Romano, J. D., and Michaelis, S. (2001) *Mol Biol Cell* **12**, 1957-1971
24. Hirokawa, T., Boon-Chieng, S., and Mitaku, S. (1998) *Bioinformatics* **14**, 378-379
25. Bateman, A., Birney, E., Durbin, R., Eddy, S. R., Howe, K. L., and Sonnhammer, E. L. (2000) *Nucleic Acids Res* **28**, 263-266
26. Lee, S., Lee, B., Jang, I., Kim, S., and Bhak, J. (2006) *Nucleic Acids Res* **34**, W99-103
27. Tusnady, G. E., and Simon, I. (1998) *J Mol Biol* **283**, 489-506
28. Tusnady, G. E., and Simon, I. (2001) *Bioinformatics* **17**, 849-850

29. Krogh, A., Larsson, B., von Heijne, G., and Sonnhammer, E. L. (2001) *J Mol Biol* **305**, 567-580
30. Kim, H., Melen, K., Osterberg, M., and von Heijne, G. (2006) *Proc Natl Acad Sci U S A* **103**, 11142-11147
31. Wilkinson, B. M., Critchley, A. J., and Stirling, C. J. (1996) *J Biol Chem* **271**, 25590-25597
32. Goder, V., Bieri, C., and Spiess, M. (1999) *J Cell Biol* **147**, 257-266
33. Nilsson, I., and von Heijne, G. (2000) *J Biol Chem* **275**, 17338-17343
34. Miller, J. P., Lo, R. S., Ben-Hur, A., Desmarais, C., Stagljar, I., Noble, W. S., and Fields, S. (2005) *Proc Natl Acad Sci U S A* **102**, 12123-12128
35. Yau, W. M., Wimley, W. C., Gawrisch, K., and White, S. H. (1998) *Biochemistry* **37**, 14713-14718

FOOTNOTES

Acknowledgements

This work was supported by an NSF 2010 Collaborative grant to TMD, a USUHS Graduate Student Research Grant to SP and an American Heart Association predoctoral fellowship to S.P. We thank Gongshe Han, Frederic Beaudoin and Dr. Jeffrey Harmon for helpful discussions.

The abbreviations used are: FAS, fatty acid synthase; FASI, fatty acid synthase type I; FA, fatty acid; VLCFA, very long-chain fatty acids; SPL, sphingolipid; ER, endoplasmic reticulum; IPC, inositolphosphorylceramide; HA, hemagglutinin; GFP, green fluorescent protein; GC, glycosylation cassette; fXa, factor Xa; TMD, transmembrane domain; EndoH, endoglycosidase H; FOA, 5-fluoroorotic acid; SC, prefix designating a *Saccharomyces cerevisiae* gene or gene product; At, prefix designating an *Arabidopsis thaliana* gene or gene product.

FIGURE LEGENDS

Figure 1. Sites of insertion of the GC cassettes into the yeast and *Arabidopsis* Tsc13p - An alignment of the human (human-TER), plant (*Arabidopsis thaliana*, At-Tsc13p), and yeast (*Saccharomyces cerevisiae*, SC-Tsc13p) Tsc13ps was used to predict locations within the protein that might accommodate insertion of the GC without disrupting function. The residues after which the GC was inserted are marked *green* for functional proteins, *blue* for non-functional but stable proteins or *red* for unstable proteins. The highly conserved residues are shaded *black*. The *blue asterisks* mark the residues identified as critical for function in this study and the *orange asterisk* (Q81) marks a residue previously shown to be important for function (7).

Figure 2. Myc-Tsc13p-HA is functional and ER localized - **A.** The *tsc13Δ* mutant is unable to lose the pTSC13-316 plasmid and is therefore unable to grow on FOA. Introduction of the *LEU2*-marked plasmid expressing the epitope-tagged MYC-Tsc13p-HA protein (but not the empty vector) allowed the *tsc13Δ* mutant to lose the *URA3*-marked pTSC13-316 plasmid and to grow on FOA. **B.** Indirect immunofluorescence shows that Myc-Tsc13p-HA localizes to the ER. Fixed and permeabilized cells were incubated with anti-myc antibody and the primary antibody was detected using Cy3-conjugated goat anti-mouse as the secondary antibody.

Figure 3. The N- and C-terminal ends of Tsc13p are located in the cytosol. Right-side-out microsomal vesicles were prepared from yeast expressing Myc-Tsc13p-HA and the vesicles were mock treated (*lane 1*), incubated with Triton X-100 (*lane 2*), or treated with proteinase K in the absence (*lane 3*) or presence of 0.4% Triton X-100 (*lane 4*). Myc-Tsc13p, Tsc13p-HA and Kar2p were detected with anti-myc-HRP (*top*), anti-HA-HRP (*middle*) and anti-Kar2p (*bottom*) antibody, respectively.

Figure 4. Topology Reporters Indicate the Presence of Several Membrane Spanning Domains in Tsc13p. **A.** The glycosylation status of the topological reporter Tsc13p-GC fusion proteins reveals the presence of at least four membrane-spanning domains. With the exception of the fusion proteins with the GC cassette inserted after amino acid 135, 159, 166, 170 and 273 the Tsc13p-GC proteins complemented the *tsc13Δ* mutant (indicated by growth on FOA). Microsomes were prepared from the *tsc13Δ* mutant yeast expressing the Tsc13p-GC fusion proteins, 10 μg of microsomal protein (with or without endoH treatment) was resolved by 12% SDS-PAGE, and the fusion proteins were detected using anti-myc. All the samples were run on the same gel except for the sample expressing the fusion with the GC inserted at position 159, which was run on a different gel. **B.** Factor Xa protease cleavage of Tsc13p-fXa fusion proteins confirms the topology of Tsc13p. Sealed right-side out microsomal vesicles were prepared from cells expressing Tsc13p-fXa proteins with a tandem repeat of the factor Xa cleavage sites inserted at the indicated positions. The microsomes were mock-digested or digested with factor Xa protease in the absence or presence of Nonidet P-40 (NP-40) on ice for 3 h. 10 μg of protein was resolved by 12% SDS-PAGE and the Myc-tagged full length or N-terminal fragments of Tsc13p were detected by immunoblotting with anti-myc antibodies. **C.** A schematic model of Tsc13p according to the results of the glycosylation and factor Xa protease susceptibility experiments. The cassette insertion sites are denoted by circles. The locations of the experimentally determined TMDs are denoted and marked 1-4. The dashed line indicates the region of Tsc13p whose topology (whether luminal or membrane embedded) cannot be resolved from the results in panels A and B.

Figure 5. The Segment of Tsc13p comprised of residues 117-200 Contains Additional Membrane Associated Domains Resulting in the Depicted Topology Model for yeast Tsc13p - **A.** Schematic representation of inside-out microsomal vesicles expressing Tsc13p with an HA

tag at 198 and fXa cleavage sites inserted after residue 117 and 200. **B.** Microsomes were prepared by bead-beating yeast cells expressing the Tsc13p with fXa cleavage sites at 117 and 200. Following incubation with fXa protease on ice for 6h, the microsomes were subjected to high speed centrifugation at 100,000 x g and the supernatant (S; lane 1) and pellet (P; lane 1) were recovered. The membrane fraction was incubated with buffer (lane 2), 0.5 M sodium chloride (lane 3), 0.2 M sodium carbonate (lane 4) and 1% Triton X-100 (lane 5) and the 100,000 x g supernatant (S) and the pellet (P) were collected and resolved by 12% SDS-PAGE. Four bands (A-D) were detected by immunoblotting with an anti-HA antibody. These represent the full length fusion protein (band A), the protein cleaved only at the fXa site at position 200 (band B), only at the fXa site at position 117 (band C) or at both fXa sites (band D). **C.** A six-membrane-spanning topology model for yeast Tsc13p. Each *circle* denotes a single amino acid, the *blue circles* denote the residues where inserted GC were not glycosylated, the *black filled circles* denote the residues where GC were glycosylated. The conserved residues that when substituted with alanine did not or did disrupt function are marked by the *green* or *red circles*, respectively. The 3 cysteine residues (at 90, 165 and 220) are marked by *yellow circles* and the tryptophan residues are marked by *purple circles*. The Q81 residue that is mutated to K in a reduced function allele of *TSC13* is indicated by the *orange circle*. The two intrinsic N-linked glycosylation sites, N38 and N255 that were not glycosylated are indicated as “Ns”. The residues predicted to lie at the ends of the TMDs are indicated. The uncertainty as to the location of TMD2 is indicated by the *dashed line*. The two highly conserved regions of Tsc13p are marked by the *blue shading*.

Figure 6. The N-terminal 117 amino acids of Tsc13p Contains the ER Targeting Signal - A. Schematic representation (left) showing the N-terminal 1-117 domain (containing TMD1; *black box*) of Tsc13p fused to the N-terminus of GFP. For immunodetection, the Myc epitope was inserted after the start codon of Tsc13p. Fluorescence microscopy revealed that the N-terminal 1-117 domain of Tsc13p conferred a typical ER localization pattern to the appended GFP protein. **B.** The 1-117-GFP fusion protein behaves as an integral membrane protein. Microsomes were prepared from yeast expressing the Myc-1-117-GFP fusion. After high speed centrifugation the membrane fraction was incubated with buffer (lane 1), 0.5 M sodium chloride (lane 2), 0.2 M sodium carbonate (lane 3) and 1% Triton X-100 (lane 4) and the 100,000 x g supernatant (S) and the pellet (P) were collected, resolved by 12% SDS-PAGE and the protein was detected by immunoblotting with anti-myc antibody.

Figure 7. Membrane Topology of the *Arabidopsis thaliana* Tsc13p (AtTSC13) - A. The glycosylation status of several AtTSC13-GC fusion proteins was assessed as described above for the yeast Tsc13p-GC fusion proteins. Briefly, microsomes were prepared from yeast expressing the indicated AtTSC13p-Suc2p fusion proteins, 10 µg of microsomal protein (with or without EndoH treatment) were resolved by 12% SDS-PAGE, transferred to nitrocellulose and the fusion proteins were detected using anti-HA antibodies. **B.** Proposed six-membrane-spanning topology model for the *A. thaliana* TSC13 ortholog. The circles represent the amino acids after which the GC was inserted.

Figure 8. Mutational Analysis of Yeast Tsc13p - A. Several conserved charged residues (*colored circles* in Fig. 5C) were mutated to alanine and the mutant Tsc13p proteins were tested for function by the complementation assay (see Experimental Procedures). **B.** The glycosylation status of Tsc13p-GC fusion proteins carrying the K140A and R141A mutations was assayed. Microsomes were prepared from yeast harboring Tsc13p-GC fusion proteins (GC after amino acid 117, 198 or 226) with either the K140A or R141A mutation as indicated. 10 µg of microsomal protein (with or without EndoH treatment) was resolved by 12% SDS-PAGE, and Tsc13p proteins were detected by immunoblotting with anti-myc.

Human-TER:MKHYEVEIIIDAKTREKICFLDKVEPHATIAEIKNLFTKTHPQWYFARQSLRIDPKGKS-----IK : 60
 At-Tsc13p:---MKVTVVSRSGREVIKAPLDLPDSATVADLQEAHHRRAKKFYPSRQRLTLPVTPGSKDKPVVIN : 63
 Sc-Tsc13p:----MPITIKSRSGIRDEIDLSKKPTLDVLLKKISANNHNISKYRIRLYKKESKQ-----V : 55

Human-TER:DEDVLQKLPVC--TTATLYFRDLGAQISWVTVFLTEYAGPIFIYLLFYFRVFIYGHKYDFTSSRH : 124
 At-Tsc13p:SKKSLKEYCDGNNSLTVVEKDLGAQVSYRTLFFFEYLGPLLIPVFYFYPVYKFLGYCEDCVIH : 128
 SC-Tsc13p:PVISSESFQEEADSMEFFIKDLGPQISWRIVFFCEYLGPVLVHSLFYLLSTIPTVVDRWHASD : 121
 *

Human-TER:T---VVHLACICHSEHYIKRILETLFVHRFSGTPIRNI FKNCTYYWGEAAWMAYYIN----- : 180
 At-Tsc13p:p---VQTYAMYWCYHYFKRILETEFVHRFSHATSPIGNVFRNCAYYWSFCAYIAYIVN----- : 184
 SC-Tsc13p:YNPFTNRVAYELIGHYGKRILETLFVHQFSLATMPINLFKNCHYWLSGLISFGYFGYGFPFG : 187
 **

Human-TER:--HPLYTEPTYGAQVVKLALALFVICQLGNFSIHMALRDLR-PAGSKTRKTFYPTKNPFTWLFLV : 243
 At-Tsc13p:--HPLYTE--VSDLQMKIGFCFGLVCQVANFYCHILLNLRDESGAGGYQIPR-----GELFNIV : 240
 SC-Tsc13p:NAKLFKYYSYIKLDDLSTLIGLVLSELWNFYCHIKLRWGDYQKKHGNAKTRVPLN--QGIFNLF : 251

Human-TER:SCPNYTYEVGSWIGFALMTQC-LPVALFSLVGFTQMTIWAQKGRHSYLKEER-----DYPPLRMP : 302
 At-Tsc13p:TCANYTTEIYQWLGFNATQT-IAGYVFLAVAALIMINWALGKHSRLRKIDGKDQKPKYPRRWI : 305
 SC-Tsc13p:VAPNYTTEVWSWIWETVFKFLFAVLFLTVSTAQYAWAQKKK-----KYHTREAF : 304

Human-TER:LTLPFLL : 308
 At-Tsc13p:LTLPFLL : 310
 SC-Tsc13p:LTLPFVF : 310

Fig. 1

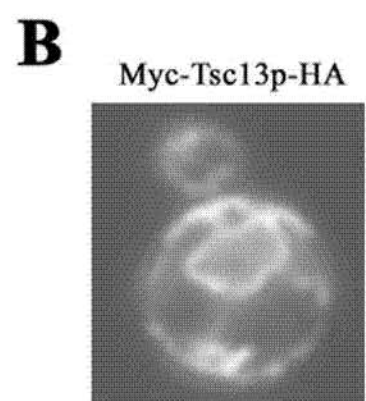
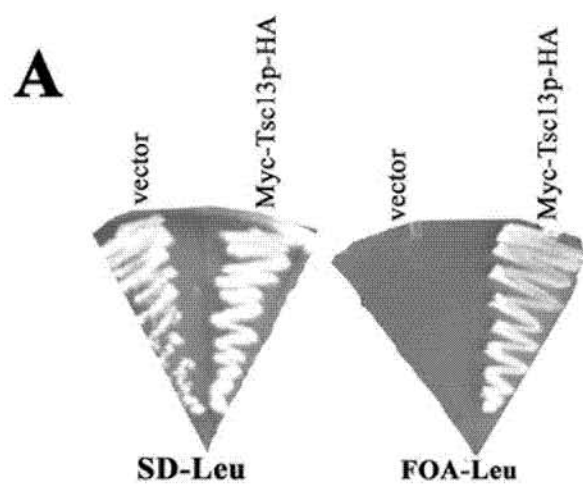


Fig 2

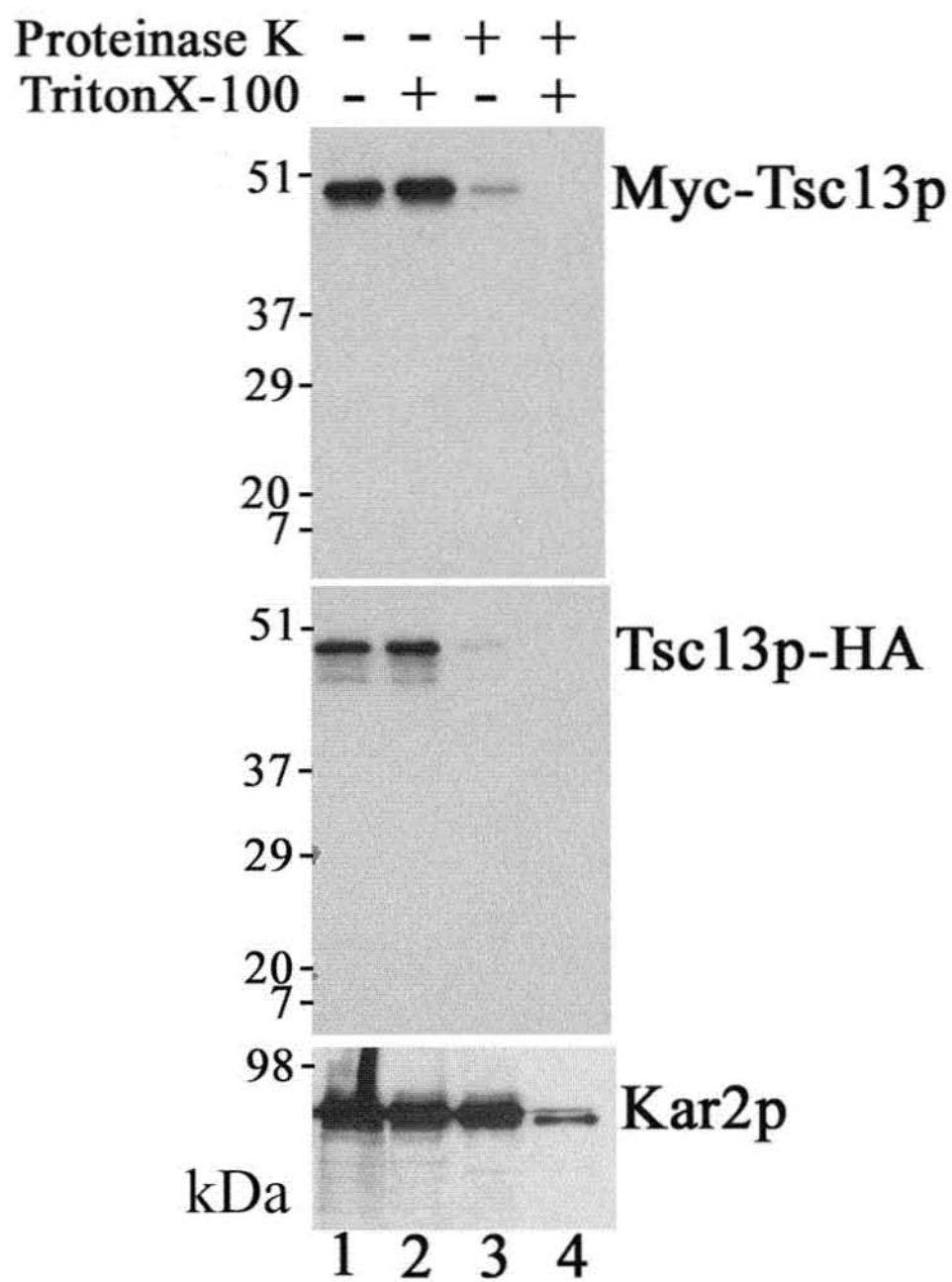
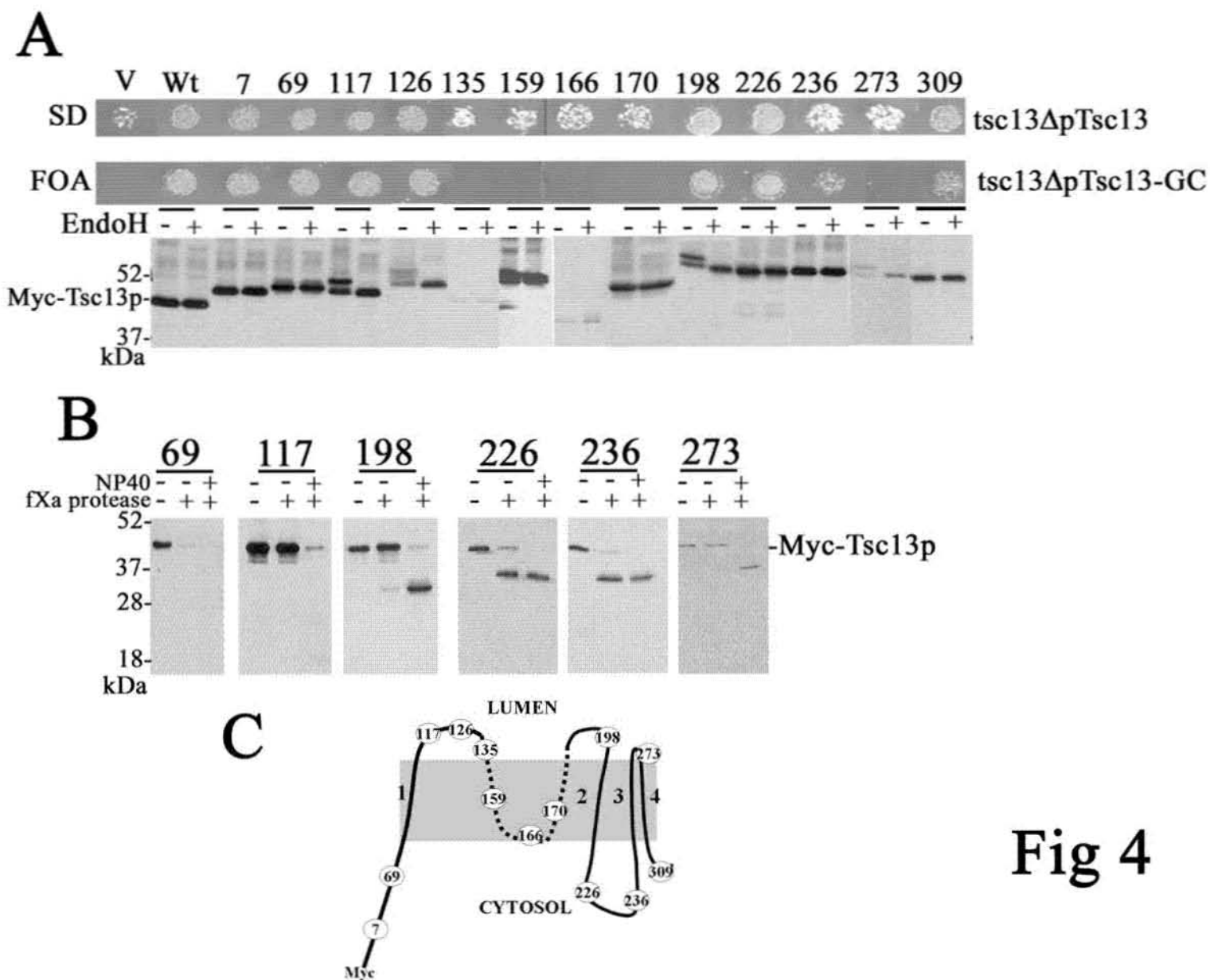


Fig 3



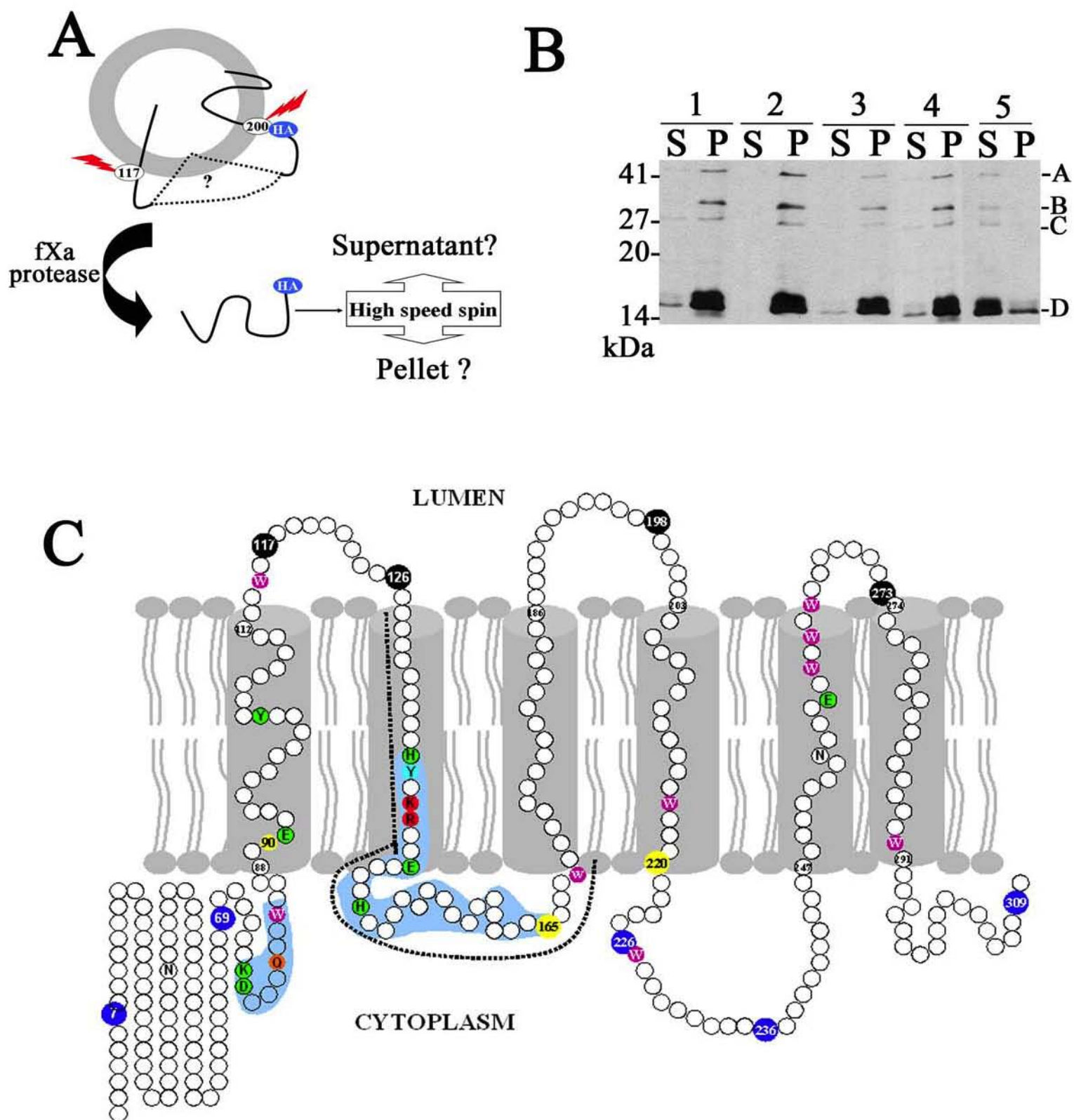


Fig 5

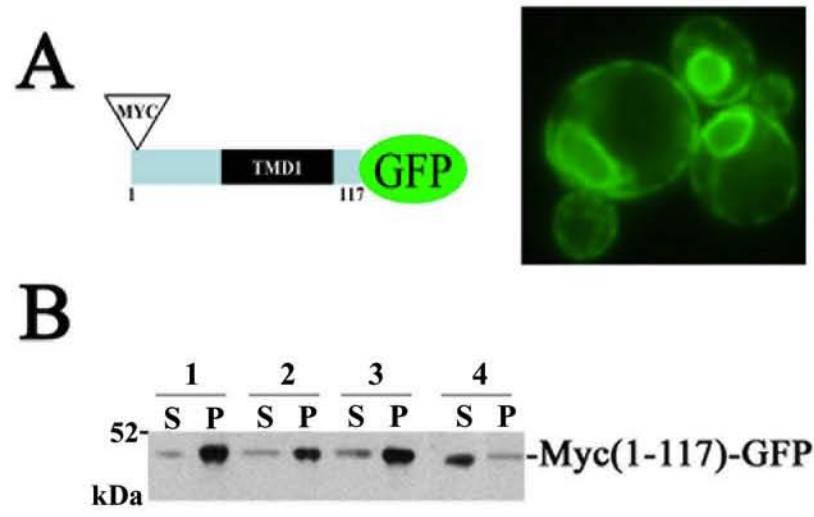


Fig 6

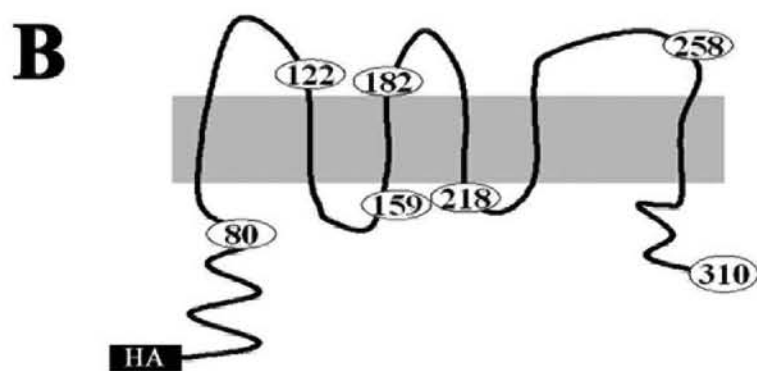
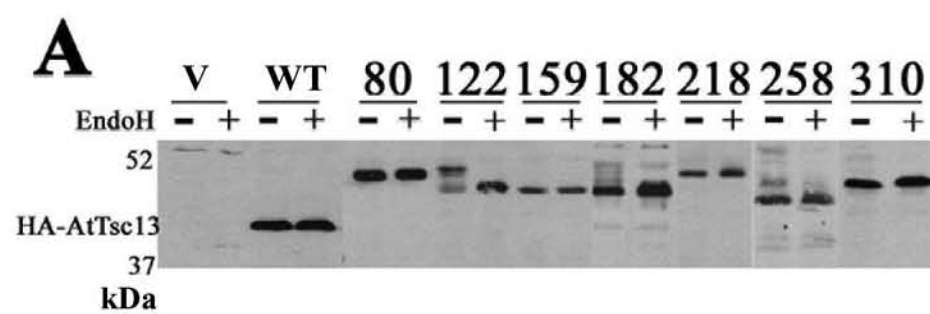
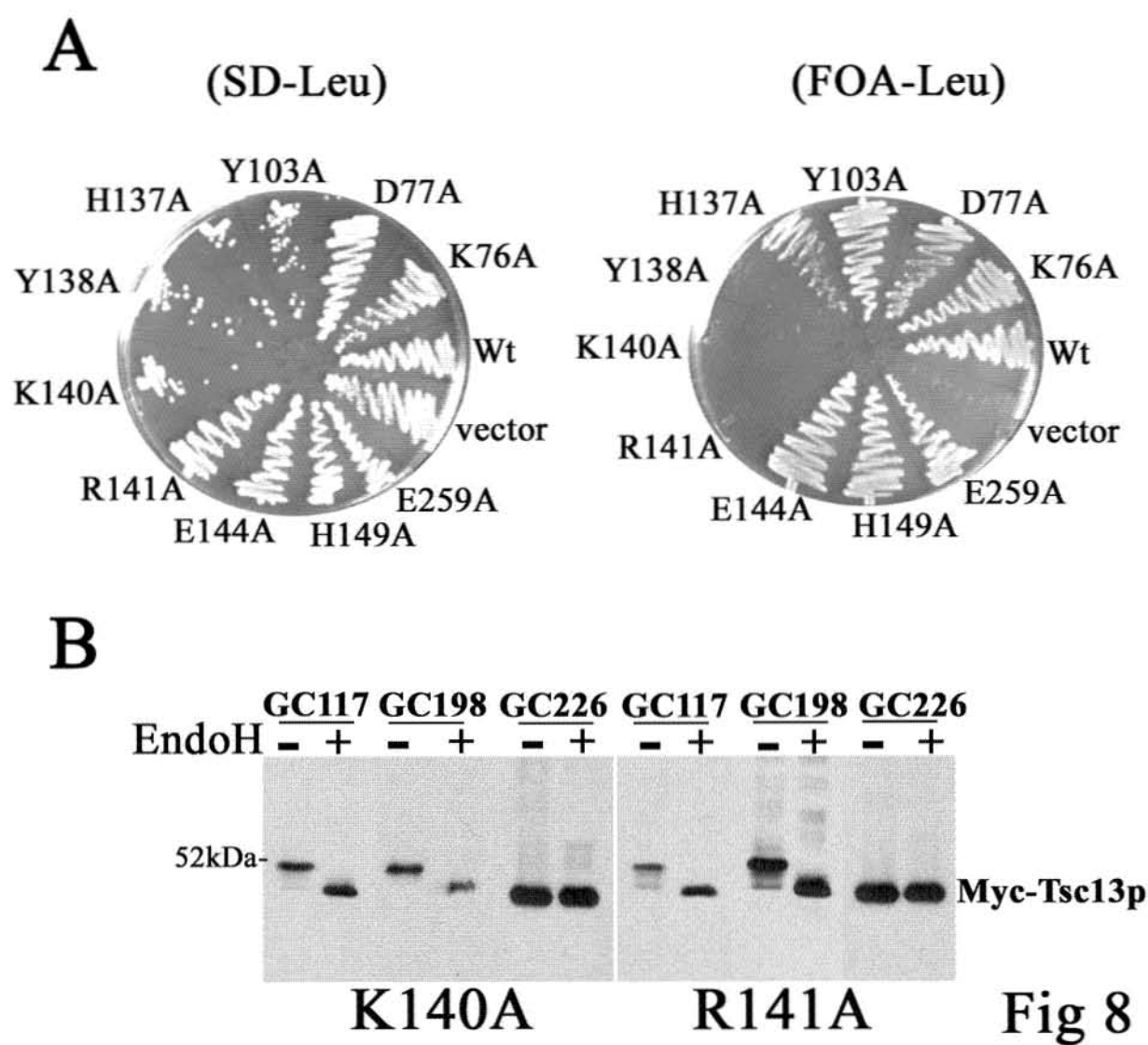


Fig 7



Topological Analysis of *Saccharomyces cerevisiae* Ybr159p, the Major 3-ketoreductase of the Microsomal Fatty Acid Elongating System

Shilpi Paul, Kenneth Gable and Teresa M. Dunn¹

Department of Biochemistry and Molecular Biology, Uniformed Services University of the Health Sciences, 4301 Jones Bridge Road, Bethesda, MD 20184

Running Title: Transmembrane topology of Ybr159p

Address Correspondence To: Teresa Dunn, ¹Department of Biochemistry and Molecular Biology, Uniformed Services University of the Health Sciences, 4301 Jones Bridge Road, Bethesda, MD 20184, tdunn@usuhs.mil, Phone: 301-295-3592, FAX: 301-295-3512

SUMMARY

The very long chain fatty acids are major acyl components of sphingolipids in humans and yeast. These fatty acids are generated by a microsomal chain-elongating enzyme system, called the elongase. Although several genes encoding the enzymes required for the biochemical steps of fatty acid elongation have been identified, the membrane bound nature of the elongase proteins has hindered their purification. In this study the topology of the Ybr159p protein, which is the major 3-ketoreductase of the elongase system in *Saccharomyces cerevisiae*, was investigated. The results indicate that both the N- and C-termini of the protein are cytosolic and that the protein is tightly associated with the endoplasmic reticulum by membrane associated domains located in the N-terminus. The active site, including the NADPH binding site, of Ybr159p is in the cytoplasm. The C-terminally located dilysine motif was found to be absolutely required for endoplasmic reticular retention of Ybr159p.

INTRODUCTION

Very long chain fatty acids (VLCFAs) are essential components of cuticular waxes and seed triacylglycerols in plants and of several classes of lipids, most notably, the sphingolipids in all eukaryotic cells. The VLCFAs are synthesized by an endoplasmic reticulum (ER) membrane associated elongase complex, which is comprised of four distinct enzymatic activities that sequentially catalyze condensation between a CoA esterified fatty acyl substrate and malonyl-CoA, a 3-ketoacyl-CoA reduction, a 3-hydroxyacyl-CoA dehydration, and a final enoyl-CoA reduction to yield a fatty acid that is two carbon units longer than the primer [24]. Several genes encoding the enzymes of the elongase system have been identified, although the dehydratase component remains unidentified.

The *YBR159w* gene was identified by screening yeast mutants that were knocked out for candidate 3-keto reductase genes for loss of elongated polyunsaturated fatty acids (PUFAs) that were produced by heterologous expression of *Pea1p*, a PUFA elongase enzyme of *C. elegans* [3]. *Ybr159p* showed limited homology to human estradiol-17 β -hydroxysteroid dehydrogenase (17 β -HSD) (32% similarity), a member of the short-chain alcohol dehydrogenase superfamily [3]. *Ybr159p* orthologs were identified from several organisms, and all contain a diagnostic NAD(P)H binding motif [4], a Y-X₃-K motif identified as catalytically essential for 17 β -HSD [4], and a predicted dilysine ER retention motif at the carboxy terminus. The *ybr159 Δ* yeast mutant shared several phenotypes that had been observed in other fatty acid elongation deficient mutants, including low C26 fatty acid levels, the accumulation of long chain bases (LCBs) and the presence of ceramides with fatty acyl chains of 16 to 22 carbons rather than the C26-ceramides of wild-type yeast [9, 16, 22]. Furthermore, *in vitro* elongation assays conducted using microsomes prepared from the *ybr159 Δ* mutant cells showed a specific defect in 3-ketoreductase activity, further confirming that *YBR159w* encodes the major 3-ketoreductase of VLCFA synthesis [9].

Two orthologs of *YBR159w* from maize (*Zea mays L.*), *gl8a* and *gl8b*, were found to be

required for the normal accumulation of cuticular waxes on seedling leaves. Mutant plants lacking both of these genes showed a defect in embryonic development [5]. Although the *ybr159Δ* mutant grew poorly, it was viable, indicating the presence of another protein with 3-ketoreductase activity that could participate in fatty acid elongation. The deletion of the *AYR1* gene encoding a 1-acyl-dihydroxyacetone-phosphate reductase homolog [1] together with the *ybr159Δ* mutation led to synthetic lethality, suggesting that Ybr1p might possess the residual 3-ketoreductase activity of fatty acid elongation[9].

Ybr159p was shown to be an ER-membrane associated protein and to coimmunoprecipitate and colocalize with other elongase proteins, Elo3p and Tsc13p [9]. To understand the molecular mechanism of Ybr159p and its organization within the membrane and within the elongase complex, information about the structure of the protein is needed. However, the high hydrophobic nature of the elongase proteins has hindered their purification. In the absence of high-resolution structural data, detailed topological models are important for the design and interpretation of structure-function studies of membrane proteins. In the present study, several approaches were used to provide a detailed topological analysis of Ybr159p. The results indicate that both the N- and C-termini of Ybr159p face the cytosol and that there are two membrane spanning domains in the N-terminus. Based on this model, the predicted active site, comprised of the NAD(P)H binding and the YX₃K catalytic motifs is located in the cytosol.

EXPERIMENTAL PROCEDURES

Yeast Strains and Media - Yeast media were prepared, and cells were grown according to standard procedures [26]. The yeast strain used in this study was *Mata ybr159::TRP1 ura3-52 trp1 leu2 lys2* (TDY 1590).

Disruption of the YBR159w gene and construction of a tagged yeast YBR159 -

The dual epitope tagged Myc-Ybr159p-HA was generated by introducing a *NheI* after residue 347 on the plasmid MYC-YBR159-426 by QuikChange XL site-directed mutagenesis

(Stratagene), and ligating a *SpeI*-ended 3X-HA cassette into the *NheI* site. To generate 1-343-GFP fusion protein, an *NheI* site was inserted after residue 343 in the MYC-YBR159-426 plasmid. The plasmid was digested with *NheI* and an *XbaI*-ended GFP-encoding fragment containing a stop codon [10] was ligated into the *NheI* site. All constructs were verified by DNA sequencing.

YBR159-SUC2 Topology Reporter Plasmids – *YBR159w* gene fusion alleles with the invertase glycosylation cassette (Suc2A or GC) inserted were constructed in two steps. In the first step, in-frame *NheI* restriction sites were introduced at 11 positions (indicated in Fig. 1) within the *YBR159w* gene. For each mutagenesis reaction, the MYC-YBR159-426 plasmid was used as template and a pair of mutagenic primers containing the *NheI* site flanked by 12 nucleotides of homology to *YBR159w* was used for the mutagenesis. Following mutagenesis and transformation into *Escherichia coli*, plasmids were isolated and screened for the presence of the *NheI* site. In the second step, a *SpeI*-ended GC cassette encoding the 53-amino acid domain from the Suc2p protein that has 3 sites for N-linked glycosylation was inserted into the *NheI* sites created in step 1. All constructs were verified by DNA sequencing.

Construction of YBR159-fXa Fusion Alleles – factor Xa cleavage sites were inserted into the *NheI* sites that were introduced into the MYC-YBR159-426 plasmid (described above). Pairs of oligonucleotides were designed that would anneal to encode a repeat of the fXa protease recognition site (IEGR) and have overhanging ends suitable for ligation into the *NheI* sites of pMYC-YBR159-426 (described above). The oligonucleotides were annealed by mixing, heating at 95°C for 5 min and cooling on ice. The *YBR159-fXa* fusion alleles were verified by DNA sequencing.

Membrane Based Split-ubiquitin Assay - The yeast strains (L40 and AMR 70) carrying the yeast expression plasmids p415-Cub-PLV and p414-HA2-NubG-ADH1 with Cub-PLV or NubG fused before the stop codon of the elongase genes were a generous gift from Stanley Fields (HHMI, University of Washington, Seattle, WA 98195). The *MATa* L40 strain that contained either the empty p415-Cub-PLV vector or a vector with the Cub-PLV fused to the elongase genes was

pairwise crossed with the *MATα* AMR70 strain that contained either the empty p414-HA2-NubG-ADH1 vector or a vector with NubG fused to the elongase genes. The diploids were selected media lacking leucine and tryptophan, grown to an A_{600} of 0.5 and diluted (1/5000) into the wells of a microtiter plate. The cells were transferred to plates containing media lacking leucine and tryptophan or to plates containing media lacking leucine, tryptophan, and histidine and containing 3 mM 3-amino-1,2,4-triazole (if required). The plates were incubated at 30°C for 7 days prior to photographing. Protein-protein interactions were indicated by histidine prototrophy as described [20].

Determination of the Glycosylation Status of the Ybr159p-Suc2p Fusion Proteins - Microsomes were prepared by bead beating and the glycosylation status of the *Ybr159p-Suc2p* fusion proteins was analyzed as described previously [10], except that the samples were incubated at 70°C for 10 min with denaturing buffer both prior to adding EndoH and before loading onto the gel.

Right-side-out Microsome Vesicle Preparation and Cleavage with Factor Xa Protease - Preparation of microsomes for analyzing the fusion proteins containing the fXa cleavage sites was performed essentially as described by Romano and Michaelis [25] with minor modifications. Spheroplasts were generated, lysed with lysis buffer, and the homogenates were cleared of debris. The microsomal membrane fraction was recovered by centrifugation at 100,000Xg for 30 min at 4°C, washed once with storage buffer (20 mM Tris-HCl, pH 7.5, containing 250 mM sorbitol, 50 mM potassium acetate, and 1 mM β -mercaptoethanol), resuspended in storage buffer at 4 mg/ml protein, and stored at -80°C. The fXa protease cleavage assay was performed as previously described [10] and the products were separated by SDS-PAGE and detected by immunoblotting.

Protease Protection Assay – Right-side-out microsomes were prepared from yeast expressing Myc-Ybr159p-HA fusion protein. Protease protection assays were performed as described [25] and the samples were resolved by SDS-PAGE and analyzed by immunoblotting.

Immunoblotting-- Proteins were resolved using 12% SDS-PAGE, transferred to nitrocellulose and the blots were blocked in 0.1M Tris, pH7.5, 0.15M NaCl, 0.1% Tween 20, 5 % dry milk. The Myc-Ybr159p was detected with horseradish peroxidase-conjugated monoclonal anti-Myc antibodies (Sigma) at 1/2500, HA-tagged proteins were detected using horseradish peroxidase-conjugated monoclonal anti-HA antibodies (from Roche Molecular Biochemicals) at 1/1000 and Kar2p was detected using anti-Kar2p (1:10,000) primary antibody followed by incubation with horseradish peroxidase-conjugated goat anti-rabbit antibody (Bio-Rad). The bound antibodies were detected by the ECL detection system (Amersham Biosciences).

Fatty Acid Analysis—Cells (5×10^8) in mid-logarithmic growth were harvested and resuspended in 100 μ l of distilled H₂O along with C21 and C23 fatty acids as internal standards. Fatty acids were extracted, and the fatty acid methyl esters were prepared as previously described [16]. Gas chromatography/mass spectrometry (GCMS) was performed using an HP-6890 Series GC system with a Supelcowax 10 column, coupled to an HP-5973 Mass Selective Detector.

Immunofluorescence and Fluorescence Microscopy - Fluorescence microscopy of the Ybr159p:1-343-GFP fusion protein was performed as described previously [9]. Staining for visualization of the Golgi apparatus with BODIPY-TR ceramide (Invitrogen) was performed following the manufacturer's protocol with minor modifications. Yeast expressing the Ybr159p:1-343-GFP plasmid were grown overnight in selective media. Cells were collected in the logarithmic phase, washed, and incubated at 4°C for 30 minutes with 5 μ M ceramide/BSA in the selective media. The ceramide/BSA complex was prepared by the following procedure: an approximately 1 mM sphingolipid stock solution in chloroform:ethanol (19:1 v/v) was prepared. 50 μ L of sphingolipid stock solution was dispensed into a small glass test tube and dried under a stream of nitrogen, which was redissolved in 200 μ L of absolute ethanol. 3.4 mg of defatted BSA was added to 10 ml of selective media and mixed by agitating on a vortex mixer. Following incubation in the ceramide/BSA media, the cells were rinsed several times with ice-cold medium and incubated in fresh selective medium at 37°C for an additional 30 minutes. The cells were washed with fresh

medium and examined using an IX70 inverted fluorescence microscope (Olympus) equipped with a HiQ fluorescein filter set (for GFP, excitation/emission was 460–490 nm/510 nm; for BODIPY TR excitation/emission was 510–550 nm/590 nm) and a Planapochromatic X100 oil immersion objective lens and a 100-watt mercury lamp. Images were collected with a Princeton Instruments 5-MHz MicroMax cooled CCD camera, a shutter and controller unit, and IPLab software (version 3.5; Scanalytic Co.). Signals from the fluorescein isothiocyanate (Ybr159-GFP) and BODIPY-TR ceramide fluorescence channels were merged to unveil colocalization of signals. The BODIPY-TR ceramide showed prominent labeling of the Golgi apparatus and weaker labeling of other intracellular membranes.

RESULTS

Membrane Topology Predictions for Ybr159p – Ybr159p, the major 3-ketoreductase of the fatty acid elongation system, is an integral ER membrane protein. Determination of the topology of Ybr159p is an important step toward understanding both its mechanism and its organization within the elongase complex. Ybr159p shows similarity with the short-chain dehydrogenase/reductase (SDR) family members. While many SDRs are soluble enzymes, 11 β -hydroxysteroid dehydrogenase (HSD) is an ER-associated enzyme. The structures of several soluble SDRs have been solved including that of the soluble domain of 11 β -HSD1. There are two isoforms of HSD. The 11 β -HSD1 isoform has a single N-terminal membrane spanning domain that is oriented such that the N-terminus is in the cytosol and the remainder of the protein, including the active site, is in the lumen. Remarkably, the N-terminus of 11 β -HSD2 is in the lumen and it is followed by three N-terminal membrane spanning domains such that the majority of this isozyme, including the catalytic domain faces the cytoplasm.[21]. Thus, the HSDs are unusual as their active sites including the NADPH binding sites of the two isoforms are located on opposite sides of the membrane. The contradicting topologies of the two isoforms of HSD highlights the importance of experimentally establishing the topology of the homologous

Ybr159p protein.

Based on the Kyte-Doolittle hydropathy plot shown in Fig. 1A, the N-terminus of Ybr159p contains high hydrophobic peak with hydrophobicity value ~ 2.0 , while rest of the protein is amphiphilic in nature. Several programs including SOSUI, localizome and TMHMM predicted a single membrane spanning domain situated between residues 20-45, and placed the N-terminus in the cytosol and the C-terminus in the lumen (Fig. 1B). SOSUI is a program that takes into account the Kyte Doolittle hydropathy, amphiphilicity, amino acid charge, and the length of protein sequence (limited to 20-5000 amino acids) [11]. Localizome uses hmmpfam (software for biological sequence analysis) to detect the presence of Pfam domains [2] and a prediction algorithm, Phobius, to predict the TM helices. The results are combined and checked against the TM topology rules stored in a protein domain database called LocaloDom [19]. TMHMM, is based on a hidden Markov Model [17]. Other computer algorithms predicted more complex topologies. For example, HMMTOP predicted three additional membrane spans (169-186, 203-220 and 309-328) with both ends located in the cytosol while TmPRED predicted two membrane spans between 20-54 and two more between 170 and 225, with the N-terminus in the cytosol (Fig. 1B). TmPRED identifies and scores putative transmembrane segments in a query protein by comparing its sequence with a database of experimentally defined transmembrane segments [27]. HMMTOP (Hidden Markov Model for Topology Prediction) is based on the principle that topology of TM proteins is determined by the difference in amino acid distribution in various structural parts of these proteins rather than by specific amino acid composition [28, 29]. In the experiments described below, these possible topological models for Ybr159p were experimentally evaluated.

Mapping the Orientation of the Ybr159p Termini by Protease Protection - To determine the orientation of the N and C terminal ends of Ybr159p, the N-terminus was tagged by inserting a Myc epitope after the start codon, and the C-terminus was tagged by inserting an HA epitope

before the stop codon. To ascertain that insertion of the epitope tags did not alter the structure of Ybr159p, the function of the epitope-tagged protein was tested. A plasmid expressing the Myc-Ybr159p-HA protein was transformed into *ybr159Δ* cells, fatty acids were extracted and analyzed by GCMS (see “Experimental Procedures”). As shown in Fig. 2, the *ybr159Δ* mutant shows reduced levels of C₂₆ fatty acid and accumulation of 3-OH fatty acids of different chain lengths (C₁₆, C₁₈ and C₂₀) [9]. However, expression of Myc-Ybr159p-HA restored wild-type fatty acid content by lowering the level of the 3-OH (C₁₆, C₁₈ and C₂₀) fatty acids (Fig. 2) and restoring the C₂₆, indicating that insertion of the N- and C-terminal epitope tags did not disrupt the function of Ybr159p.

To localize the N- and C-termini of Ybr159p with respect to the ER membrane, protease protection assays were conducted. Sealed right-side-out ER membrane vesicles were isolated by gently lysing yeast spheroplasts prepared from cells expressing Myc-Ybr159p-HA, and sensitivity of the protein to proteinase K in the presence or absence of detergent was examined. The microsomes were digested with proteinase K and analyzed by immunoblotting with either anti-Myc or anti-HA antibodies. The immunoblots indicated that both the N-terminal Myc-tag and the C-terminal HA-tag were sensitive to proteinase K even in the absence of detergent as no protected immunoreactive protein fragments were detected in either case (Fig. 3).

If the N-terminus had been luminal, a protected Myc fragment of at least 8 kDa (consisting of Myc and the first 45 amino acids, if 20-45 is the first TMD) should have been observed and similarly if the C-terminus were in the ER lumen, a protected HA-tagged fragment would have been seen. This indicates that both the N- and C-termini of Ybr159p are cytosolically oriented, and that Ybr159p has an even number of membrane spanning domains. The integrity of the sealed right-side-out vesicles was confirmed by the observation that the ER luminal Kar2p protein was insensitive to proteinase K until the vesicles were disrupted with detergent. As has been previously reported, in the presence of detergent, proteinase K clipped Kar2p to a smaller size but did not completely degrade it [25].

Mapping the Orientation of the C-terminal by Split-ubiquitin Yeast Two-hybrid Approach - The membrane-based split-ubiquitin method has been used to study protein-protein interactions between membrane bound proteins. The system utilizes complementation between separable domains of ubiquitin, the N-terminal domain (Nub, amino acids 1-34) and the C-terminal domain (Cub, amino acids 35-76), which is followed by a transcription factor (PLV) that if liberated can activate expression of reporter genes (*HIS3* and *LacZ*) [13]. Wild-type Nub (NubI, with I being isoleucine at position 13) spontaneously assembles with Cub-PLV, resulting in proteolytic cleavage at the C terminus of Cub-PLV by a ubiquitin-specific protease(s) and subsequent release of the PLV transcription factor. However, a mutant of Nub (NubG) in which the isoleucine at 13 is changed to glycine has reduced affinity for the Cub-PLV domain and reconstitution of the ubiquitin becomes dependent upon the fusion of the Nub and Cub domains to two interacting proteins that bring the two halves of ubiquitin together. As a result, the interaction between two proteins can be monitored by the cleavage and subsequent activation of the reporter genes (Fig. 4A). A prerequisite of the split-ubiquitin system is that Nub and Cub domains must be fused to the membrane protein such that they are oriented in the cytosol because the ubiquitin-specific protease(s) is a cytosolic enzyme. A recent study reported the use of this split-ubiquitin approach to study the topological features of the yeast oligosaccharyl transferase subunits [30]. We have previously reported that Ybr159p associates with other components of the ER-associated elongase system, including Elo3p and Tsc13p [9]. To investigate the orientation of the C-terminus of Ybr159p, the NubG or the Cub-PLV domain was fused to the C-terminus of Ybr159p and to the C-termini of the Elops and Tsc13p. The C-termini of the Elops and Tsc13p were chosen for tagging based on evidence that the C-terminal ends of these proteins are cytosolic (our unpublished data). Furthermore, in a recent study to determine the topology of the *S. cerevisiae* membrane proteome, a topological reporter cassette (Suc2p/HIS4C) was fused at the C-terminus of several proteins. The lack of glycosylation of the Suc2p along with the catalytic activity of the

His4Cp domain, indicated that the reporter at the C-terminus of all three Elops and the Tsc13p proteins was cytosolic [15]. Yeast strains expressing either Ybr159p-NubG or Ybr159p-Cub-PLV were mated with strains expressing the Cub or NubG domains fused to the C-termini of several other elongase proteins. The diploids were selected and screened for their ability to grow on plates lacking histidine. If the NubG and Cub-PVL-fused elongase proteins are able to interact, the PLV transcription factor is liberated and the *HIS3* reporter gene can be expressed, allowing the strain to grow in media lacking histidine. Our results indicate an interaction of the Ybr159p-NubG (or Cub-PLV) with both Tsc13p-Cub-PLV (or Tsc13p-NubG) and the Elops (tagged with ½ Ub on the C-terminus) (Fig. 4B). These results provide additional evidence that the C-terminus of Ybr159p is located in the cytoplasm.

The Native Glycosylation Sites at Residues 173 and 325 of Ybr159p are not Modified – An established approach to map the topology of ER proteins takes advantage of the lumen specific glycosylation machinery. The glycosylation status of the two potential N-linked glycosylation sites (NXS/T) at residues 173 and 325 of Ybr159p was evaluated. As shown in Fig. 6A, treatment with endoglycosidase H (EndoH) did not alter the electrophoretic mobility of Myc-Ybr159p and thus the potential N-linked glycosylation sites in the native Ybr159p sequence are not glycosylated. The lack of glycosylation at residue 325 is consistent with the assignment of the C-terminus of Ybr159p to the cytosol.

Analysis of Ybr159pGC Fusion Proteins Reveals Membrane-associated Domains at the N-terminus- To further investigate the topology of the Ybr159p, a set of fusion proteins containing a glycosylation reporter cassette (GC) inserted in-frame at 11 positions (Fig. 5) along the length of Ybr159p was constructed (Fig. 6A). The cassette consists of a 53-amino acid domain comprising residues 80-133 of invertase (Suc2p) that contains three NXS/T sites for N-linked glycosylation. These sites are located far enough from the ends of the cassette to insure that if the GC is inserted

anywhere in the luminal loop of a fusion protein, the acceptor sites will be sufficiently far from the membrane to be recognized by the glycosylation machinery [8]. The cassettes were inserted into Ybr159p at positions that would make it possible to distinguish the different topological models predicted by the hydropathy analyses (Fig. 1B). In addition, by inserting the cassette into sites within Ybr159p that are not highly conserved in Ybr159p orthologs, we sought to identify sites that might be sufficiently flexible to tolerate an insertion without disrupting function (Fig. 5).

A restriction site (*NheI*) encoding two amino acids was inserted at different locations of the protein for further insertion of the topology reporter cassette. The GC cassette with compatible ends was ligated to these restriction sites. The Ybr159-GC fusion proteins were evaluated for function by testing for their ability to restore wild-type fatty acid content in the *ybr159Δ* cells (Fig. 2). Not surprisingly, since in most cases insertion of only the restriction site (encoding two amino acids) disrupted function, most of the Ybr159p-GC fusion proteins were not functional. In fact, only the Ybr159p-GC fusions with the Suc2p domain inserted at residue 18 restored wild-type activity, while those with the domain inserted at position 7 and 347 were partially active (Fig. 2). Although insertion of the cassette into most sites along the central portion of the protein led to loss of activity, the fusion proteins were stable, thus allowing further analysis. In this regard, it is important to point out that this reporter cassette has been successfully used in topology studies of other membrane proteins [8, 10, 15] and that its insertion into the luminal loops between transmembrane domains has not been found to interfere with their insertion or to alter their orientation.

The region between amino acid 7 and 55 possesses high hydrophobicity (Fig. 1A), and all algorithms predict the presence of a membrane spanning domain between residues 16 to 45 (while TMpred predicts a second TMD between 37 and 54). The GC cassettes inserted at several locations in and around this hydrophobic segment (7, 18, 45 and 66) showed partial glycosylation as indicated by the increased electrophoretic mobility of the fusion proteins following EndoH

treatment (Fig. 6A). While the GC cassette must reside in the lumen of the ER to be glycosylated, it is not possible to conclude that there are actual luminal domains defined by the insertions at residues 7, 18, 45 and 66. Rather it is possible that the hydrophilic GC cassette, if inserted into a membrane-embedded domain, extends into lumen where it can be glycosylated, perhaps explaining the inefficient glycosylation that is observed.

It is very clear that the electrophoretic mobilities of the fusion proteins with the GC located at position 102, 127, 196, 206, 280, 290 and 347 were not altered after treatment with EndoH, demonstrating that these regions of Ybr159p are located in the cytosol (Fig. 6A). In particular, with the caveat that these proteins are not functional, these data suggest that there are no additional TMDs between 169 and 192, between 204 and 225 and between 309 and 328 because the GC cassette at 196, 206 and 347 is clearly not lumenally disposed.

Analysis of Ybr159p Topology by fXa Insertion - To further investigate the topology of Ybr159p, tandem fXa protease cleavage sites (IEGRIEGR) were inserted at several positions [10], and their accessibility to fXa protease in sealed right-side-out membrane vesicles was assessed. A tandem recognition sequence was inserted to increase the probability of cleavage by the fXa protease, which cuts on the C-terminal side of the arginine in the IEGR tetrapeptide. The Ybr159p-fXa fusion proteins were expressed in *ybr159Δ* mutant cells, sealed right-side-out vesicles were prepared, and the sensitivity to fXa protease cleavage was assayed in the absence or presence of detergent. The integrity of the vesicle preparations was verified by showing that the luminal ER protein, Kar2p, was accessible to proteinase K only in the presence of detergent (data not shown). The fXa site inserted at position 45 was partially accessible to fXa protease only after treatment with detergent (Fig. 6B), further confirming that this region is not present in the cytosol. These experiments revealed that the fXa protease recognition sites at 196, 220 and 290 were accessible to the protease even in the absence of detergent (Fig. 6B), which is consistent with our glycosylation results. Taken together, the glycosylation and fXa protease cleavage results suggest

that Ybr159p contains membrane spanning regions, or possibly a membrane-embedded region at the N-terminus with major portion of the protein residing in the cytosol. According to this model, the putative NADPH binding site and the essential catalytic motif lies in the cytoplasm (Fig. 6C). These results suggest that Ybr159p is topologically more similar to the HSD2 isozyme that has a cytosolic active site than to the HSD1 enzyme, which has a lumenally disposed active site (discussed below) (Fig. 8).

The dilysine motif at the C-terminus of Ybr159p is required for ER retention -The KKXX motif is known to function in ER retention for several proteins [12], as well as for retrieval of proteins from the Golgi to ER [7]. Two dilysine motifs are present at the C-terminus of Ybr159p, at position K338K339 and K345K346. To determine whether the lysines at 345,346 are required for ER retention, we fused residues 1-343 of Ybr159p to GFP and compared the localization of this fusion protein to that of the full-length Ybr159p-GFP fusion protein by fluorescence microscopy. The fluorescence microscopy of the Ybr159p¹⁻³⁴³-GFP fusion protein displayed a punctate localization pattern (Fig. 7) similar to that which has been reported for Golgi-localized proteins. This pattern is completely distinct from that displayed for the intact Ybr159p-GFP, which revealed nuclear rimming and sub-plasma membrane labeling that is typical of ER localized proteins in yeast [9]. To further investigate whether the Ybr159p¹⁻³⁴³-GFP resides in the Golgi, colocalization experiments were done with a known Golgi marker, BODIPY TR ceramide. Fluorescence microscopy of live Ybr159p¹⁻³⁴³-GFP-expressing yeast cells that had been incubated with BODIPY TR ceramide revealed that the structures labeled with the two fluorescently labeled probes were completely overlapping (Fig. 7). BODIPY TR ceramide is known to stain the Golgi apparatus [6, 23]. These results indicate that the C-terminal dilysine motif in Ybr159p is absolutely required for ER retrieval.

DISCUSSION

The topology of Ybr159p, the major 3-ketoreductase of the ER-associated elongase

system was investigated by several approaches. Since the exact features of membrane proteins that dictate how they insert into membranes are not fully understood, the available algorithms for predicting membrane topologies can only serve as heuristic guides for the actual topology. Various programs predicted different numbers of membrane-spanning domains (1 or 4) for Ybr159p. Our data are most consistent with the presence of membrane-associated region at the N-terminus as shown schematically in Fig. 6C. All the programs predicted the N-terminus located in the cytosol, which is consistent with the proteinase K data. But the partial glycosylation of GC at position 7 and 18 contradicts their location in the cytosol. Due to the inability to glycosylate the majority of the fusion protein with GC at several locations at the N-terminus, as well as, the lack of any visible protected Myc fragment in our proteinase K experiment, suggests that the N-terminus is not in the lumen. The membrane association of the N-terminus is favored by the high hydrophobicity of this region and all programs predicted membrane spanning domains from 20-45 and TmPRED predicted from 16-37 and 37-54. Our data combined with the topology predictions, suggest that the N-terminus is membrane associated, however, the exact location of the domains cannot be predicted (denoted by *dashed line* in Fig. 6C).

HMMTOP and TmPRED predicted cytosolic orientation of the C-terminus. Our protease protection assay and split-ubiquitin assay also indicates that the C-terminus is in the cytosol. The evidence that the C-terminal dilysine motif is required for ER-retention of Ybr59p further confirms that the C-terminus is exposed to the cytoplasmic side of the ER. Several ER membrane bound proteins, for example the ceramide synthase (Lag1p and Lac1p) [14] showed a cytoplasmically oriented C-terminus that contains an ER-retention motif. Our glycosylation results are consistent with the cytosolic location of the C-terminus. GC inserted at several locations after residue 66 were not glycosylated, indicating that major portion of the protein is located in the cytoplasm. The fXa sites inserted at 196, 220 and 290 shows accessibility to fXa protease even in the absence of detergent confirming the glycosylation result. Taking together,

the glycosylation, fXa assays and also the high hydrophobicity of ~2.0, strongly suggest the presence of membrane spanning domains only at the N-terminus, with the remainder of the protein located in the cytoplasm. Based on this model, the predicted NADPH binding site and the catalytic domain of Ybr159p lies in the cytoplasm.

Since the majority of the Ybr159p was found to be very intolerant of amino acid insertions, even small 2-amino acid insertions caused loss of function. Therefore, our glycosylation and fXa protease results need to be cautiously interpreted. Nonetheless, the fact that most of the proteins were stable suggests that they folded normally and that they very likely adopted a native membrane topology can only be interpreted as suggestive. However our topology model has established the foundation for further structure-function studies on Ybr159p.

Ybr159p shows similarity with the short-chain dehydrogenase/reductase (SDR) family members, including the well-studied N-terminally membrane-anchored HSD1 and HSD2. The active site of HSD1 resides in the lumen, whereas, of HSD2 is located in the cytosol. Since our data suggest that the C-terminus, including the active site of Ybr159p is located in the cytosol, indicate similarity with HSD2 instead of HSD1 (Fig. 8).

REFERENCES

1. Athenstaedt, K. and G. Daum, *1-Acyldihydroxyacetone-phosphate reductase (Ayr1p) of the yeast Saccharomyces cerevisiae encoded by the open reading frame YIL124w is a major component of lipid particles*. J Biol Chem, 2000. **275**(1): p. 235-40.
2. Bateman, A., et al., *The Pfam protein families database*. Nucleic Acids Res, 2000. **28**(1): p. 263-6.
3. Beaudoin, F., et al., *A Saccharomyces cerevisiae gene required for heterologous fatty acid elongase activity encodes a microsomal beta-keto-reductase*. J Biol Chem, 2002. **277**(13): p. 11481-8.
4. Chang, S.I. and G.G. Hammes, *Homology analysis of the protein sequences of fatty acid synthases from chicken liver, rat mammary gland, and yeast*. Proc Natl Acad Sci U S A, 1989. **86**(21): p. 8373-6.
5. Dietrich, C.R., et al., *Characterization of two GL8 paralogs reveals that the 3-ketoacyl reductase component of fatty acid elongase is essential for maize (Zea mays L.) development*. Plant J, 2005. **42**(6): p. 844-61.
6. Egelund, J., et al., *Arabidopsis thaliana RGXT1 and RGXT2 encode Golgi-localized (1,3)-alpha-D-xylosyltransferases involved in the synthesis of pectic rhamnogalacturonan-II*. Plant Cell, 2006. **18**(10): p. 2593-607.
7. Gaynor, E.C., et al., *Signal-mediated retrieval of a membrane protein from the Golgi to the ER in yeast*. J Cell Biol, 1994. **127**(3): p. 653-65.
8. Gilstring, C.F. and P.O. Ljungdahl, *A method for determining the in vivo topology of yeast polytopic membrane proteins demonstrates that Gap1p fully integrates into the membrane independently of Shr3p*. J Biol Chem, 2000. **275**(40): p. 31488-95.
9. Han, G., et al., *The Saccharomyces cerevisiae YBR159w gene encodes the 3-ketoreductase of the microsomal fatty acid elongase*. J Biol Chem, 2002. **277**(38): p. 35440-9.
10. Han, G., et al., *The topology of the Lcb1p subunit of yeast serine palmitoyltransferase*. J Biol Chem, 2004. **279**(51): p. 53707-16.
11. Hirokawa, T., S. Boon-Chieng, and S. Mitaku, *SOSUI: classification and secondary structure prediction system for membrane proteins*. Bioinformatics,

1998. **14**(4): p. 378-9.
12. Jackson, M.R., T. Nilsson, and P.A. Peterson, *Retrieval of transmembrane proteins to the endoplasmic reticulum*. J Cell Biol, 1993. **121**(2): p. 317-33.
 13. Johnsson, N. and A. Varshavsky, *Split ubiquitin as a sensor of protein interactions in vivo*. Proc Natl Acad Sci U S A, 1994. **91**(22): p. 10340-4.
 14. Kageyama-Yahara, N. and H. Riezman, *Transmembrane topology of ceramide synthase in yeast*. Biochem J, 2006. **398**(3): p. 585-93.
 15. Kim, H., et al., *A global topology map of the Saccharomyces cerevisiae membrane proteome*. Proc Natl Acad Sci U S A, 2006. **103**(30): p. 11142-7.
 16. Kohlwein, S.D., et al., *Tsc13p is required for fatty acid elongation and localizes to a novel structure at the nuclear-vacuolar interface in Saccharomyces cerevisiae*. Mol Cell Biol, 2001. **21**(1): p. 109-25.
 17. Krogh, A., et al., *Predicting transmembrane protein topology with a hidden Markov model: application to complete genomes*. J Mol Biol, 2001. **305**(3): p. 567-80.
 18. Kyte, J. and R.F. Doolittle, *A simple method for displaying the hydropathic character of a protein*. J Mol Biol, 1982. **157**(1): p. 105-32.
 19. Lee, S., et al., *Localizome: a server for identifying transmembrane topologies and TM helices of eukaryotic proteins utilizing domain information*. Nucleic Acids Res, 2006. **34**(Web Server issue): p. W99-103.
 20. Miller, J.P., et al., *Large-scale identification of yeast integral membrane protein interactions*. Proc Natl Acad Sci U S A, 2005. **102**(34): p. 12123-8.
 21. Odermatt, A., et al., *The N-terminal anchor sequences of 11beta-hydroxysteroid dehydrogenases determine their orientation in the endoplasmic reticulum membrane*. J Biol Chem, 1999. **274**(40): p. 28762-70.
 22. Oh, C.S., et al., *ELO2 and ELO3, homologues of the Saccharomyces cerevisiae ELO1 gene, function in fatty acid elongation and are required for sphingolipid formation*. J Biol Chem, 1997. **272**(28): p. 17376-84.
 23. Pagano, R.E., et al., *A novel fluorescent ceramide analogue for studying membrane traffic in animal cells: accumulation at the Golgi apparatus results in altered spectral properties of the sphingolipid precursor*. J Cell Biol, 1991. **113**(6): p. 1267-79.
 24. Poulos, A., *Very long chain fatty acids in higher animals--a review*. Lipids, 1995. **30**(1): p. 1-14.
 25. Romano, J.D. and S. Michaelis, *Topological and mutational analysis of Saccharomyces cerevisiae Ste14p, founding member of the isoprenylcysteine*

- carboxyl methyltransferase family*. Mol Biol Cell, 2001. **12**(7): p. 1957-71.
26. Sherman, F., Fink, G. R., and Hicks, J. B., *Methods in Yeast Genetics*, 1986.
 27. Stoffel, K.H.W., *TMbase - A database of membrane spanning proteins segments*. Biol. Chem. Hoppe-Seyler, 1993: p. 374,166.
 28. Tusnady, G.E. and I. Simon, *Principles governing amino acid composition of integral membrane proteins: application to topology prediction*. J Mol Biol, 1998. **283**(2): p. 489-506.
 29. Tusnady, G.E. and I. Simon, *The HMMTOP transmembrane topology prediction server*. Bioinformatics, 2001. **17**(9): p. 849-50.
 30. Yan, A., E. Wu, and W.J. Lennarz, *Studies of yeast oligosaccharyl transferase subunits using the split-ubiquitin system: topological features and in vivo interactions*. Proc Natl Acad Sci U S A, 2005. **102**(20): p. 7121-6.

FOOTNOTES

Acknowledgements

This work was supported by an NSF 2010 Collaborative grant to TMD, a USUHS Graduate Student Research Grant to SP and an American Heart Association predoctoral fellowship to S.P. We thank Gongshe Han, Frederic Beaudoin and Dr. Jeffrey Harmon for helpful discussions. We thank Dr. Stanley Fields (HHMI, University of Washington, Seattle, WA 98195) for the NubG and Cub elongase constructs.

The abbreviations used are: FA, fatty acid; VLCFA, very long-chain fatty acids; ER, endoplasmic reticulum; HA, hemagglutinin; GFP, green fluorescent protein; GC, glycosylation cassette; fXa, factor Xa; TMD, transmembrane domain; EndoH, endoglycosidase H; SC, prefix designating a *Saccharomyces cerevisiae* gene or gene product; HSD, hydroxysteroid dehydrogenase; PUFA, polyunsaturated fatty acid.

FIGURE LEGENDS

Figure 1. Hydropathy Plot of Ybr159p – **A.** Hydropathy plot of *Saccharomyces cerevisiae* Ybr159p was generated according to the algorithm of Kyte and Doolittle [165] with a window of 13 amino acids. Hydrophobic amino acids are displayed above, and hydrophilic amino acids are below the zero line. **B.** Topology models predicted by different algorithms. Above the *grey box* lies the ER lumen and below is the cytosol. The residues marking the start and end of the membrane domains are indicated. Localizome, TMHMM and SOSUI predicted one TMD, HMMTOP and TmPRED predicted four TMDs.

Figure 2. Fatty Acid Profile of the Ybr159p Fusion Proteins Expressed in *ybr159Δ* mutant by GCMS - Fatty acids were extracted from *ybr159Δ* mutant cells expressing vector alone or wild-type Ybr159p or Ybr159p fusion proteins. The fatty acids were converted to methyl esters, and analyzed by GCMS. C21/23 fatty acids were added to the cells as internal standards prior to extraction of the fatty acids and were used for normalization but are not shown in the traces. The majority of the intracellular fatty acids are saturated and monounsaturated C16 and C18 (not shown in these traces) with the elongated (C18) saturated fatty acids representing only 5% of the total fatty acids [35]. In wild-type yeast a high proportion (50%) of the C26 is -hydroxylated, also not shown in these traces. The ability of the fusion proteins expressed in *ybr159Δ* mutant to restore wild-type fatty acid profile is mentioned on the right side either as *yes* (restores wild-type activity), *partial* (partial complementation) or *no* (failure to complement).

Figure 3. Protease Protection of Myc-Ybr159p-HA - Intact right-side out microsomal vesicles prepared from yeast harboring Myc-Ybr159p-HA was mock treated (*lane 1*), incubated with Triton X-100 (*lane 2*), or treated with proteinase K in the absence (*lane 3*) or presence of 0.4% Triton X-100 (*lane 4*). Myc-Ybr159p, Ybr159p-HA and Kar2p were detected with anti-myc-HRP (*top*), anti-HA-HRP (*middle*) and anti-Kar2p (*bottom*) antibody, respectively.

Figure 4. Split-ubiquitin Assay of the Elongase Proteins - **A.** Schematic representation of the split-ubiquitin assay. The Mata strain expressing the elongase proteins with C-terminally fused Cub-PLV are crossed with Mata α strain expressing elongase protein with C-terminally tagged NubG and the diploids are selected. If the two proteins interact, the Cub and Nub moieties will come close together and will be recognized and cleaved by the cytosolic ubiquitin-specific protease(s). The transcription factor (PLV) released will enter the nucleus and turn on the

reporter gene (*HIS3*). **B.** Protein-protein interaction assay. The diploids were selected on the SD-LT plates (*upper panel*) and were also pinned on plates lacking histidine (*lower panel*) to screen for interactions. The yeast expressing the Ybr159p-NubG and Ybr159p-Cub-PLV are marked by *asterisks*.

Figure 5. Sites of Insertion of the GC cassettes into the yeast Ybr159p - An alignment of the human (human-KAR), plant (*Arabidopsis thaliana*, At-Ybr159p), and yeast (*Saccharomyces cerevisiae*, SC-Ybr159p) Ybr159ps was used to predict locations within the protein that might accommodate insertion of the GC without disrupting function. The residues after which the GC was inserted are marked *green* for functional protein, *blue* for partial functional or *red* for non-functional but stable proteins. The highly conserved residues are shaded *black*. The NAD(P)H binding site is marked by a *blue line*, the intrinsic glycosylation sites by *green line*, and the active site residues are denoted by *red asterisks*.

Figure 6. Topology reporters Indicate the Membrane association of the N-terminus and cytosolic location of the C-terminus of Ybr159p - **A.** The glycosylation status of Ybr159p-GC fusion proteins reveals the membrane association of the N-terminus. The numbers represent the amino acids after which the GC was inserted. Microsomes were prepared from yeast expressing the Ybr159p-GC fusion proteins and 10 µg of microsomal protein (with or without EndoH treatment) were resolved by 12% SDS-PAGE and the fusion proteins were detected using anti-myc. **B.** Factor Xa protease cleavage of Ybr159p-fXa fusion proteins confirms the topology of Ybr159p. Sealed right-side out microsomal vesicles were prepared from cells expressing Ybr159p-fXa proteins with a tandem repeat of the factor Xa cleavage sites inserted at the indicated positions. The microsomes were mock-digested or digested with factor Xa protease in the absence or presence of Nonidet P-40 (NP-40) on ice for 3 h. 10 µg of protein was resolved by 12% SDS-PAGE and the Myc-tagged full length or N-terminal fragments of Ybr159p were detected by immunoblotting with anti-myc antibodies. **C.** A N-terminal membrane-associated and C-terminal cytoplasmic topology model for yeast Ybr159p. Each *circle* denotes a single amino acid, the *black circles* denote the residues where the inserted GC were partially glycosylated and the *green circles* denote the residues where GC were not glycosylated. The residues of the putative NADPH binding site are marked *blue* and the catalytic site *red*. The two intrinsic N-linked glycosylation sites, N173 and N325 that were not glycosylated are indicated as “Ns”. The *dashed line* marks the N-terminal membrane anchored region, where the exact TMD(s) cannot be predicted.

Figure 7. The Dilysine motif at the C-terminus of Ybr159p is Required for ER Retention -

Fluorescence microscopy of the Ybr159p¹⁻³⁴³-GFP fusion protein lacking the dilysine motif (K345K346) reveals punctate localization pattern in the cytoplasm (*left panel*) and the yeast incubated with BODIPY TR ceramide marks the Golgi apparatus (*middle panel*). Merging *left* and the *middle panel* indicates that 1-343-GFP co-localizes with the BODIPY TR ceramide (*right panel*) in the Golgi apparatus.

Figure 8. Position of the active site of Ybr159p compared with the Human Steroid Dehydrogenases (HSDs) - The *right panel* shows an alignment of the HSD1, HSD2 and yeast (*Saccharomyces cerevisiae*, SC-Ybr159p) Ybr159p. The NADPH binding site is marked by the *grey box* and the catalytic site by *black box*. The topology of these proteins is depicted on the *left panel*, with the active site denoted by *asterisk*. The active site of HSD1 is in the lumen, whereas, the active sites of Ybr159p and HSD2 resides in the cytosol.

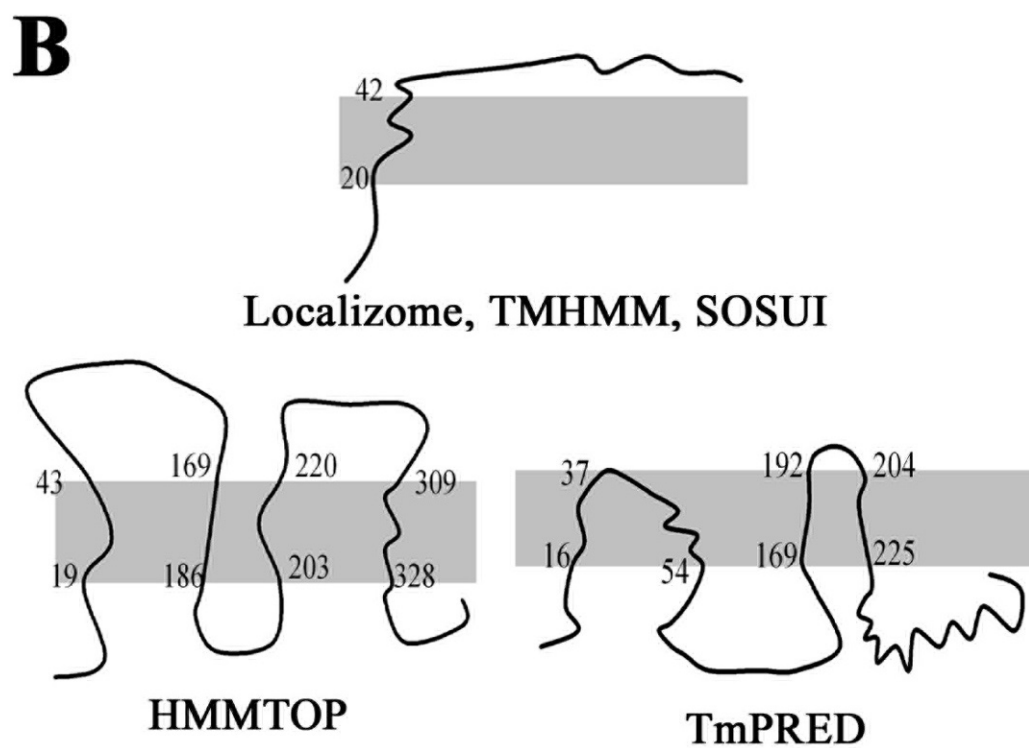
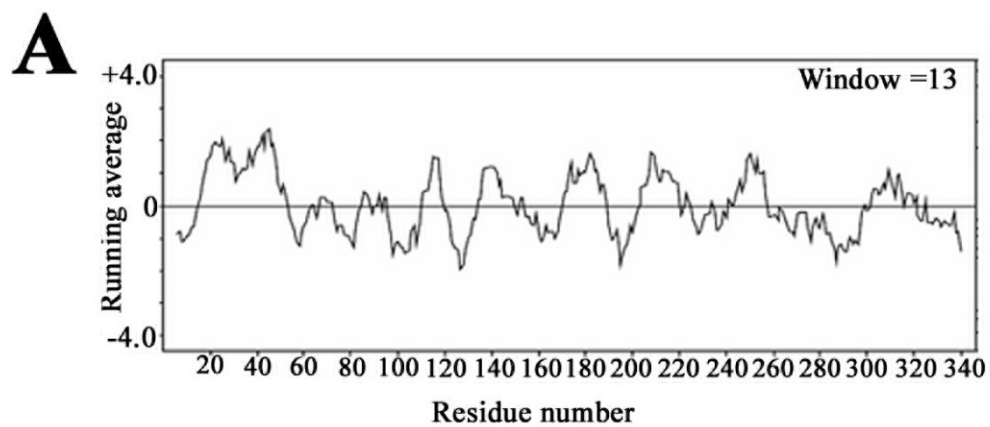


Fig 1

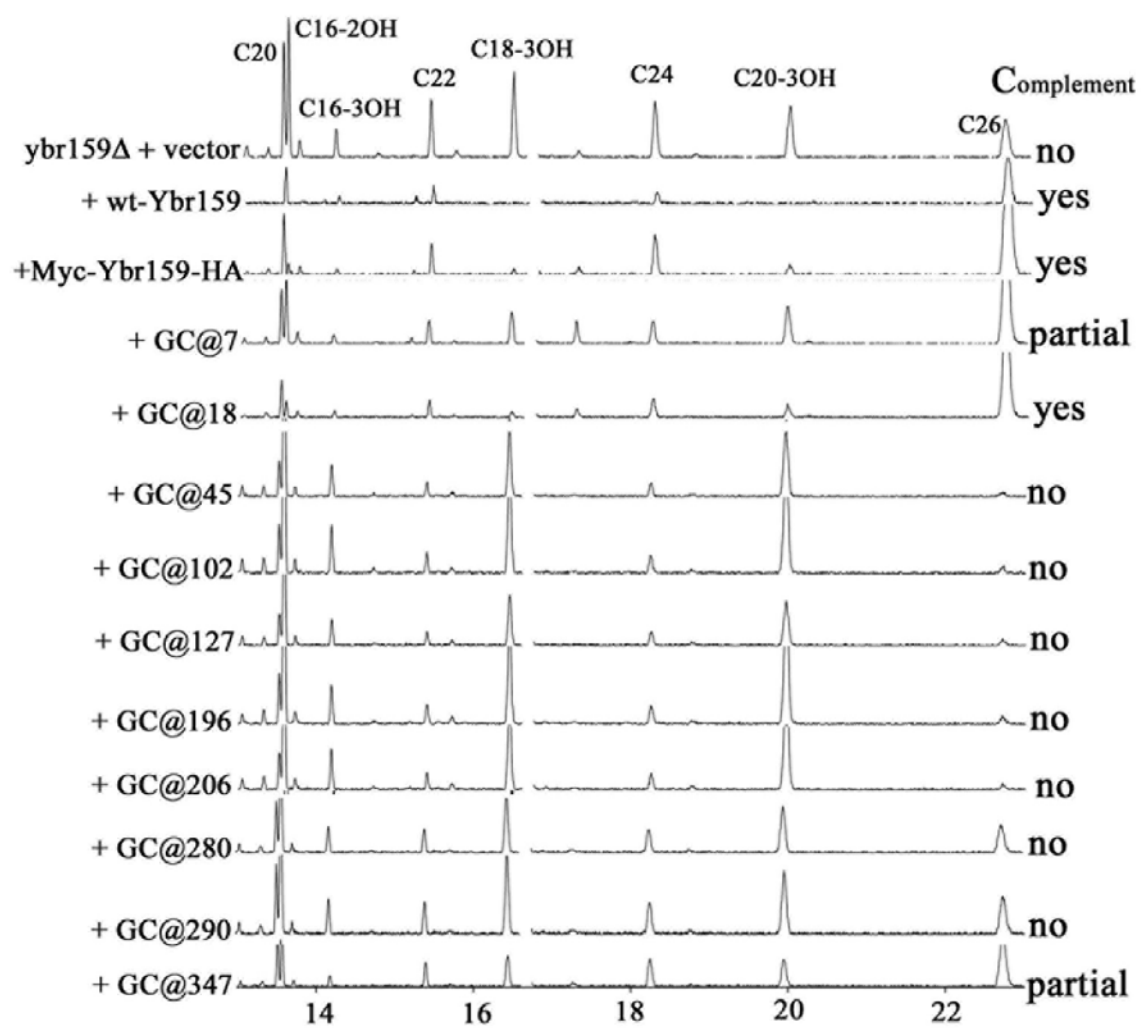


Fig 2

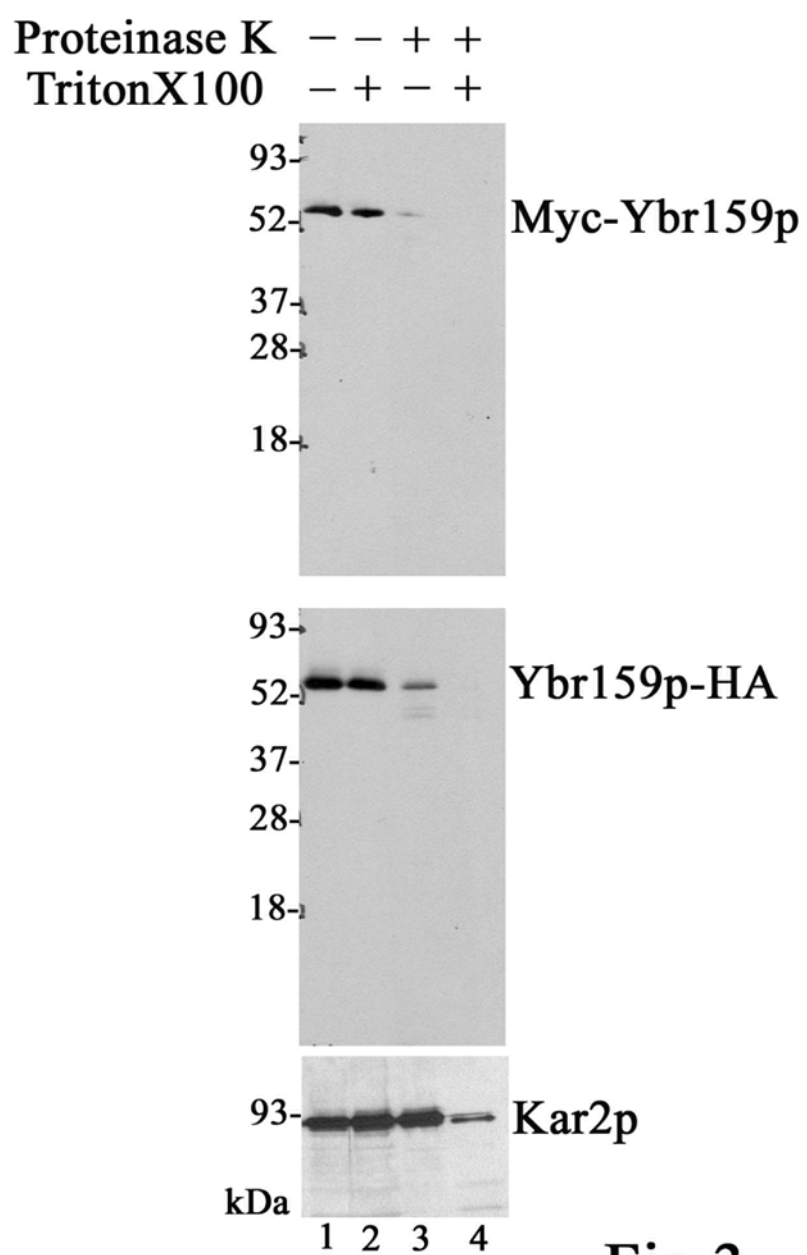


Fig 3

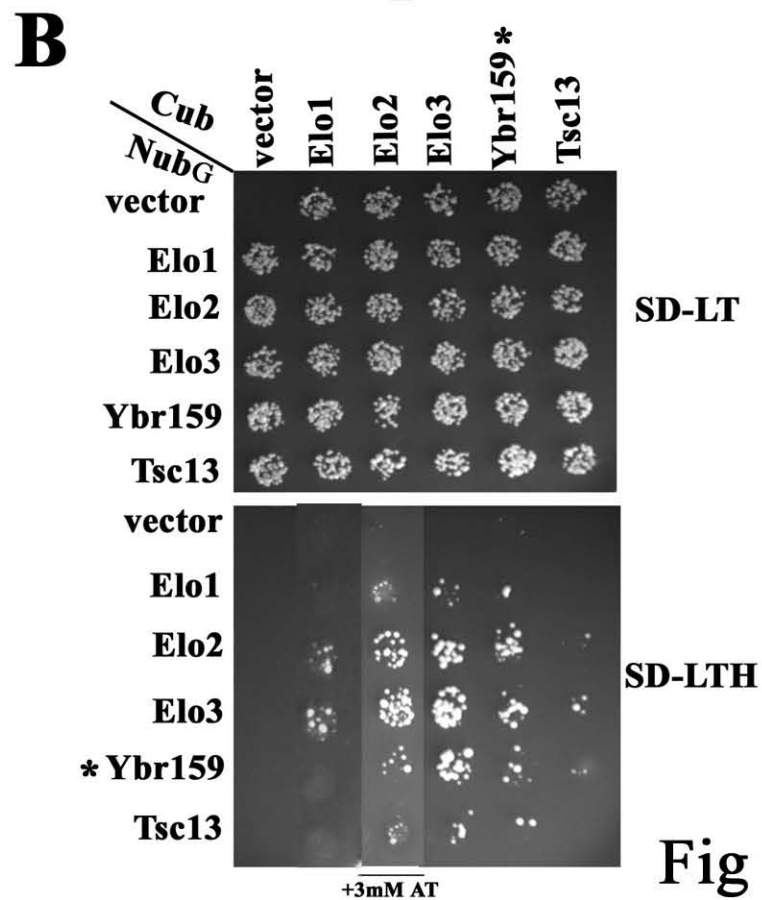
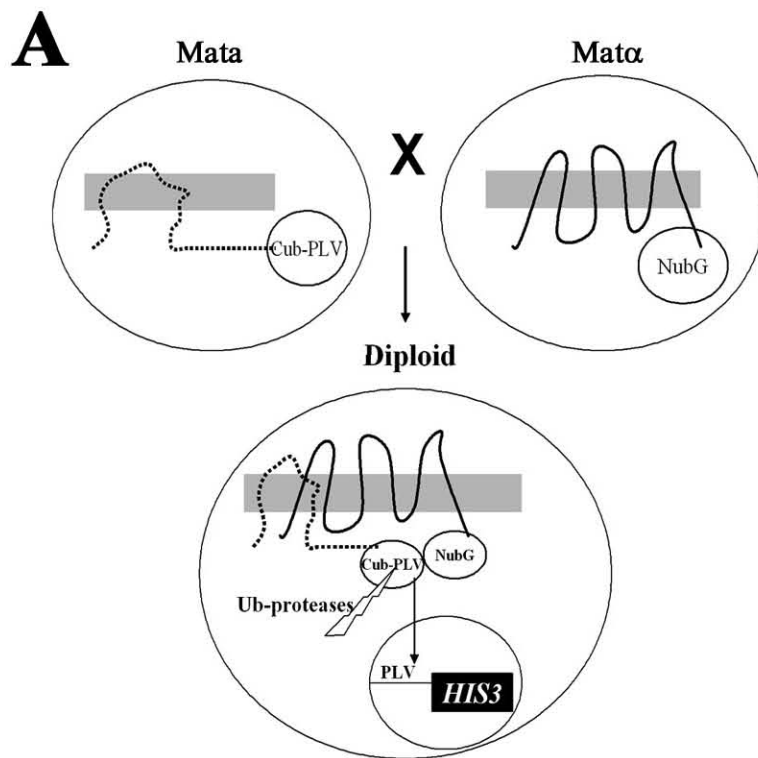


Fig 4

Human KAR: -----MESALPAAGFLYWVGAGTVAYLAIRISYSLFTALRVWGVGNEAGVG--PGLGEWAVV : 55
 At-Ybr159p: -----MEICTYFKSQPTWLLIIFVLG-SISIFKFIPTLLRSEYIYFIRPSKNLRRYGSWAI : 56
 SC-Ybr159p: MTFMQQIQEAGERFRCINGLLWVVFGLVLCCTLSLRFLALIFLELLPAVNFDKYGAKTGKYC : 67

Human KAR: TGSTDGIGKSYAEELAKHGKVVLLISRSKDKLDQVSSEIKKKFKVETRTIAVLFASEDIYD---KIK : 119
 At-Ybr159p: TGPTDGIGKAFQLAQKGLNLILVARNPDKLKDVSDSIRSKYSQTQILTVMDFSGDIDEGVKRIK : 123
 SC-Ybr159p: TGASDGIGKEFARQMAKRGFNVLVLSRQSKLEAQKELEDQHHVVVKILAIIDIEDKEIN-YESIK : 133

Human KAR: TGLAGLEIGILVNNVGMSEYIEYFLDVPDLNVIKKMININILSVCKMTQLVLPGMVE----- : 178
 At-Ybr159p: ESIEGLDVGILINNAGMSYPYAKYFHEVD--EELINNLIKINVEGTIKVTOQAVLPNMLK----- : 180
 SC-Ybr159p: ELCAQLFITVLVNNVGQSHSIFVPFLETE--EKELRNIIITNNTATLLITQIITAPKIVETVKAEEK : 198

Human KAR: -RSKGAILNISSGSGMLP--VPLLTIIYSATKTFVDFFSQCLHEEYRSKGVFVQSVLPYFVATKLAKI : 242
 At-Ybr159p: -RKKGAIIINMGSGAAALIPSYEFYSVYAGAKTYVLOFTKCLIVEYKKSgidVQCQVPLVATKMTKI : 246
 SC-Ybr159p: SGTIRGLITMGSGFGIIP--TPLLATYSGSKSFLOGWSNSLAGELSKDAIDVELIISYLVTSMSKI : 263

Human KAR: RKPTLDKPSPETFVKSIAKTVG-----LSRTNGYLIHALMGSIISNLP---SWIYLKIVNMNK : 299
 At-Ybr159p: RRASFVASPEGYAKAALRFVG-----YEAQCTPYWPHALMGAVVSALP---ESVFESFNIRKCL : 303
 SC-Ybr159p: RRSSLMIENPQCFVKSILRSVGRRCGIQERYATMTPYWAHAYQFVITETFGVYSKIVNSINYSFHK : 330

Human KAR: STRAHYLLKTKIN---- : 312
 At-Ybr159p: QIRKKGLQKDSMKKE-- : 318
 SC-Ybr159p: SIRIRALKKAARQVKKE : 347

Fig 1

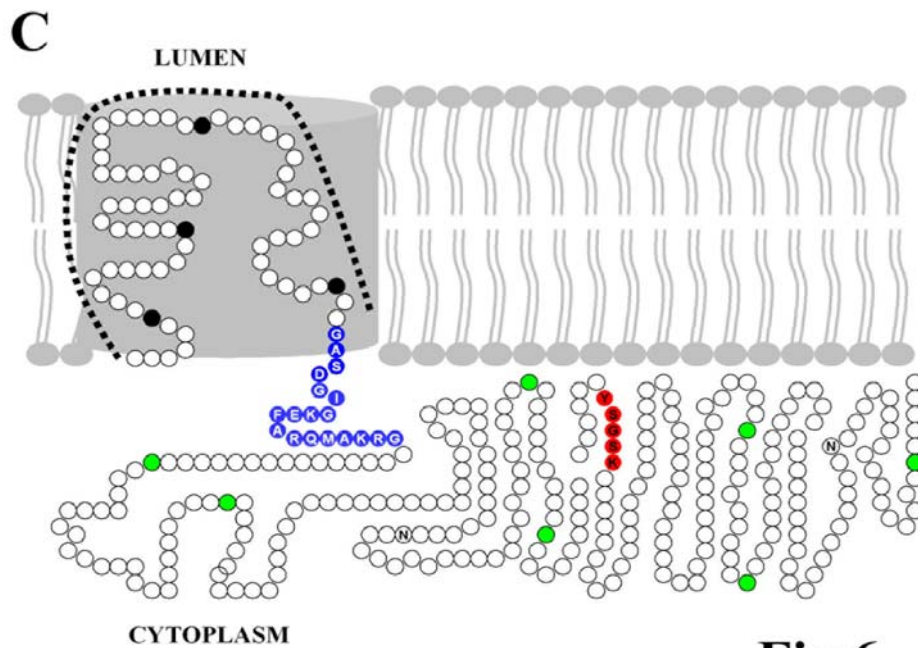
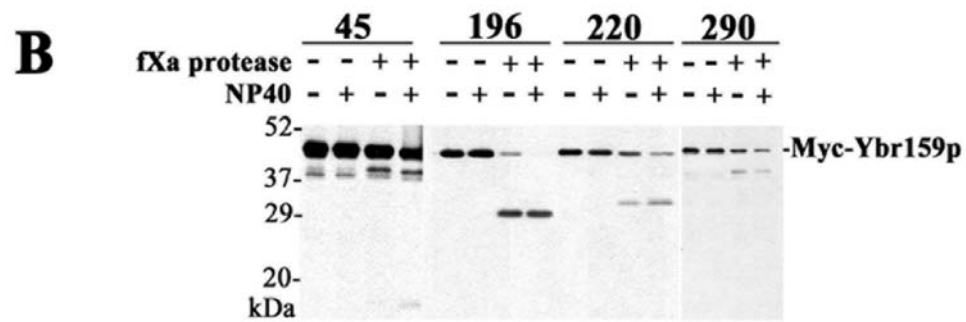
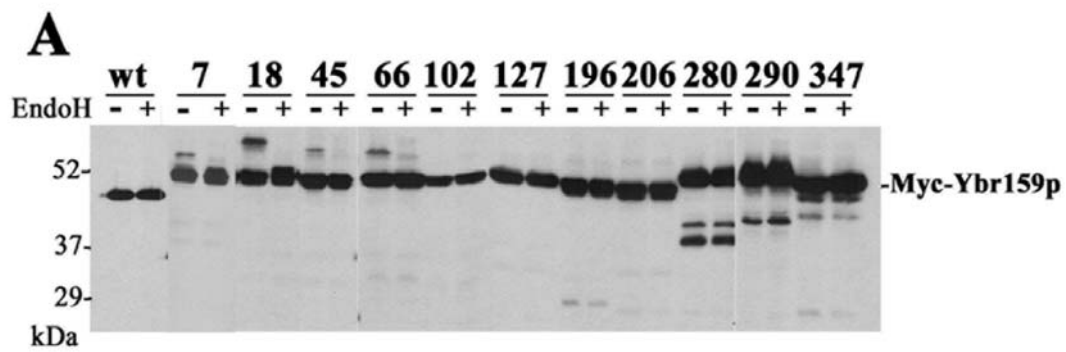


Fig 6



Fig 7

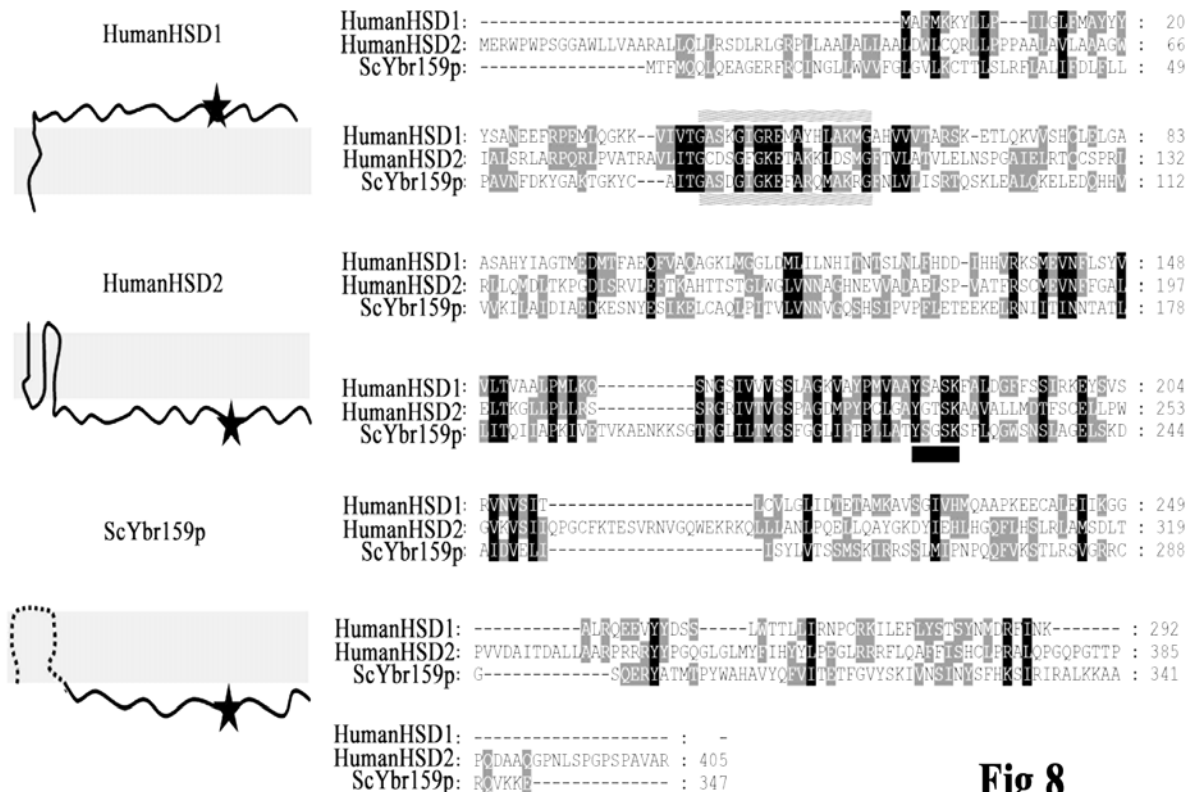


Fig 8

DISCUSSION

In spite of a large and growing body of data that support the metabolic significance of VLCFAs, the biochemical characterization of the elongase components required for their syntheses is very limited. Among the unresolved questions are the precise membrane topologies and organizations of the elongase proteins with respect to one another, the exact role of the Elop proteins in the condensation step, the enzymatic mechanism of each step in the elongation pathway, the mapping of the active sites of the component enzymes and a molecular understanding of how the intermediate substrates are passed from one active site to the next. A detailed characterization of the elongase proteins is needed in order to resolve these and other questions about the organization, mechanism and regulation of the elongase complex.

The work presented in this study has employed the budding yeast, *Saccharomyces cerevisiae* as a model system for investigating the elongase system of enzymes for several reasons: many of the genes encoding the enzymes involved in VLCFA and sphingolipid biosynthesis have been identified in this organism; these enzymes are highly conserved from yeast to mammals; and yeast mutants lacking these enzymes are available and their phenotypes well characterized. Moreover, the yeast model system provided the opportunity to combine powerful classical and molecular genetic approaches with cell biology and traditional biochemical approaches in the studies of VLCFA synthesis.

This work demonstrates that *Arabidopsis* FAE-KCSs can substitute for the yeast Elops. Although the Elops and FAE-KCS proteins lack similarity, both of these protein families works in conjunction with the common elongase components to generate

VLCFAs that are further incorporated into sphingolipids. The *in vivo* and *in vitro* data revealed that the FAE-KCSs have different substrate specificities, as do the Elop proteins. The coimmunoprecipitation data indicated a physical association of the FAE-KCSs with the reductases. To gain insight into the organization of the elongase complex, structural information about the elongase components is important. Although the ultimate goal would be to have a high resolution structure of the component enzymes, the problems associated with purification and crystallization of membrane bound proteins necessitate other approaches to these questions. For example, the detailed topological analyses and mutational studies of the reductases of the elongase complex that were performed in this study provide important insights about where the active sites of these proteins reside. Based on several biochemical approaches, we propose a six-membrane spanning topology model for the yeast and the *Arabidopsis* Tsc13p. Further characterization identified two functionally critical residues of Tsc13p. This study also demonstrates that the active site of Ybr159p is located in the cytosol.

The Elops are required in the condensation step

Although Elops lack the hallmarks of the well-characterized condensing enzymes, they were proposed to catalyze condensation in VLCFA synthesis [37] for several reasons. First, mutants lacking specific Elop proteins were found to be deficient in the synthesis of specific VLCFA species, and it seemed likely that the committed step would be condensation. Second, heterologous expression of Elop proteins from other species resulted in the synthesis of novel VLCFAs in yeast, again suggesting that they were responsible for the condensation step. Finally, there are no candidate classical 3-keto-CoA synthases in the yeast genome, and thus, the condensation step must be catalyzed by

a novel type of 3-keto-CoA synthase. Nonetheless, all these arguments are circumstantial, and to date no one has directly demonstrated that the Elop proteins are sufficient for the condensation step of FA elongation. To address this question more directly, *in vitro* elongase assays were performed with wild-type and *elo1* Δ , *elo2* Δ , and *elo3* Δ yeast microsomes using different chain length primary acyl CoAs in the presence and absence of NADPH, to specifically measure the condensation step. Consistent with earlier *in vivo* studies showing that Elo1p is required for elongation of myristate to palmitate [36, 166], our elongase assays with microsomes prepared from cells lacking Elo1p showed failure to form the C16–3-keto product from C14-CoA. Furthermore, microsomes prepared from the *elo2* Δ mutant showed low condensation activity toward the C16 and C18-CoA substrates, and those from the *elo3* Δ mutant produced very little C24–3-keto product with the C22-CoA substrate and no C26–3-keto product with the C24-CoA substrate. Because the condensation step was measured directly in these assays, it was possible to conclude that the Elops are absolutely required for the condensation step of FA elongation. Of course, while it was possible to conclude that the Elop proteins are directly involved in condensation, it is not possible to conclude that they are sufficient for condensation. This will require purification of the Elop proteins or a demonstration that heterologous expression of an Elop protein in a host that lacks FA elongation (e.g., *E. coli*) is sufficient to confer condensation activity.

Several Arabidopsis FAE-KCSs substitute for the Elops

FAE1 is a well-characterized condensing enzyme that catalyzes the condensation step of VLCFA synthesis in plants. The FAE-KCSs are found in plants, photosynthetic algae and in a marine parasitic protozoon (*Perkinus marinus*), but they are absent other

eukaryotes, including animals and fungus. Our study shows that the *Arabidopsis* FAE1 gene, upon heterologous expression in yeast, rescues the lethality of the *elo2Δelo3Δ* yeast double mutant. In an effort to identify other FAE-KCSs (there are 22 predicted FAE-KCS encoding genes in the *Arabidopsis* genome) that can substitute for the Elo2/3p, we screened an *Arabidopsis* cDNA expression library and found three other FAE-KCSs that were able to substitute for the Elo2/3p proteins. Our *in vivo* FA analysis and *in vitro* elongase assays with microsomes from these FAE-KCS-rescued yeast *elo2Δelo3Δ* mutants demonstrated that these different FAE-KCSs possess different substrate specificities. Those that rescued the *elo2Δelo3Δ* mutants all restored the synthesis of C₂₀ or longer VLCFAs.

The presence of 22 predicted *Arabidopsis* FAE-KCSs, raises the possibility that there might be additional FAE-KCSs that could substitute for Elo2/3p. The inability to detect any other FAE-KCSs in the cDNA library screen could be due to several reasons. It is possible that several of the FAE-KCSs were poorly represented in the *Arabidopsis* yeast expression library. Even if they are represented well in the library the possibility of mutations or errors while cloning in the yeast expression vector might disrupt their function. For example, we did not recover FAE1 in the cDNA library screen, despite the fact that it could be PCR amplified from the library suggesting the possibility of error while cloning the gene in the *Arabidopsis* yeast expression library, rendering inactive protein. Several FAE-KCSs (including *Atlg19440* and *At2g26640*) were shown to have no or very low activity with C_{16/18/20} substrates [87]. This suggests that the five PCR amplified FAE-KCSs (*At2g26250*, *Atlg01120*, *At2g26640*, *Atlg19440*, and *Atlg25450*) in our study, which did not rescue the *elo2Δelo3Δ* double mutant, might have failed to

utilize the substrates available in yeast. Both our *in vitro* and *in vivo* analyses show that C₂₂ is the minimum chain length FA that was generated by the FAE-KCSs that rescued the Elop lacking yeast strain, suggesting the need of C₂₂ as the minimum chain length FA for the survival of yeast. Thus not all FAE-KCSs are likely to substitute for Elo2/3p since the ones that do must be able to utilize substrates present in yeast and also synthesize saturated FAs with chain lengths of C₂₂ or greater. It will be interesting to characterize the substrate specificities of the FAE-like -KCSs using the *in vitro* elongase assays or *in vivo* FA analysis of the yeast expressing FAE-KCSs growing in medium supplemented with different chain length FAs.

FAE-KCSs and Elops utilize similar elongase components

The elongase components are known to exist in a complex [34, 35]. Thus, it was quite remarkable that the FAE-KCSs were able to substitute for the Elops. Despite the lack of sequence homology between the Elops and the FAE-KCSs, our genetic evidence suggests that the FAE-KCSs, like the Elops, depend on the reductases of the elongase complex. The genetic evidence is based on the failure of heterologously expressed FAE-KCSs to rescue the lethality associated with *tsc13Δ* or the slow growth phenotype of *ybr159Δ*. The genetic data prompted us to determine whether the FAE-KCSs physically associate with the reductases as do the Elop proteins. Indeed, coimmunoprecipitation experiments strongly support the conclusion that FAE1 can physically associate with both the yeast and *Arabidopsis* Ybr159p and Tsc13p reductases. Similarly, the FAE-KCS encoded by the *At2g16280* gene (that also rescued the *elo2Δelo3Δ* double mutant) also coimmunoprecipitated with both yeast and *Arabidopsis* Tsc13p. Coexpression of both Elops and the FAE1 fails to show a physical interaction between the proteins,

suggesting that when FAE-KCSs and Elops coexist, the elongase complexes can form with either an Elop protein or a FAE-KCS protein, but not with both (Fig. 11).

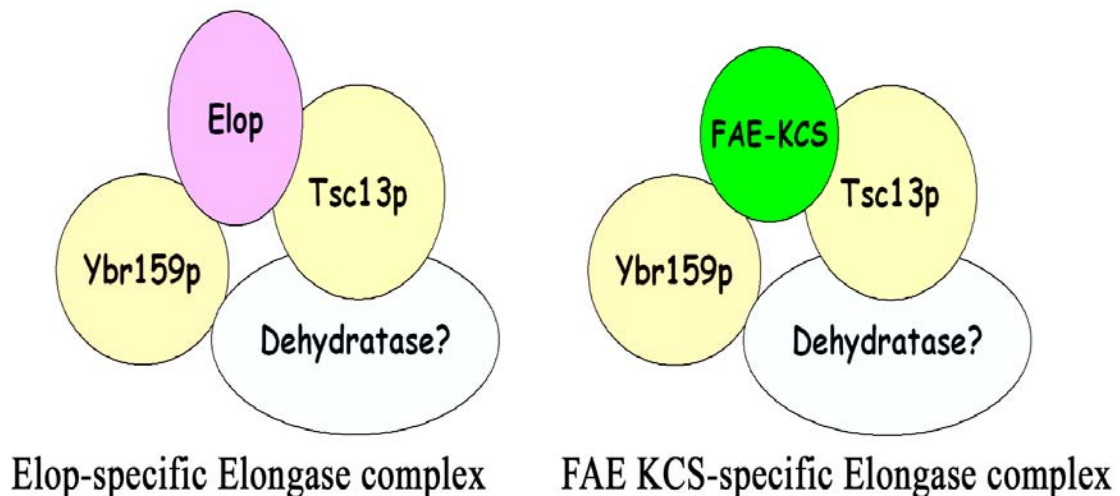


Figure 11. Schematic representation of the Elongase Complex. Based on our data, either Elop-specific (*left*) or FAE-KCS-specific (*right*) elongase complex exist. The elongase complex also shows that the Elop or the FAE—KCSs are associated with similar reductases. The dehydratase is marked by a *question mark* as the gene encoding the dehydratase is unknown.

The VLCFAs Synthesized by the FAE-KCS rescued yeast are incorporated into sphingolipids

In yeast the VLCFAs are major component of the complex sphingolipids, i.e., the inositolphosphoceramides (IPCs) and mannosylated IPCs (MIPC and M(IP)₂C) (Fig. 10). However, in a screen for suppressors of yeast mutants lacking serine palmitoyltransferase, Dickson and coworkers [108, 109] found that yeast lacking complex sphingolipids could survive if they had a mutated acyltransferase that

synthesized VLCFA-containing phosphatidylinositols. Thus, it was possible that the VLCFAs produced by FAE-KCS were incorporated into PI rather than into the complex sphingolipids. To test this possibility, the IPCs/MIPCs were extracted from the FAE-KCS- rescued yeast strains and analyzed. These studies revealed that the VLCFAs derived from the FAE-KCSs were indeed incorporated into the complex sphingolipids. Unlike the wild-type yeast that generates IPC containing α -OH-C26 FA, the FAE-KCS rescued yeast produced relatively hydrophilic IPCs. The data are consistent with the FA analyses, as the FAE-KCSs that generated mainly C20 FAs, produced C20-containing IPCs. Interestingly, these IPC species are not mannosylated, except C24-IPC generated by the At2g16280-rescued mutant, suggesting that the enzymes for mannosylation are specific for IPC substrates with an acyl chain of 24 or more carbons.

Topological mapping of the reductases of the elongase complex

Although several components of the elongase complex have been identified and their roles in FA elongation determined, their molecular mechanisms and their organizations within the complex are unknown, in part due to a lack of structural knowledge. The membrane bound nature of the elongase proteins has hindered their purification and crystallization. In the absence of high-resolution structural data, detailed topological mapping of the reductases of the elongase complex was performed in order to gain a more detailed understanding of their association with the membrane and with one another.

A. Six membrane-spanning topology model of yeast and Arabidopsis Tsc13p, the enoyl-CoA reductases

As various programs predicted different topologies for Tsc13p, we used several

biochemical approaches to map the location of the luminal and cytosolic domains. Our proteinase K results suggested a cytosolic localization of both the N- and C-termini of yeast Tsc13p. The epitope tagged Tsc13p showed ER localization and also rescued the lethality of *tsc13Δ* mutant, thus indicating that insertion of the N- and C-terminal epitope tags did not disrupt the function of Tsc13p. Because the immunolocalization studies were performed with the yeast grown on minimal media and at the midlogarithmic phase, we were unable to detect Tsc13p in the NVJ. Previous studies showed that yeast grown on complete media and at the stationary phase leads to enrichment of Tsc13p at the NVJ [35]. The cytosolic location of the N-terminus was further demonstrated by the absence of glycosylation of the intrinsic glycosylation site at N38 and a glycosylation reporter cassette inserted at position 7 and 69. This was further confirmed by the ability of fXa protease to cleave a fXa site inserted at position 69 even in the absence of detergent. The failure to glycosylate the GC at position 309, confirms our proteinase K result that the C-terminus is cytosolic. Two independent reports also suggested a cytosolic orientation of the C-terminus [167, 168].

We further analyzed the topology in detail by inserting the GC at several locations throughout the length of the protein. The electrophoretic mobility of the fusion proteins with cassettes inserted at 117, 126, 198 and 273 was altered after EndoH treatment, indicating glycosylation and luminal localization. However, GC at positions 159, 170, 226 and 236 were not glycosylated. The glycosylation data indicates that residues 117 and 126 are located in the first luminal loop. The N-terminal segment (1-117) containing TMD1 was found to contain sufficient information to target the protein to the ER membrane. As the GC at positions between 126 and 198 resulted in mislocalization

and/or disruption of function, it is unclear whether this segment is luminal or whether it contains additional membrane associated domains. Evidence for additional membrane associated domains within this segment of the protein was provided using a novel strategy. By inserting fXa sites at 117 and at 200 and an HA epitope at 198, this fragment of the protein was clipped out its membrane association was evaluated. The results revealed evidence of tight membrane association of the 117-200 fragment, which was solubilized with detergent but not with salt or high pH buffers. Were this domain a large luminal loop, this fragment would have been soluble. With residues 126 and 198 being in the lumen, we propose that there are at least two membrane spans between 126 and 198, a model that is consistent with the predictions of two algorithms, Localizome and HMMTOP. Our data most strongly support a six-membrane spanning topology model for the yeast Tsc13p, consistent with the topology predicted by HMMTOP and Localizome.

The *Arabidopsis* ortholog of Tsc13p (AtTsc13p) complements the yeast *tsc13Δ* mutant [118], prompting us to analyze the topology of this protein by heterologous expression in yeast. The results provided evidence of a similar six membrane-spanning topology model for AtTsc13p. In the case of the *Arabidopsis* protein, the presence of two membrane spans with a cytosolic loop between the TMD2 and TMD3 were identified in the region analogous to the yeast 126 to 198 segment, providing additional support for the proposed 6-membrane spanning model.

Tsc13p shows significant similarity at the C-terminal 150 amino acids with steroid-5 α reductases and both enzymes catalyze the reduction of a double bond that is α,β to a carbonyl group. However, nothing is known about the active site residues of

these proteins. The enoyl-ACP reductase of the FAS system is well-characterized but Tsc13p lacks similarity with this soluble reductase. The sequence alignment of yeast, plant, and mammalian Tsc13ps identified two highly conserved domains. Based on our six-membrane spanning model, the first highly conserved domain is positioned close to the membrane in the first cytosolic loop (Fig. 11A). The exact location of the second highly conserved domain vis a vis the membrane is not certain due to ambiguity about the precise location of TMD2, however, it is likely to be in a cytosolic domain just preceding, and possibly extending into TMD2. It is often the case that charged residues within membrane spanning domains are critical for function. Our topological model includes several charged residues within TMDs. To identify residues important for maintaining function, we mutated several conserved residues, including several charged residues in the conserved domains, to alanine in the yeast Tsc13p. Two residues, K140 and R141 are identified as critical for function, but not for maintaining the topology. These residues reside in the second conserved domain and are predicted to lie in or near the cytosolic end of TMD2.

B. Topology model of yeast Ybr159p, the 3-ketoreductase

Ybr159p bears homology to human estradiol-hydroxysteroid dehydrogenase (HSD), which belongs to the short-chain dehydrogenase/reductase (SDR) superfamily. These proteins, including Ybr159p, consist of a putative NADH binding motif and a catalytic domain. The two isoforms of HSDs (HSD1 and HSD2) are N-terminally associated with the membrane, but possess opposite topologies. The N-terminus of HSD1 is predicted to be in the cytosol, with the major portion of the protein, including the active site located in the lumen. By contrast, the N-terminus of HSD2 is predicted to be in the lumen with the

majority of the protein including the catalytic residues and the NADH binding site located in the cytosol.

Our data provides evidence that Ybr159p bears topological similarity with the HSD2 isozyme in that the active site is located in the cytosol. The cytosolic orientation of the C-terminus is indicated by the sensitivity of the C-terminal epitope tag to proteinase K even in the absence of detergent. Furthermore, our split ubiquitin experiments show that Ybr159p has a C-terminally positioned ½ ubiquitin that interacts with other ½-ubiquitin tagged elongase proteins in a manner consistent with the C-terminus being cytosolic. The presence of a C-terminal dilysine motif in Ybr159p, which we found to be essential for ER retrieval, also is consistent with the conclusion that the C-terminus of Ybr159p is exposed to the cytoplasmic face of the ER. The absence of glycosylation of the intrinsic glycosylation site at position N325, and also of the glycosylation cassette inserted at 347, is also consistent with the cytosolic orientation of the C-terminus. The glycosylation cassette was inserted at several other locations throughout the length of the protein for detailed topological analysis. The GC cassette inserted at 7 different positions after residue 66 does not show any glycosylation, suggesting that the majority of Ybr159p is cytosolic. This was confirmed by the accessibility of the fXa sites inserted at positions 196, 220 and 290 to fXa protease even in the absence of detergent. However, the GCs at position 7, 18, 45 and 66 showed partial glycosylation. Several programs predict a membrane spanning domain from 20-45 and TmPRED predicts two membrane spans from 16-37 and 37-54. This region also shows high hydrophobicity, suggesting its membrane association. While the GC cassette must reside in the lumen of the ER to be glycosylated, it is possible that the GC cassette inserted into the membrane-embedded

domain extends into the lumen and is glycosylated. This might explain the inefficient glycosylation observed at several positions (7, 18, 45 and 66) at the N-terminus. Based on our experiments, we propose a membrane associated region at the N-terminus of Ybr159p, although the exact start and end residues of the membrane associated domains cannot be detected. However, our data strongly suggests that the major C-terminal portion of Ybr159p, including the active site, resides in the cytosol (Fig. 11B).

To solve the topology of the N-terminus of Ybr159p other topological mapping approaches might be useful. Ybr159p has 5 cysteines (C16, C32, C65, C136, and C288), which based on the alignment of the orthologs is not conserved. Thus, it appears that none of them are likely to be critical for function and can be mutagenized to serines or alanines to generate a functional cysteineless mutant. However, with appropriate controls information can be obtained even if the cysteineless mutant is inactive. The localization of the cysteines with respect to the ER membrane can be determined by incubating sealed right-side out vesicles with membrane impermeable cysteine modifying agents. Cysteines present only in the cytosolic loops of the protein will be modified, compared to the luminal or membrane embedded cysteines that will remain unmodified.

Comparing the topology of Tsc13p and Ybr159p

Based on this study a long 88 amino acid containing N-terminal loop of Tsc13p is detected in the cytosol. In contrast, our experiments suggest membrane association of the N-terminus of Ybr159p, although the exact location of the N-terminus cannot be determined. The C-terminus of both Tsc13p and Ybr159p are identified to be cytosolically oriented. Although, both the proteins utilize NADPH for their enzymatic reactions, however, a classical NADPH binding motif is lacking in the Tsc13p protein

sequence. In contrast, Ybr159p contain both the putative NADPH binding site and the active site, which based on the topology model reside in the cytosol. Based on the model proposed in this study, majority of Ybr159p including the putative active site reside in the cytosol. In contrast, majority of Tsc13p protein is found to be embedded in the membrane containing six-membrane spanning domains. The proposed topology model of Tsc13p places the highly conserved domain containing the functionally important K140 and R141 residues, in or at the cytosolic face of TMD2.

FUTURE DIRECTIONS

Although several of the genes of the VLCFA synthesis pathway have been identified, the gene encoding the dehydratase is still unknown. There is still the possibility that the Elop proteins are regulatory subunits that act in conjunction with an additional protein to catalyze condensation. Thus, future studies should be aimed at identifying any additional unknown components of the elongase complex. An approach to identify the additional elongase components might take advantage of the split ubiquitin system. A NubG fused yeast cDNA library could be transformed into cells expressing either Tsc13p-Cub-PLV or Ybr159p-Cub-PLV as the bait protein. As our studies demonstrated that the C-termini of both the reductases are cytosolically orientated, the Cub-PLV tagged at the C-termini of the reductases would be suitable for screening the library. With a good cDNA library, the major portion of the yeast proteome could be screened, as the prey proteins can be either soluble or membrane bound in this assay.

Although both N- and C-terminally tagged NubG constructs would be used, if both ends of a potential prey protein are luminal, the interacting partner would be missed since both $\frac{1}{2}$ ubiquitins must reside in the cytosol to result in cleavage and reporter activation. The positive interacting candidates will be further confirmed for physical interaction by coimmunoprecipitation assays after coexpressing epitope tagged prey and bait proteins in yeast. An alternative method to identify the unknown elongase components would be to immunopurify the components of the elongase complex, possibly after chemical crosslinking. The topological information of the cytosolically disposed domains obtained from our study should provide information for selecting appropriate cross-linkers for purifying the complex for the purpose of identifying unknown elongase components by mass spectrometry.

The enoyl CoA reductase and the 3-ketoreductase use NADPH as cofactor and Ybr159p possess the classical NADH binding motif. Tsc13p lacks the signature sequence of a conventional NADH binding site, although the motif has been identified in steroid 5 α -reductases, with which Tsc13p shows high similarity. The lack of such a sequence in Tsc13p, raises the possibility of the existence of a novel type of NADPH binding site, or possibly an unidentified subunit of the enoyl reductase(s) component that possesses the NADPH binding motif. To determine whether NADPH binds to Tsc13p, and if so to identify the binding site, an experimental procedure similar to that previously used to determine the binding site in steroid 5 α -reductases [169] might be used. Yeast microsomes expressing epitope-tagged Tsc13p would be incubated with [2'-³²P]2-azido-NADP⁺, a competitive inhibitor of NADPH [169], and crosslinked by UV photolysis. The epitope-tagged Tsc13p would be immunopurified and electrophoresed to separate the

components of the elongase complex on an SDS-PAGE and then detected by immunoblotting with antibody against the epitope tag. If the immunoreactive band also shows [^{32}P] labelling, Tsc13p would have bound the [$2'-^{32}\text{P}$]2-azido-NADP $^{+}$. To identify the binding sequence, the protein could be eluted from the gel, digested with trypsin, followed by immobilized-Al $^{3+}$ affinity chromatography. The [$2'-^{32}\text{P}$]2-azido-NADP $^{+}$ labeled peptide will be retained on the column, and following elution, the purified peptide could be sequenced.

HSD1 and HSD2 have their active sites oriented in the lumen and the cytosol, respectively. Based on this study, the active site of Ybr159p resides in the cytosol. To investigate whether altering the orientation of the active site of Ybr159p from cytosol to the lumen of the ER causes loss of function, a chimeric protein might be generated. The first 66 amino acids from Ybr159p could be exchanged with either the first 39 amino acids of HSD1 or the first 87 amino acids of HSD2. HSD1 contains one TMD within the first 39 amino acids and the N-terminus is located in the cytosol. In contrast, HSD2 has the N-terminus oriented in the lumen and three TMDs are predicted within the first 87 residues. The N terminus of HSD1 or HSD2 was shown to be sufficient to determine the orientation of the protein in the ER membrane [170]. Thus, the active site of the fusion proteins with either the N-terminus of HSD1 or HSD2 fused to amino acids 66-347 of Ybr159p would be expected to reside in the lumen or cytosol, respectively (Fig. 12). The location of the epitope-tagged C-terminus of the fusion proteins could be determined by preparing sealed right-side out vesicles and assaying for accessibility of the epitope to proteinase K. If the C-terminus is in the cytosol, the epitope will be accessible to the proteinase K but a protected fragment will be detected if lumenally orientated. This

result could be further coupled with glycosylation data by inserting GC at a few locations and testing for EndoH sensitivity. Factor Xa protease cleavage sites could also be inserted and checked for accessibility to fXa protease to confirm the glycosylation data.

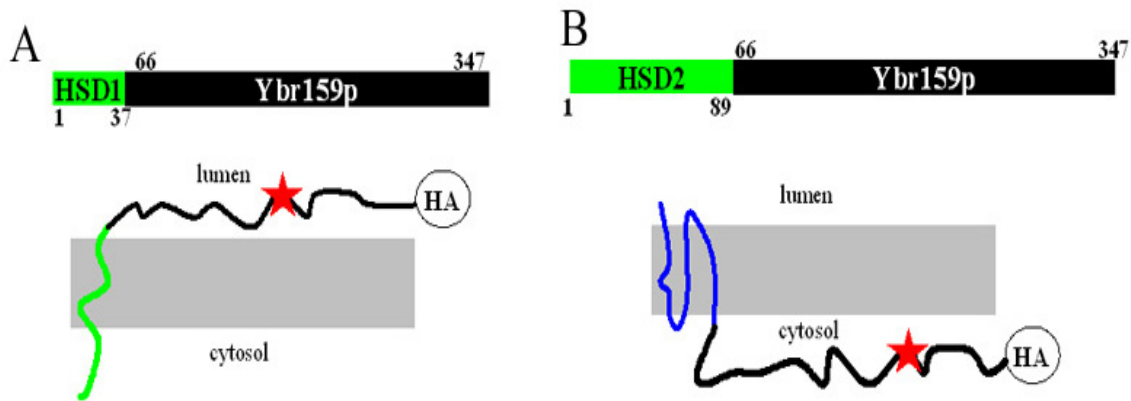


Figure 12. Schematic of altering the location of the active site of Ybr159p. (A) 1-37 amino acids of HSD1 fused to 66-347 of Ybr159p. The active site of the fusion protein (*red asterisk*) is expected in the lumen. (B) 1-89 of HSD2 fused to 66-347 of Ybr159p. The active site of the fusion protein (*red asterisk*)

CONCLUSION

The contents of this dissertation have focused on characterizing the components of the ER membrane bound elongase complex required for VLCFA synthesis, using the budding yeast *Saccharomyces cerevisiae* as the model system. This body of work makes several significant contributions to the overall understanding of the elongase proteins in

both plants and yeast. Our study suggests that although the Elop proteins lack all the hallmarks of the well-characterized 3-keto-CoA synthase family of condensing enzymes, they are indeed essential for the condensation step, and that they therefore represent either a novel type of condensing enzyme or possibly a regulatory subunit that is required for substrate recognition by an as yet unidentified condensing enzyme. In considering the possibility that all of the proteins involved in condensation may not yet have been identified, it is worth pointing out that the dehydratase component of FA elongation has yet to be identified. Of particular importance, our data demonstrates that although the Elops lack sequence homology with the FAE-KCS proteins, both work in conjunction with the common reductases of the elongase complex. The ability of these dissimilar proteins to physically associate with common reductases raises the possibility that FAE-KCSs and the Elops evolved independently as distinct condensing enzymes and yet are able to interact with the other elongase components. Although we showed that the FAE-KCSs can substitute for the Elops, the FAE-KCS rescued yeast strains possess several similar phenotypes to mutants with reduced sphingolipid synthesis, like the inability to grow at temperatures above 30°C. This may reflect a role of the VLCFA-containing sphingolipids in lowering membrane fluidity at elevated temperatures.

As an important step toward resolving the organization of the the elongase proteins, we performed detailed topological analyses of the reductases of the elongase complex. We successfully demonstrated a similar topology model for both the *Arabidopsis* and yeast Tsc13p, which comprises six-membrane spanning domains with both termini residing in the cytosol (Fig. 13A). Furthermore, this is the first study to identify functionally critical residues of the enoyl-CoA reductase. Based on our model,

the first conserved domain is located in the first cytosolic loop close to the membrane, and the second conserved domain containing the functionally critical residues in or near the cytosolic end of TMD2 (Fig. 13A). Finally, we were able to show that similar to HSD2 proteins, the yeast Ybr159p has the active site located in the cytosol (Fig. 13B). Insertion of glycosylation cassettes at several locations throughout the protein suggested a three membrane-spanning topology model for both yeast Elo2p and Elo3p (unpublished data from the lab). According to this model, the N-terminus and the conserved histidine motif are located in the lumen (Fig. 13C).

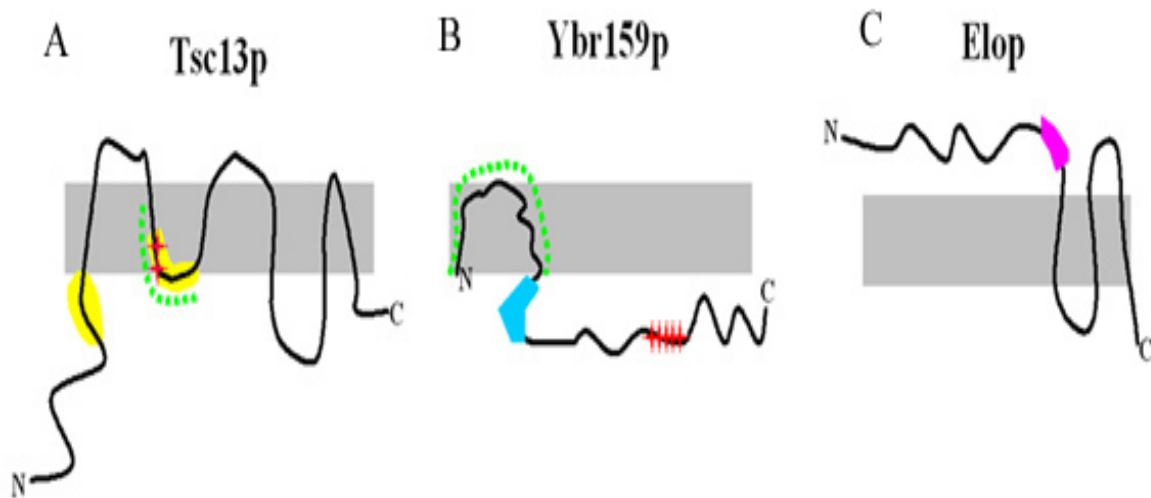


Figure 13. Schematic representation of the topology models of the yeast elongase components. (A) Six-membrane spanning model of Tsc13p. The two highly conserved domains are marked *yellow*, and the two functionally critical residues are denoted by *red asterisk*. The uncertainty as to the location of TMD2 is indicated by the *green dashed line*. (B) N-terminal membrane association and C-terminus cytosolically oriented in Ybr159p. The *green dashed line* denotes the uncertainty of the TMDs at the N-terminus. The NADPH binding site is marked *blue*, and the *red asterisks* denote the active site residues. (C) Three membrane-spanning model of Elo2p and Elo3p. The highly conserved histidine motif is marked *pink*. Lumen is *above* the *grey box* and cytosol is *below*.

BIBLIOGRAPHY

1. Schneiter, R., Hitomi, M., Ivessa, A.S., Fasch, E.V., Kohlwein, S.D. and Tartakoff, A.M., *A yeast acetyl coenzyme A carboxylase mutant links very-long-chain fatty acid synthesis to the structure and function of the nuclear membrane-pore complex*. Mol Cell Biol, 1996. **16**(12): p. 7161-72.
2. Smith, S., *The animal fatty acid synthase: one gene, one polypeptide, seven enzymes*. Faseb J, 1994. **8**(15): p. 1248-59.
3. White, S.W., Zheng, J., Zhang, Y.M. and Rock, *The structural biology of type II fatty acid biosynthesis*. Annu Rev Biochem, 2005. **74**: p. 791-831.
4. Schweizer, E., *Fatty acid synthase complexes*. Multifunctional Proteins, ed. Bisswanger, H., Schmincke-Ott, Eva. 1980, New York: John Wiley & Sons.
5. Wakil, S.J., Stoops, J.K. and Joshi, V.C., *Fatty acid synthesis and its regulation*. Annu Rev Biochem, 1983. **52**: p. 537-79.
6. Stoops, J.K. and Wakil, S.J., *Animal fatty acid synthetase. A novel arrangement of the beta-ketoacyl synthetase sites comprising domains of the two subunits*. J Biol Chem, 1981. **256**(10): p. 5128-33.
7. Brink, J., Ludtke, S.J., Yang, C.Y., Gu, Z.W., Wakil, S.J. and Chiu, W., *Quaternary structure of human fatty acid synthase by electron cryomicroscopy*. Proc Natl Acad Sci U S A, 2002. **99**(1): p. 138-43.
8. Rangan, V.S., Joshi, A.K. and Smith, S., *Mapping the functional topology of the animal fatty acid synthase by mutant complementation in vitro*. Biochemistry, 2001. **40**(36): p. 10792-9.
9. Witkowski, A., Joshi, A.K., Rangan, V.S., Falick, A.M., Witkowska, H.E. and Smith, S., *Dibromopropanone cross-linking of the phosphopantetheine and active-site cysteine thiols of the animal fatty acid synthase can occur both inter- and intrasubunit. Reevaluation of the side-by-side, antiparallel subunit model*. J Biol Chem, 1999. **274**(17): p. 11557-63.
10. Joshi, A.K., Rangan, V.S., Witkowski, A. and Smith, S., *Engineering of an active animal fatty acid synthase dimer with only one competent subunit*. Chem Biol, 2003. **10**(2): p. 169-73.
11. Asturias, F.J., Chadick, J.Z., Cheung, I.K., Stark, H., Witkowski, A., Joshi, A.K. and Smith, S., *Structure and molecular organization of mammalian fatty acid synthase*. Nat Struct Mol Biol, 2005. **12**(3): p. 225-32.
12. Wakil, S.J., *Fatty acid synthase, a proficient multifunctional enzyme*. Biochemistry, 1989. **28**(11): p. 4523-30.
13. Joshi, A.K. and Smith, S., *Construction, expression, and characterization of a mutated animal fatty acid synthase deficient in the dehydrase function*. J Biol Chem, 1993. **268**(30): p. 22508-13.
14. Amy, C.M., Witkowski, A., Naggert, J., Williams, B., Randhawa, Z. and Smith, S., *Molecular cloning and sequencing of cDNAs encoding the entire rat fatty acid synthase*. Proc Natl Acad Sci U S A, 1989. **86**(9): p. 3114-8.
15. Holzer, K.P., Liu, W. and Hammes, G.G., *Molecular cloning and sequencing of chicken liver fatty acid synthase cDNA*. Proc Natl Acad Sci U S A, 1989. **86**(12): p. 4387-91.

16. Witkowski, A., Rangan, V.S., Randhawa, Z.I., Amy, C.M. and Smith, S., *Structural organization of the multifunctional animal fatty-acid synthase*. Eur J Biochem, 1991. **198**(3): p. 571-9.
17. Smith, S., Agradi, E., Libertini, L. and Dileepan, K.N., *Specific release of the thioesterase component of the fatty acid synthetase multienzyme complex by limited trypsinization*. Proc Natl Acad Sci U S A, 1976. **73**(4): p. 1184-8.
18. Zhang, L., Joshi, A.K., Hofmann, J., Schweizer, E. and Smith, S., *Cloning, expression, and characterization of the human mitochondrial beta-ketoacyl synthase. Complementation of the yeast CEM1 knock-out strain*. J Biol Chem, 2005. **280**(13): p. 12422-9.
19. Jordan, S.W. and Cronan, J.E., Jr., *A new metabolic link. The acyl carrier protein of lipid synthesis donates lipoic acid to the pyruvate dehydrogenase complex in Escherichia coli and mitochondria*. J Biol Chem, 1997. **272**(29): p. 17903-6.
20. Price, A.C., Zhang, Y.M., Rock, C.O. and White, S.W., *Structure of beta-ketoacyl-[acyl carrier protein] reductase from Escherichia coli: negative cooperativity and its structural basis*. Biochemistry, 2001. **40**(43): p. 12772-81.
21. Price, A.C., Zhang, Y.M., Rock, C.O. and White, S.W., *Cofactor-induced conformational rearrangements establish a catalytically competent active site and a proton relay conduit in FabG*. Structure, 2004. **12**(3): p. 417-28.
22. Roujeinikova, A., Levy, C.W., Rowsell, S., Sedelnikova, S., Baker, P.J., Minshull, C.A., Mistry, A., Colls, J.G., Camble, R., Stuitje, A.R., Slabas, A.R., Rafferty, J.B., Paupit, R.A., Viner, R. and Rice, D.W., *Crystallographic analysis of triclosan bound to enoyl reductase*. J Mol Biol, 1999. **294**(2): p. 527-35.
23. Stewart, M.J., Parikh, S., Xiao, G., Tonge, P.J. and Kisker, C., *Structural basis and mechanism of enoyl reductase inhibition by triclosan*. J Mol Biol, 1999. **290**(4): p. 859-65.
24. Baldock, C., Rafferty, J.B., Stuitje, A.R., Slabas, A.R. and Rice, D.W., *The X-ray structure of Escherichia coli enoyl reductase with bound NAD⁺ at 2.1 Å resolution*. J Mol Biol, 1998. **284**(5): p. 1529-46.
25. Baldock, C., Rafferty, J.B., Sedelnikova, S.E., Baker, P.J., Stuitje, A.R., Slabas, A.R., Hawkes, T.R. and Rice, D.W., *A mechanism of drug action revealed by structural studies of enoyl reductase*. Science, 1996. **274**(5295): p. 2107-10.
26. Cohen-Gonsaud, M., Ducasse, S., Hoh, F., Zerbib, D., Labesse, G. and Quemard, A., *Crystal structure of MabA from Mycobacterium tuberculosis, a reductase involved in long-chain fatty acid biosynthesis*. J Mol Biol, 2002. **320**(2): p. 249-61.
27. Rozwarski, D.A., Grant, G.A., Barton, D.H., Jacobs, W.R., Jr. and Sacchettini, J.C., *Modification of the NADH of the isoniazid target (InhA) from Mycobacterium tuberculosis*. Science, 1998. **279**(5347): p. 98-102.
28. Fisher, M., Kroon, J.T., Martindale, W., Stuitje, A.R., Slabas, A.R. and Rafferty, J.B., *The X-ray structure of Brassica napus beta-keto acyl carrier protein reductase and its implications for substrate binding and catalysis*. Structure, 2000. **8**(4): p. 339-47.
29. Rafferty, J.B., Simon, J.W., Baldock, C., Artymiuk, P.J., Baker, P.J., Stuitje, A.R., Slabas, A.R. and Rice, D.W., *Common themes in redox chemistry emerge from the X-ray structure of oilseed rape (Brassica napus) enoyl acyl carrier protein*

- reductase*. Structure, 1995. **3**(9): p. 927-38.
30. Heath, R.J. and Rock, C.O., *Roles of the FabA and FabZ beta-hydroxyacyl-acyl carrier protein dehydratases in Escherichia coli fatty acid biosynthesis*. J Biol Chem, 1996. **271**(44): p. 27795-801.
 31. Heath, R.J. and Rock, C.O., *The Claisen condensation in biology*. Nat Prod Rep, 2002. **19**(5): p. 581-96.
 32. Nugteren, D.H., *The enzymic chain elongation of fatty acids by rat-liver microsomes*. Biochim Biophys Acta, 1965. **106**(2): p. 280-90.
 33. Cinti, D.L., Cook, L., Nagi, M.N. and Suneja, S.K., *The fatty acid chain elongation system of mammalian endoplasmic reticulum*. Prog Lipid Res, 1992. **31**(1): p. 1-51.
 34. Han, G., Gable, K., Kohlwein, S.D., Beaudoin, F., Napier, J.A. and Dunn, T.M., *The Saccharomyces cerevisiae YBR159w gene encodes the 3-ketoreductase of the microsomal fatty acid elongase*. J Biol Chem, 2002. **277**(38): p. 35440-9.
 35. Kohlwein, S.D., Eder, S., Oh, C.S., Martin, C.E., Gable, K., Bacikova, D. and Dunn, T., *Tsc13p is required for fatty acid elongation and localizes to a novel structure at the nuclear-vacuolar interface in Saccharomyces cerevisiae*. Mol Cell Biol, 2001. **21**(1): p. 109-25.
 36. Toke, D.A. and Martin, C.E., *Isolation and characterization of a gene affecting fatty acid elongation in Saccharomyces cerevisiae*. J Biol Chem, 1996. **271**(31): p. 18413-22.
 37. Oh, C.S., Toke, D.A., Mandala, S. and Martin, C.E., *ELO2 and ELO3, homologues of the Saccharomyces cerevisiae ELO1 gene, function in fatty acid elongation and are required for sphingolipid formation*. J Biol Chem, 1997. **272**(28): p. 17376-84.
 38. el-Sherbeini, M. and Clemas, J.A., *Cloning and characterization of GNS1: a Saccharomyces cerevisiae gene involved in synthesis of 1,3-beta-glucan in vitro*. J Bacteriol, 1995. **177**(11): p. 3227-34.
 39. Ladeveze, V., Marcireau, C., Delourme, D. and Karst, F., *General resistance to sterol biosynthesis inhibitors in Saccharomyces cerevisiae*. Lipids, 1993. **28**(10): p. 907-12.
 40. Garcia-Arranz, M., Maldonado, A.M., Mazon, M.J. and Portillo, F., *Transcriptional control of yeast plasma membrane H(+)-ATPase by glucose. Cloning and characterization of a new gene involved in this regulation*. J Biol Chem, 1994. **269**(27): p. 18076-82.
 41. Desfarges, L., Durrens, P., Juguelin, H., Cassagne, C., Bonneu, M. and Aigle, M., *Yeast mutants affected in viability upon starvation have a modified phospholipid composition*. Yeast, 1993. **9**(3): p. 267-77.
 42. Silve, S., Leplattois, P., Josse, A., Dupuy, P.H., Lanau, C., Kaghad, M., Dhers, C., Picard, C., Rahier, A., Taton, M., Le Fur, G., Caput, D., Ferrara, P. and Loison, G., *The immunosuppressant SR 31747 blocks cell proliferation by inhibiting a steroid isomerase in Saccharomyces cerevisiae*. Mol Cell Biol, 1996. **16**(6): p. 2719-27.
 43. Revardel, E., Bonneu, M., Durrens, P. and Aigle, M., *Characterization of a new gene family developing pleiotropic phenotypes upon mutation in Saccharomyces cerevisiae*. Biochim Biophys Acta, 1995. **1263**(3): p. 261-5.

44. Tvrdik, P., Asadi, A., Kozak, L.P., Nedergaard, J., Cannon, B. and Jacobsson, A., *Cig30, a mouse member of a novel membrane protein gene family, is involved in the recruitment of brown adipose tissue*. J Biol Chem, 1997. **272**(50): p. 31738-46.
45. Westerberg, R., Mansson, J.E., Golozoubova, V., Shabalina, I.G., Backlund, E.C., Tvrdik, P., Retterstol, K., Capecchi, M.R. and Jacobsson, A., *ELOVL3 is an important component for early onset of lipid recruitment in brown adipose tissue*. J Biol Chem, 2006. **281**(8): p. 4958-68.
46. Tvrdik, P., Westerberg, R., Silve, S., Asadi, A., Jakobsson, A., Cannon, B., Loison, G. and Jacobsson, A., *Role of a new mammalian gene family in the biosynthesis of very long chain fatty acids and sphingolipids*. J Cell Biol, 2000. **149**(3): p. 707-18.
47. Gill, I. and Valivety, R., *Polyunsaturated fatty acids, Part 1: Occurrence, biological activities and applications*. Trends Biotechnol, 1997. **15**(10): p. 401-9.
48. Broun, P., Gettner, S. and Somerville, C., *Genetic engineering of plant lipids*. Annu Rev Nutr, 1999. **19**: p. 197-216.
49. Leonard, A.E., Kelder, B., Bobik, E.G., Chuang, L.T., Lewis, C.J., Kopchick, J.J., Mukerji, P. and Huang, Y.S., *Identification and expression of mammalian long-chain PUFA elongation enzymes*. Lipids, 2002. **37**(8): p. 733-40.
50. Jakobsson, A., Westerberg, R. and Jacobsson, A., *Fatty acid elongases in mammals: their regulation and roles in metabolism*. Prog Lipid Res, 2006. **45**(3): p. 237-49.
51. Zhang, K., Kniazeva, M., Han, M., Li, W., Yu, Z., Yang, Z., Li, Y., Metzker, M.L., Allikmets, R., Zack, D.J., Kakuk, L.E., Lagali, P.S., Wong, P.W., MacDonald, I.M., Sieving, P.A., Figueroa, D.J., Austin, C.P., Gould, R.J., Ayyagari, R. and Petrukhin, K., *A 5-bp deletion in ELOVL4 is associated with two related forms of autosomal dominant macular dystrophy*. Nat Genet, 2001. **27**(1): p. 89-93.
52. de Antueno, R.J., Knickle, L.C., Smith, H., Elliot, M.L., Allen, S.J., Nwaka, S. and Winther, M.D., *Activity of human Delta5 and Delta6 desaturases on multiple n-3 and n-6 polyunsaturated fatty acids*. FEBS Lett, 2001. **509**(1): p. 77-80.
53. Inagaki, K., Aki, T., Fukuda, Y., Kawamoto, S., Shigeta, S., Ono, K. and Suzuki, O., *Identification and expression of a rat fatty acid elongase involved in the biosynthesis of C18 fatty acids*. Biosci Biotechnol Biochem, 2002. **66**(3): p. 613-21.
54. Das, T., Thurmond, J.M., Bobik, E., Leonard, A.E., Parker-Barnes, J.M., Huang, Y.S. and Mukerji, P., *Polyunsaturated fatty acid-specific elongation enzymes*. Biochem Soc Trans, 2000. **28**(6): p. 658-60.
55. Parker-Barnes, J.M., Das, T., Bobik, E., Leonard, A.E., Thurmond, J.M., Chuang, L.T., Huang, Y.S. and Mukerji, P., *Identification and characterization of an enzyme involved in the elongation of n-6 and n-3 polyunsaturated fatty acids*. Proc Natl Acad Sci U S A, 2000. **97**(15): p. 8284-9.
56. Beaudoin, F., Michaelson, L.V., Lewis, M.J., Shewry, P.R., Sayanova, O. and Napier, J.A., *Production of C20 polyunsaturated fatty acids (PUFAs) by pathway engineering: identification of a PUFA elongase component from Caenorhabditis elegans*. Biochem Soc Trans, 2000. **28**(6): p. 661-3.

57. Pereira, S.L., Leonard, A.E., Huang, Y.S., Chuang, L.T. and Mukerji, P., *Identification of two novel microalgal enzymes involved in the conversion of the omega3-fatty acid, eicosapentaenoic acid, into docosahexaenoic acid*. Biochem J, 2004. **384**(Pt 2): p. 357-66.
58. Zank, T.K., Zahringer, U., Beckmann, C., Pohnert, G., Boland, W., Holtorf, H., Reski, R., Lerchl, J. and Heinz, E., *Cloning and functional characterisation of an enzyme involved in the elongation of Delta6-polyunsaturated fatty acids from the moss Physcomitrella patens*. Plant J, 2002. **31**(3): p. 255-68.
59. Qi, B., Beaudoin, F., Fraser, T., Stobart, A.K., Napier, J.A. and Lazarus, C.M., *Identification of a cDNA encoding a novel C18-Delta(9) polyunsaturated fatty acid-specific elongating activity from the docosahexaenoic acid (DHA)-producing microalga, Isochrysis galbana*. FEBS Lett, 2002. **510**(3): p. 159-65.
60. Hastings, N., Agaba, M.K., Tocher, D.R., Zheng, X., Dickson, C.A., Dick, J.R. and Teale, A.J., *Molecular cloning and functional characterization of fatty acyl desaturase and elongase cDNAs involved in the production of eicosapentaenoic and docosahexaenoic acids from alpha-linolenic acid in Atlantic salmon (Salmo salar)*. Mar Biotechnol (NY), 2004. **6**(5): p. 463-74.
61. Ferguson, M.A., Low, M.G. and Cross, G.A., *Glycosyl-sn-1,2-dimyristylphosphatidylinositol is covalently linked to Trypanosoma brucei variant surface glycoprotein*. J Biol Chem, 1985. **260**(27): p. 14547-55.
62. Lee, S.H., Stephens, J.L., Paul, K.S. and Englund, P.T., *Fatty acid synthesis by elongases in trypanosomes*. Cell, 2006. **126**(4): p. 691-9.
63. Post-Beittenmiller, D., *Biochemistry And Molecular Biology Of Wax Production In Plants*. Annu Rev Plant Physiol Plant Mol Biol, 1996. **47**: p. 405-430.
64. Katavic, V., Reed, D.W., Taylor, D.C., Giblin, E.M., Barton, D.L., Zou, J., Mackenzie, S.L., Covello, P.S. and Kunst, L., *Alteration of seed fatty acid composition by an ethyl methanesulfonate-induced mutation in Arabidopsis thaliana affecting diacylglycerol acyltransferase activity*. Plant Physiol, 1995. **108**(1): p. 399-409.
65. James, D.W., Jr., Lim, E., Keller, J., Plooy, I., Ralston, E. and Dooner, H.K., *Directed tagging of the Arabidopsis FATTY ACID ELONGATION1 (FAE1) gene with the maize transposon activator*. Plant Cell, 1995. **7**(3): p. 309-19.
66. Rossak, M., Smith, M. and Kunst, L., *Expression of the FAE1 gene and FAE1 promoter activity in developing seeds of Arabidopsis thaliana*. Plant Mol Biol, 2001. **46**(6): p. 717-25.
67. James, D.W., and Dooner, H.K., *Isolation of EMS-induced mutants in Arabidopsis altered in seed fatty acid composition*. Theor. Appl. Genet., 1990. **80**: p. 241-245.
68. Lemieux, B., Miquel, M., Somerville, C., and Browse, J., *Mutants of Arabidopsis with alterations in seed lipid fatty acid composition*. Theor. Appl. Genet., 1990. **80**: p. 234-240.
69. Kunst, L., Taylor, D.C., and Underhill, E.W., *Fatty acid elongation in developing seeds of Arabidopsis thaliana*. Plant Physiol. Biochem., 1992. **30**: p. 425-434.
70. P. Barret, R.D., M. Renard, F. Domergue, R. Lessire, M. Delseny and T. J. Roscoe, *A rapeseed FAE1 gene is linked to the E1 locus associated with variation in the content of erucic acid*. TAG Theoretical and Applied Genetics, 1998. **96** (2): p. 177-186.

71. S. Das, T.J.R., M. Delseny, P. S. Srivastava and M. Lakshmikumaran, *Cloning and molecular characterization of the Fatty Acid Elongase 1 (FAE 1) gene from high and low erucic acid lines of Brassica campestris and Brassica oleracea* • ARTICLE. Plant Science, 2002. **162**(2): p. 245-250.
72. Lassner, M.W., Lardizabal, K. and Metz, J.G., *A jojoba beta-Ketoacyl-CoA synthase cDNA complements the canola fatty acid elongation mutation in transgenic plants*. Plant Cell, 1996. **8**(2): p. 281-92.
73. Moon, H., Smith, M.A. and Kunst, L., *A condensing enzyme from the seeds of Lesquerella fendleri that specifically elongates hydroxy fatty acids*. Plant Physiol, 2001. **127**(4): p. 1635-43.
74. Cahoon, E.B., Marillia, E.F., Stecca, K.L., Hall, S.E., Taylor, D.C. and Kinney, A.J., *Production of fatty acid components of meadowfoam oil in somatic soybean embryos*. Plant Physiol, 2000. **124**(1): p. 243-51.
75. Azachi, M., Sadka, A., Fisher, M., Goldshlag, P., Gokhman, I. and Zamir, A., *Salt induction of fatty acid elongase and membrane lipid modifications in the extreme halotolerant alga Dunaliella salina*. Plant Physiol, 2002. **129**(3): p. 1320-9.
76. *Analysis of the genome sequence of the flowering plant Arabidopsis thaliana*. Nature, 2000. **408**(6814): p. 796-815.
77. Gray, J.E., Holroyd, G.H., van der Lee, F.M., Bahrami, A.R., Sijmons, P.C., Woodward, F.I., Schuch, W. and Hetherington, A.M., *The HIC signalling pathway links CO₂ perception to stomatal development*. Nature, 2000. **408**(6813): p. 713-6.
78. Millar, A.A., Clemens, S., Zachgo, S., Giblin, E.M., Taylor, D.C. and Kunst, L., *CUT1, an Arabidopsis gene required for cuticular wax biosynthesis and pollen fertility, encodes a very-long-chain fatty acid condensing enzyme*. Plant Cell, 1999. **11**(5): p. 825-38.
79. Yephremov, A., Wisman, E., Huijser, P., Huijser, C., Wellesen, K. and Saedler, H., *Characterization of the FIDDLEHEAD gene of Arabidopsis reveals a link between adhesion response and cell differentiation in the epidermis*. Plant Cell, 1999. **11**(11): p. 2187-201.
80. Lolle, S.J., Berlyn, G.P., Engstrom, E.M., Krolkowski, K.A., Reiter, W.D. and Pruitt, R.E., *Developmental regulation of cell interactions in the Arabidopsis fiddlehead-1 mutant: a role for the epidermal cell wall and cuticle*. Dev Biol, 1997. **189**(2): p. 311-21.
81. Lolle, S.J., Cheung, A.Y. and Sussex, I.M., *Fiddlehead: an Arabidopsis mutant constitutively expressing an organ fusion program that involves interactions between epidermal cells*. Dev Biol, 1992. **152**(2): p. 383-92.
82. Pruitt, R.E., Vielle-Calzada, J.P., Ploense, S.E., Grossniklaus, U. and Lolle, S.J., *FIDDLEHEAD, a gene required to suppress epidermal cell interactions in Arabidopsis, encodes a putative lipid biosynthetic enzyme*. Proc Natl Acad Sci U S A, 2000. **97**(3): p. 1311-6.
83. Hooker, T.S., Millar, A.A. and Kunst, L., *Significance of the expression of the CER6 condensing enzyme for cuticular wax production in Arabidopsis*. Plant Physiol, 2002. **129**(4): p. 1568-80.
84. Fiebig, A., Mayfield, J.A., Miley, N.L., Chau, S., Fischer, R.L. and Preuss, D., *Alterations in CER6, a gene identical to CUT1, differentially affect long-chain*

- lipid content on the surface of pollen and stems*. Plant Cell, 2000. **12**(10): p. 2001-8.
85. Todd, J., Post-Beittenmiller, D. and Jaworski, J.G., *KCS1 encodes a fatty acid elongase 3-ketoacyl-CoA synthase affecting wax biosynthesis in Arabidopsis thaliana*. Plant J, 1999. **17**(2): p. 119-30.
 86. Trenkamp, S., Martin, W. and Tietjen, K., *Specific and differential inhibition of very-long-chain fatty acid elongases from Arabidopsis thaliana by different herbicides*. Proc Natl Acad Sci U S A, 2004. **101**(32): p. 11903-8.
 87. Blacklock, B.J. and Jaworski, J.G., *Substrate specificity of Arabidopsis 3-ketoacyl-CoA synthases*. Biochem Biophys Res Commun, 2006. **346**(2): p. 583-90.
 88. Ghanevati, M. and Jaworski, J.G., *Active-site residues of a plant membrane-bound fatty acid elongase beta-ketoacyl-CoA synthase, FAE1 KCS*. Biochim Biophys Acta, 2001. **1530**(1): p. 77-85.
 89. Schroder, G., Brown, J.W. and Schroder, J., *Molecular analysis of resveratrol synthase. cDNA, genomic clones and relationship with chalcone synthase*. Eur J Biochem, 1988. **172**(1): p. 161-9.
 90. Ghanevati, M. and Jaworski, J.G., *Engineering and mechanistic studies of the Arabidopsis FAE1 beta-ketoacyl-CoA synthase, FAE1 KCS*. Eur J Biochem, 2002. **269**(14): p. 3531-9.
 91. Clough, R.C., Matthis, A.L., Barnum, S.R. and Jaworski, J.G., *Purification and characterization of 3-ketoacyl-acyl carrier protein synthase III from spinach. A condensing enzyme utilizing acetyl-coenzyme A to initiate fatty acid synthesis*. J Biol Chem, 1992. **267**(29): p. 20992-8.
 92. Tsay, J.T., Oh, W., Larson, T.J., Jackowski, S. and Rock, C.O., *Isolation and characterization of the beta-ketoacyl-acyl carrier protein synthase III gene (fabH) from Escherichia coli K-12*. J Biol Chem, 1992. **267**(10): p. 6807-14.
 93. Martin, C.R., *Structure, function, and regulation of the chalcone synthase*. Int Rev Cytol, 1993. **147**: p. 233-84.
 94. Downey, R.K.a.R., G., *Brassica species*. Oil Crops of the World, ed. G. Robbelen, R.K.D.a.A.A. 1989, New York: McGraw-Hill Publishing Company.
 95. Blacklock, B.J. and Jaworski, J.G., *Studies into factors contributing to substrate specificity of membrane-bound 3-ketoacyl-CoA synthases*. Eur J Biochem, 2002. **269**(19): p. 4789-98.
 96. Venegas-Caleron, M., Beaudoin, F., Sayanova, O. and Napier, J.A., *Cotranscribed genes for long chain polyunsaturated fatty acid biosynthesis in the protozoon perkinsus marinus contain a plant-like FAE1 3-ketoacyl-CoA synthase*. J Biol Chem, 2006.
 97. Bernert, J.T., Jr. and Sprecher, H., *An analysis of partial reactions in the overall chain elongation of saturated and unsaturated fatty acids by rat liver microsomes*. J Biol Chem, 1977. **252**(19): p. 6736-44.
 98. Hogan, E.L., *Myelin*, ed. Morrell, P., ed. 1977, New York and London: Plenum Press. 489-520.
 99. Suneja, S.K., Nagi, M.N., Cook, L. and Cinti, D.L., *Decreased long-chain fatty acyl CoA elongation activity in quaking and jimpy mouse brain: deficiency in one enzyme or multiple enzyme activities?* J Neurochem, 1991. **57**(1): p. 140-6.

100. Millar, A.A. and Kunst, L., *Very-long-chain fatty acid biosynthesis is controlled through the expression and specificity of the condensing enzyme*. Plant J, 1997. **12**(1): p. 121-31.
101. Beaudoin, F., Michaelson, L.V., Hey, S.J., Lewis, M.J., Shewry, P.R., Sayanova, O. and Napier, J.A., *Heterologous reconstitution in yeast of the polyunsaturated fatty acid biosynthetic pathway*. Proc Natl Acad Sci U S A, 2000. **97**(12): p. 6421-6.
102. Beaudoin, F., Gable, K., Sayanova, O., Dunn, T. and Napier, J.A., *A Saccharomyces cerevisiae gene required for heterologous fatty acid elongase activity encodes a microsomal beta-keto-reductase*. J Biol Chem, 2002. **277**(13): p. 11481-8.
103. Chang, S.I. and Hammes, G.G., *Homology analysis of the protein sequences of fatty acid synthases from chicken liver, rat mammary gland, and yeast*. Proc Natl Acad Sci U S A, 1989. **86**(21): p. 8373-6.
104. Puranen, T., Poutanen, M., Ghosh, D., Vihko, P. and Vihko, R., *Characterization of structural and functional properties of human 17 beta-hydroxysteroid dehydrogenase type 1 using recombinant enzymes and site-directed mutagenesis*. Mol Endocrinol, 1997. **11**(1): p. 77-86.
105. Xu, X., Dietrich, C.R., Delledonne, M., Xia, Y., Wen, T.J., Robertson, D.S., Nikolau, B.J. and Schnable, P.S., *Sequence analysis of the cloned glossy8 gene of maize suggests that it may code for a beta-ketoacyl reductase required for the biosynthesis of cuticular waxes*. Plant Physiol, 1997. **115**(2): p. 501-10.
106. Haak, D., Gable, K., Beeler, T. and Dunn, T., *Hydroxylation of Saccharomyces cerevisiae ceramides requires Sur2p and Scs7p*. J Biol Chem, 1997. **272**(47): p. 29704-10.
107. Mitchell, A.G. and Martin, C.E., *Fah1p, a Saccharomyces cerevisiae cytochrome b5 fusion protein, and its Arabidopsis thaliana homolog that lacks the cytochrome b5 domain both function in the alpha-hydroxylation of sphingolipid-associated very long chain fatty acids*. J Biol Chem, 1997. **272**(45): p. 28281-8.
108. Lester, R.L. and Dickson, R.C., *Sphingolipids with inositolphosphate-containing head groups*. Adv Lipid Res, 1993. **26**: p. 253-74.
109. Nagiec, M.M., Wells, G.B., Lester, R.L. and Dickson, R.C., *A suppressor gene that enables Saccharomyces cerevisiae to grow without making sphingolipids encodes a protein that resembles an Escherichia coli fatty acyltransferase*. J Biol Chem, 1993. **268**(29): p. 22156-63.
110. Beeler, T., Gable, K., Zhao, C. and Dunn, T., *A novel protein, CSG2p, is required for Ca²⁺ regulation in Saccharomyces cerevisiae*. J Biol Chem, 1994. **269**(10): p. 7279-84.
111. Athenstaedt, K. and Daum, G., *1-Acyldihydroxyacetone-phosphate reductase (Ayr1p) of the yeast Saccharomyces cerevisiae encoded by the open reading frame YIL124w is a major component of lipid particles*. J Biol Chem, 2000. **275**(1): p. 235-40.
112. Beeler, T., Bacikova, D., Gable, K., Hopkins, L., Johnson, C., Slife, H. and Dunn, T., *The Saccharomyces cerevisiae TSC10/YBR265w gene encoding 3-ketosphinganine reductase is identified in a screen for temperature-sensitive suppressors of the Ca²⁺-sensitive csg2Delta mutant*. J Biol Chem, 1998. **273**(46):

- p. 30688-94.
113. Tuller, G., Prein, B., Jandrositz, A., Daum, G. and Kohlwein, S.D., *Deletion of six open reading frames from the left arm of chromosome IV of Saccharomyces cerevisiae*. Yeast, 1999. **15**(12): p. 1275-85.
 114. Knoll, A., Bessoule, J.J., Sargueil, F. and Cassagne, C., *Dehydration of 3-hydroxyacyl-CoA in brain very-long-chain fatty acid synthesis*. Neurochem Int, 1999. **34**(4): p. 255-67.
 115. Johnston, I.G., Rush, S.J., Gurd, J.W. and Brown, I.R., *Molecular cloning of a novel mRNA using an antibody directed against synaptic glycoproteins*. J Neurosci Res, 1992. **32**(2): p. 159-66.
 116. Pan, X., Roberts, P., Chen, Y., Kvam, E., Shulga, N., Huang, K., Lemmon, S. and Goldfarb, D.S., *Nucleus-vacuole junctions in Saccharomyces cerevisiae are formed through the direct interaction of Vac8p with Nvj1p*. Mol Biol Cell, 2000. **11**(7): p. 2445-57.
 117. Kvam, E., Gable, K., Dunn, T.M. and Goldfarb, D.S., *Targeting of Tsc13p to nucleus-vacuole junctions: a role for very-long-chain fatty acids in the biogenesis of microautophagic vesicles*. Mol Biol Cell, 2005. **16**(9): p. 3987-98.
 118. Gable, K., Garton, S., Napier, J.A. and Dunn, T.M., *Functional characterization of the Arabidopsis thaliana orthologue of Tsc13p, the enoyl reductase of the yeast microsomal fatty acid elongating system*. J Exp Bot, 2004. **55**(396): p. 543-5.
 119. Zheng, H., Rowland, O. and Kunst, L., *Disruptions of the Arabidopsis Enoyl-CoA reductase gene reveal an essential role for very-long-chain fatty acid synthesis in cell expansion during plant morphogenesis*. Plant Cell, 2005. **17**(5): p. 1467-81.
 120. Bogdanov, M., Zhang, W., Xie, J. and Dowhan, W., *Transmembrane protein topology mapping by the substituted cysteine accessibility method (SCAM(TM)): application to lipid-specific membrane protein topogenesis*. Methods, 2005. **36**(2): p. 148-71.
 121. Romano, J.D. and Michaelis, S., *Topological and mutational analysis of Saccharomyces cerevisiae Ste14p, founding member of the isoprenylcysteine carboxyl methyltransferase family*. Mol Biol Cell, 2001. **12**(7): p. 1957-71.
 122. Gilstring, C.F. and Ljungdahl, P.O., *A method for determining the in vivo topology of yeast polytopic membrane proteins demonstrates that Gap1p fully integrates into the membrane independently of Shr3p*. J Biol Chem, 2000. **275**(40): p. 31488-95.
 123. Han, G., Gable, K., Yan, L., Natarajan, M., Krishnamurthy, J., Gupta, S.D., Borovitskaya, A., Harmon, J.M. and Dunn, T.M., *The topology of the Lcb1p subunit of yeast serine palmitoyltransferase*. J Biol Chem, 2004. **279**(51): p. 53707-16.
 124. Kihara, A., Sano, T., Iwaki, S. and Igarashi, Y., *Transmembrane topology of sphingoid long-chain base-1-phosphate phosphatase, Lcb3p*. Genes Cells, 2003. **8**(6): p. 525-35.
 125. Nishi, T., Kawasaki-Nishi, S. and Forgac, M., *The first putative transmembrane segment of subunit c" (Vma16p) of the yeast V-ATPase is not necessary for function*. J Biol Chem, 2003. **278**(8): p. 5821-7.
 126. Wilkinson, B.M., Critchley, A.J. and Stirling, C.J., *Determination of the transmembrane topology of yeast Sec61p, an essential component of the*

- endoplasmic reticulum translocation complex*. J Biol Chem, 1996. **271**(41): p. 25590-7.
127. Leng, X.H., Nishi, T. and Forgac, M., *Transmembrane topography of the 100-kDa a subunit (Vph1p) of the yeast vacuolar proton-translocating ATPase*. J Biol Chem, 1999. **274**(21): p. 14655-61.
 128. Johnsson, N. and Varshavsky, A., *Split ubiquitin as a sensor of protein interactions in vivo*. Proc Natl Acad Sci U S A, 1994. **91**(22): p. 10340-4.
 129. Yan, A., Wu, E. and Lennarz, W.J., *Studies of yeast oligosaccharyl transferase subunits using the split-ubiquitin system: topological features and in vivo interactions*. Proc Natl Acad Sci U S A, 2005. **102**(20): p. 7121-6.
 130. Dietrich, C.R., Perera, M.A., M, D.Y.-N., Meeley, R.B., Nikolau, B.J. and Schnable, P.S., *Characterization of two GL8 paralogs reveals that the 3-ketoacyl reductase component of fatty acid elongase is essential for maize (Zea mays L.) development*. Plant J, 2005. **42**(6): p. 844-61.
 131. Baud, S., Bellec, Y., Miquel, M., Bellini, C., Caboche, M., Lepiniec, L., Faure, J.D. and Rochat, C., *gurke and pasticcino3 mutants affected in embryo development are impaired in acetyl-CoA carboxylase*. EMBO Rep, 2004. **5**(5): p. 515-20.
 132. Jung, K.H., Han, M.J., Lee, D.Y., Lee, Y.S., Schreiber, L., Franke, R., Faust, A., Yephremov, A., Saedler, H., Kim, Y.W., Hwang, I. and An, G., *Wax-deficient anther1 Is Involved in Cuticle and Wax Production in Rice Anther Walls and Is Required for Pollen Development*. Plant Cell, 2006. **18**(11): p. 3015-32.
 133. Preuss, D., Lemieux, B., Yen, G. and Davis, R.W., *A conditional sterile mutation eliminates surface components from Arabidopsis pollen and disrupts cell signaling during fertilization*. Genes Dev, 1993. **7**(6): p. 974-85.
 134. Park, J.A., Kim, T.W., Kim, S.K., Kim, W.T. and Pai, H.S., *Silencing of NbECR encoding a putative enoyl-CoA reductase results in disorganized membrane structures and epidermal cell ablation in Nicotiana benthamiana*. FEBS Lett, 2005. **579**(20): p. 4459-64.
 135. Westerberg, R., Tvrdik, P., Unden, A.B., Mansson, J.E., Norlen, L., Jakobsson, A., Holleran, W.H., Elias, P.M., Asadi, A., Flodby, P., Toftgard, R., Capecci, M.R. and Jakobsson, A., *Role for ELOVL3 and fatty acid chain length in development of hair and skin function*. J Biol Chem, 2004. **279**(7): p. 5621-9.
 136. Schaefer, E.J., Bongard, V., Beiser, A.S., Lamon-Fava, S., Robins, S.J., Au, R., Tucker, K.L., Kyle, D.J., Wilson, P.W. and Wolf, P.A., *Plasma phosphatidylcholine docosahexaenoic acid content and risk of dementia and Alzheimer disease: the Framingham Heart Study*. Arch Neurol, 2006. **63**(11): p. 1545-50.
 137. Mariani, C. and Wolters-Arts, M., *Complex waxes*. Plant Cell, 2000. **12**(10): p. 1795-8.
 138. Harwood, J.L., *The Biochemistry of Plants*, ed. Stumpf, P.K.C., E. 1980, New York): Academic. pp. 2-56.
 139. Kolattukudy, P.E., Fernandes, N.D., Azad, A.K., Fitzmaurice, A.M. and Sirakova, T.D., *Biochemistry and molecular genetics of cell-wall lipid biosynthesis in mycobacteria*. Mol Microbiol, 1997. **24**(2): p. 263-70.
 140. Daffe, M. and Draper, P., *The envelope layers of mycobacteria with reference to*

- their pathogenicity*. Adv Microb Physiol, 1998. **39**: p. 131-203.
141. Leonard, C., Lipid Technol., 1994. **4**: p. 79-83.
 142. Ruf, T., Valencak, T., Tataruch, F. and Arnold, W., *Running Speed in Mammals Increases with Muscle n-6 Polyunsaturated Fatty Acid Content*. PLoS ONE, 2006. **1**: p. e65.
 143. Cole, G.M., Lim, G.P., Yang, F., Teter, B., Begum, A., Ma, Q., Harris-White, M.E. and Frautschy, S.A., *Prevention of Alzheimer's disease: Omega-3 fatty acid and phenolic anti-oxidant interventions*. Neurobiol Aging, 2005. **26 Suppl 1**: p. 133-6.
 144. Riemersma, R.A., Wood, D.A., Butler, S., Elton, R.A., Oliver, M., Salo, M., Nikkari, T., Vartiainen, E., Puska, P., Gey, F. and et al., *Linoleic acid content in adipose tissue and coronary heart disease*. Br Med J (Clin Res Ed), 1986. **292**(6533): p. 1423-7.
 145. Singer, P., Jaeger, W., Voigt, S. and Thiel, H., *Defective desaturation and elongation of n-6 and n-3 fatty acids in hypertensive patients*. Prostaglandins Leukot Med, 1984. **15**(2): p. 159-65.
 146. Hakomori, S., *Glycosphingolipids in cellular interaction, differentiation, and oncogenesis*. Annu Rev Biochem, 1981. **50**: p. 733-64.
 147. Hechtberger, P., Zinser, E., Saf, R., Hummel, K., Paltauf, F. and Daum, G., *Characterization, quantification and subcellular localization of inositol-containing sphingolipids of the yeast, Saccharomyces cerevisiae*. Eur J Biochem, 1994. **225**(2): p. 641-9.
 148. Horvath, A., Sutterlin, C., Manning-Krieg, U., Movva, N.R. and Riezman, H., *Ceramide synthesis enhances transport of GPI-anchored proteins to the Golgi apparatus in yeast*. Embo J, 1994. **13**(16): p. 3687-95.
 149. Bagnat, M., Keranen, S., Shevchenko, A., Shevchenko, A. and Simons, K., *Lipid rafts function in biosynthetic delivery of proteins to the cell surface in yeast*. Proc Natl Acad Sci U S A, 2000. **97**(7): p. 3254-9.
 150. Simons, K. and van Meer, G., *Lipid sorting in epithelial cells*. Biochemistry, 1988. **27**(17): p. 6197-202.
 151. Bhat, R.A. and Panstruga, R., *Lipid rafts in plants*. Planta, 2005. **223**(1): p. 5-19.
 152. Simons, K. and Ikonen, E., *Functional rafts in cell membranes*. Nature, 1997. **387**(6633): p. 569-72.
 153. Friedrichson, T. and Kurzchalia, T.V., *Microdomains of GPI-anchored proteins in living cells revealed by crosslinking*. Nature, 1998. **394**(6695): p. 802-5.
 154. Ikonen, E., *Roles of lipid rafts in membrane transport*. Curr Opin Cell Biol, 2001. **13**(4): p. 470-7.
 155. Smart, E.J., Graf, G.A., McNiven, M.A., Sessa, W.C., Engelman, J.A., Scherer, P.E., Okamoto, T. and Lisanti, M.P., *Caveolins, liquid-ordered domains, and signal transduction*. Mol Cell Biol, 1999. **19**(11): p. 7289-304.
 156. Simons, K. and Toomre, D., *Lipid rafts and signal transduction*. Nat Rev Mol Cell Biol, 2000. **1**(1): p. 31-9.
 157. Perry, D.K. and Hannun, Y.A., *The role of ceramide in cell signaling*. Biochim Biophys Acta, 1998. **1436**(1-2): p. 233-43.
 158. Hannun, Y.A. and Luberto, C., *Ceramide in the eukaryotic stress response*. Trends Cell Biol, 2000. **10**(2): p. 73-80.

159. Hannun, Y.A. and Obeid, L.M., *The Ceramide-centric universe of lipid-mediated cell regulation: stress encounters of the lipid kind*. J Biol Chem, 2002. **277**(29): p. 25847-50.
160. Acharya, U., Patel, S., Koundakjian, E., Nagashima, K., Han, X. and Acharya, J.K., *Modulating sphingolipid biosynthetic pathway rescues photoreceptor degeneration*. Science, 2003. **299**(5613): p. 1740-3.
161. Pettus, B.J., Chalfant, C.E. and Hannun, Y.A., *Ceramide in apoptosis: an overview and current perspectives*. Biochim Biophys Acta, 2002. **1585**(2-3): p. 114-25.
162. Wu, Z., Tandon, R., Ziemicki, J., Nagano, J., Hujer, K.M., Miller, R.T. and Huang, C., *Role of ceramide in Ca²⁺-sensing receptor-induced apoptosis*. J Lipid Res, 2005. **46**(7): p. 1396-404.
163. Sirakova, T.D., Thirumala, A.K., Dubey, V.S., Sprecher, H. and Kolattukudy, P.E., *The Mycobacterium tuberculosis pks2 gene encodes the synthase for the hepta- and octamethyl-branched fatty acids required for sulfolipid synthesis*. J Biol Chem, 2001. **276**(20): p. 16833-9.
164. Kohlwein, S.D., Eder, S., Oh, C.S., Martin, C.E., Gable, K., Bacikova, D. and Dunn, T., *Tsc13p is required for fatty acid elongation and localizes to a novel structure at the nuclear-vacuolar interface in Saccharomyces cerevisiae*. Mol Cell Biol, 2001. **21**(1): p. 109-25.
165. Kyte, J. and Doolittle, R.F., *A simple method for displaying the hydropathic character of a protein*. J Mol Biol, 1982. **157**(1): p. 105-32.
166. Schneiter, R., Tatzer, V., Gogg, G., Leitner, E. and Kohlwein, S.D., *Elo1p-dependent carboxy-terminal elongation of C14:1Delta(9) to C16:1Delta(11) fatty acids in Saccharomyces cerevisiae*. J Bacteriol, 2000. **182**(13): p. 3655-60.
167. Miller, J.P., Lo, R.S., Ben-Hur, A., Desmarais, C., Stagljar, I., Noble, W.S. and Fields, S., *Large-scale identification of yeast integral membrane protein interactions*. Proc Natl Acad Sci U S A, 2005. **102**(34): p. 12123-8.
168. Kim, H., Melen, K., Osterberg, M. and von Heijne, G., *A global topology map of the Saccharomyces cerevisiae membrane proteome*. Proc Natl Acad Sci U S A, 2006. **103**(30): p. 11142-7.
169. Bhattacharya AK, C.A., Shuffett M, Haley BE and Collins DC, *Photoaffinity labeling of rat liver microsomal steroid 5 α -reductase by 2-azido-NADP⁺*. Steroids, 1999. **59**(11): p. 634-41.
170. Odermatt, A., Arnold, P., Stauffer, A., Frey, B.M. and Frey, F.J., *The N-terminal anchor sequences of 11beta-hydroxysteroid dehydrogenases determine their orientation in the endoplasmic reticulum membrane*. J Biol Chem, 1999. **274**(40): p. 28762-70.

APPENDIX

Statement of Author's Contribution:

The author was personally involved in the planning and execution of all experiments described in this dissertation, and played a crucial role in the writing of the papers presented here. Furthermore, the author has presented different stages of this work in oral presentations at a number of scientific meetings.